CFD ANALYSIS OF COLD GAS DYNAMIC SPRAY COATING UNDER DIFFERENT CONDITIONS

A Thesis Submitted
In Partial Fulfilment of the Requirements
for the Degree of

DOCTOR OF PHILOSOPHY

by

MOHSIN KHAN
(Roll No. 2K18/PhD/ME/15)

Under the Supervision of

DR. MOHAMMAD ZUNAID
DTU, DELHI
(Supervisor)

PROF. QASIM MURTAZA
DTU, DELHI
(Co-Supervisor)

Department of Mechanical Engineering

DELHI TECHNOLOGICAL UNIVERSITY
(Formerly Delhi College of Engineering)
Shahbad Daulatpur, Main Bawana Road, Delhi- 110042, India

April, 2025

DELHI TECHNOLOGICAL UNIVERSITY
(Formerly Delhi College of Engineering)
Shahbad Daulatpur, Main Bawana Road, Delhi- 42

ACKNOWLEDGEMENTS

First and foremost, I want to express my gratitude to my supervisors, Dr. Mohammad Zunaid and Prof. Qasim Murtaza, for their valuable guidance, support, and encouragement throughout my Ph.D. program. This thesis could not have attained its present form without their supervision, direction, and interest in the research work. Their painstaking efforts, methodical approach, and individual help made it possible for me to complete this work on time.

I express my gratitude to Prof. Atul Kumar Agrawal, Chairman of DRC, and SRC members Prof. M. Emran Khan, Prof. Avdhesh Sharma, Prof. S. Ambu, and Prof. Amit Pal for providing valuable comments and suggestions. I am thankful to all faculty and staff members of the Mechanical, Production & Industrial, and Automobile Engineering Department for their continued valuable support. I appreciate reviewers of research papers and industry people for sparing their valuable time and constructive comments.

I wish to thank my parents, brothers, sisters, family members, and friends whose blessings made this work a reality. I want to sincerely thank my dear mother, Smt. Jamila, for her great role in my life and their numerous sacrifices. I sincerely thank my wife, Anjum Bano, for her patience, support, and loving participation in accomplishing this research work. I would also like to recognize the support and direction of my father, Shri. Sarfuddin. Last but not least, I am thankful to the almighty God for giving me the mental and physical strength to work sincerely, diligently, and honestly and for helping and guiding me during my life and throughout my studies.

MOHSIN KHAN

DELHI TECHNOLOGICAL UNIVERSITY
(Formerly Delhi College of Engineering)
Shahbad Daulatpur, Main Bawana Road, Delhi- 42

CANDIDATE'S DECLARATION

I, MOHSIN KHAN, hereby certify that the work which is being presented in the thesis entitled "**CFD Analysis of Cold Gas Dynamic Spray Coating under Different Conditions"** in partial fulfillment of the requirements for the award of the Degree of Doctors of Philosophy, submitted in the Department of Mechanical Engineering, Delhi Technological University is an authentic record of my own work carried out during the period from **2018** to **2024** under the supervision of **Dr. Mohammad Zunaid and Prof. Qasim Murtaza.**

The matter presented in the thesis has not been submitted by me for the award of any other degree from this or any other institute.

Candidate's Signature

DELHI TECHNOLOGICAL UNIVERSITY
(Formerly Delhi College of Engineering)
Shahbad Daulatpur, Main Bawana Road, Delhi- 42

CERTIFICATE BY THE SUPERVISOR(s)

Certified that **Mohsin Khan** (Roll No. 2K18/PhD/ME/15) has carried out their search work presented in this thesis entitled **"CFD Analysis of Cold Gas Dynamic Spray Coating under Different Conditions"** for the award of the degree of **Doctor of Philosophy** from Department of Mechanical Engineering, Delhi Technological University, Delhi under our supervision. The thesis embodies the results of original work, and studies are carried out by the student himself, and the contents of the thesis do not form the basis for the award of any other degree to the candidate or to anybody else from this or any other University/ Institution.

Signature

DR. MOHAMMAD ZUNAID
(Associate Professor)
Department of Mechanical, Production & Industrial and Automobile Engineering,
Delhi Technological University,
Delhi-110042,
INDIA

Signature

PROF. QASIM MURTAZA
(Professor)
Department of Mechanical, Production & Industrial and Automobile Engineering,
Delhi Technological University,
Delhi-110042,
INDIA

Date:

CFD ANALYSIS OF COLD GAS DYNAMIC SPRAY COATING UNDER DIFFERENT CONDITIONS

Mohsin Khan

ABSTRACT

The emerging and future cold spray (CS) coating technology has limitless opportunities and possibilities. Still, parameters like particle velocity, temperature, and flow dynamics lack precise control, which may improve the coating quality, performance, and long-lasting applications. Such limitations catalyzed the evolution of simulation work. The experimental measurement is often limited by cost, time, reproducibility, failure risks, and control over variables. Complementing them with computational methods like simulations can help overcome many drawbacks.

CFD Simulation is superior to the experimental methods due to its cost-effectiveness, greater control over variables, continuous monitoring, reproducibility, optimization, detailed data collection, faster results, etc. Therefore, the CFD Simulation used for CS process technology necessitates the optimization of multiple parameters to achieve optimal coating performance. According to the literature, the critical particle velocity for effective deposition in CS lies within the range of 400 - 585 m/s for particle sizes around 20 μm.

This study calculates the particle velocity at the nozzle exit, proximate to the substrate, for varying particle sizes and propellant gas compositions under conditions yielding extreme and least velocities. A two-dimensional axisymmetric convergent-divergent nozzle model was employed and initialized with specific parameters and boundary conditions. Commercially Pure (C.P.) Titanium was selected as the coating material, with an inlet temperature of 401 K, across particle sizes of 20 μm, 40 μm, 60 μm, 80 μm, and 100 μm. The material properties include a 4850 kg/m^3 density and a specific heat capacity of 544.25 J/kg-K.

To further understand the CS process, a numerical simulation was

conducted to examine the impact of varying pressure and gas mixtures on the pre-heat temperature and impact velocity of feedstock powder particles in the Cold Spraying coating process. The analysis discovered that the pressure of 7 MPa is most effective to achieve high-impact velocities. Pure helium gas was recognized as the most suitable for maximizing the impact velocity among the gas mixtures examined. In contrast, a mixture of 80% nitrogen (N_2) and 20% helium (He) generated the maximum pre-heat temperatures. Higher impact velocities enhance the coating properties by improving particle bonding strength and the quality of the first layer deposition, which are the main factors in the Cold Spraying process.

This analysis was carried out using computational fluid dynamics (CFD), an advanced method that gives similar results via simulation to experimental results. This work analyzed the impact of the powder particle shape and size on the impact velocity using CFD for the CS coating process. The geometry for simulation was modeled using SolidWorks, while the numerical analysis was carried out using ANSYS Fluent workbench. The numerical simulation uses optimal input parameters for cold spraying. The model used for analysis was a pressure-based, axisymmetric model that explains the flow dynamics in the CS nozzle. The model was the realizable k-ε turbulence model, known for its accuracy in representing the physics of high-velocity flows. Various powder particle sizes and varying stand-off distances were used to analyze using copper as the coating material to be coated on the steel substrate. The results show the spherical powder particles were the most reliable when sprayed with a 35 mm stand-off distance.

Moreover, this study observes the effect of injector length on impact velocity, particle temperature, and substrate surface temperature in the cold spraying process. A two-dimensional axisymmetric model was created in SolidWorks, and the computational analysis performed using ANSYS Fluent was used for the simulations. Titanium powder was coated on the steel substrate as the feedstock powder. This study examined the effect of different propelling gas mixtures on particle velocity and temperature. The results indicated that particle velocity was maximized with helium, an inert gas, and minimized with pure nitrogen. On the other hand, the particle and

substrate temperatures were highest when pure nitrogen was used under identical operating conditions. Based on the findings, the 15 mm injector length is optimal for attaining a balanced performance for velocity and temperature.

Finally, the study focused on how disparities in process parameters—such as pressure, temperature, material particle size, and velocity of the coating material powder, which was taken as titanium—affect the substrate surface temperature in the CS coating process. These findings contribute a unique viewpoint to CS technology. The geometry was simulated using a two-dimensional axisymmetric model, incorporating a k-ε turbulence model with a second-order implicit pressure-based solver. Our results show the substrate surface temperature was maximum when the injector length was 15 mm. It was also observed that the optimal nozzle barrel length corresponded to the particle injector length, suggesting a critical relationship between these components in achieving optimal coating performance.

As discussed above, the results highlight several critical parameters that significantly improve experimental outcomes, including the optimal injector length, stand-off distance, and the pre-heating of powder particles. Upon analyzing the particle size and shape with various pressure ranges, the research reveals critical insights for boosting performance. Moreover, selecting the most effective carrier gases or gas mixtures is crucial for achieving maximum temperatures and impact velocities. These simulations control parameters like particle velocity, temperature, and flow dynamics, improving the performance of CS coating.

Keywords: *CFD simulation, Cold spray, Nozzle, Injector, Gas Mixture, Impact velocity, Stand-off distance, Particle shape, Particle Size*

LIST OF PUBLICATIONS

Papers published in International Journals:

1. Khan, M., Zunaid, M. & Murtaza, Q. "Effect of Process Parameters on the Substrate Surface in Cold Spray Coating" published in "International Journal of Maritime Engineering, University of Buckingham Press," ICARI, VOL 1, ISSUE 1, CURRENT TRENDS IN RESEARCH AND INNOVATION, (2024), ISSN/E-ISSN: 1479-8751/1740-0716, pp. 1-9, https://doi.org/10.5750/ijme.v1i1.1330 **(SCIE).**

2. Khan, M., Zunaid, M. & Murtaza, Q. "Computational Simulation of Cold Spray Coating for Optimal Injector Length" published in "Case Studies in Thermal Engineering," Elsevier, Volume-51, (2023), ISSN: 2214-157X, pp. 1-7 https://doi.org/10.1016/j.csite.2023.103655 **(SCIE).**

Papers published in International/ National Conferences:

1. Khan, M., Zunaid, M. & Murtaza, Q. "CFD analysis of particle shape and size on impact velocity and effect of stand-off distance in the cold spray process" published in "LNME, SPRINGER NATURE, Book Title: Recent Trends in Mechanical Engineering, Subtitle: Proceedings of PRIME 2021," Chapter-11, (2023), pp.109-119. DOI: https://doi.org/10.1007/978-981-19-7709-1_11 **(Scopus Index Proceeding).**

2. Khan, M., Zunaid, M. & Murtaza, Q. "Simulation of cold spray coating for powder pre-heat and impact velocity" published in "Materials Today:

Proceedings," Volume 46, Part-20, (2021), pp. 10837-10844. **(Scopus Index Proceeding)**

3. Khan, M., Zunaid, M. & Murtaza, Q. "Examination of Titanium Powder with Different Particle Sizes for Velocity" published in "Materials Today: Proceedings," Volume III, Part-1, (2020), pp.383-387. **(Scopus Index Proceeding).**

TABLE OF CONTENTS

LIST OF TABLES

LIST OF FIGURES

NOMENCLATURE

A	Cross-section area of point in the pipe (m^2)
A_1	Cross-section area of the lower section of the pipe (m^2)
A_2	Cross-section area of the upper section of the pipe (m^2)
A_p	Surface area of particle (m^2)
$A_{.D.}$	Cross-sectional area of particles (m^2)
C_D	Drag Coefficient
f	Flow Rate (m^3/s)
$F_{.D.}$	Drag Force (N)
g	Gravitational Acceleration, (m/s^2)
K.E.	Kinetic energy (Joules, J)
m_1	Mass flux for the lower section pf pipe with cross-sectional area A_1, (kg)
m_2	Mass flux for the upper section of pipe with cross-sectional area A_2, (kg)
m	Mass, (kg)
P	Pressure, (Pa or N/m^2)
P.E.	Potential Energy, (Joules, J)
Q	Heat, (Joules, J)
R	Volume Flow Rate, (m^3/s)
t	Time, (s)
U	Internal Energy (Joules, J)

u	Velocity Vector, (m/s)
V_p	Volume of particle (m^3)
v_1	The velocity of the lower section of the flowing fluid in the pipe (m/s)
v_2	The velocity of the upper section of the flowing fluid in the pipe (m/s)
v	The average speed of the flowing fluid in the pipe (m/s)
V	Volume (m^3)
v_p	Particle velocity (m/s)
W	Work (Joules, J)
x_1	Distance covered by the flowing fluid in the lower section of the pipe (m)
x_2	Distance covered by the flowing fluid in the upper section of the pipe (m)

Subscripts

1	Lower end of the pipe
2	Upper end of the pipe
in	Inlet
out	Outlet
stored	Stored
p	Particle
D	Drag

Greek Symbols

ρ	Fluid density (kg/m³)
τ	Shear Stress / Stress tensor (Pa or N/m²)
μ	Absolute Viscosity of water (Ns/m^2)
$\dot{\gamma}$	Share Rate
ψ	Shape Factor
л	Pi

Abbreviations

2D	Two Dimensional
3D	Three Dimensional
HVOF	High-Velocity Oxy-Fuel
CGDS	Cold Gas Dynamic Spraying
DCSS	Dry Cast Storage System
CS	Cold Spray
SiC	Silicon Carbonate
AM	Additive Manufacturing
Ti	Titanium
TiO_2	Titania
Al	Aluminium
Cu	Copper
Zn	Zinc
Mg	Magnesium

H.A.	Hydroxyapatite
Ni	Nitride
U.V.	Ultraviolet
IMC	Indomethacin
A.D.	Aerosol Deposition
CFD	Computational Fluid Dynamics
CEL	Coupled-Eulerian Lagrangian
CV	Critical Velocity
JC	Johnson-Cook
K.E.	Kinetic Energy
T.E.	Thermal Energy
CAD	Computer-Aided Design
C-D	Convergent-Divergent
SF	Shape Factor
SPH	Smooth Particle Hydrodynamics
SIMPLE	Semi-Implicit Method for Pressure-Linked Equations
MUSCL	Monotonic Upstream-cantered Scheme for Conservation Laws

CHAPTER 1

INTRODUCTION

1.1 Introduction

The coating may be defined as the covering applied on an object's surface; here, the object is referred to as a substrate. The covering is applied to fulfill the purpose of decoration, function, or both. It may be on some parts or the whole surface of the substrate. To understand the above in simple words, we can say printing is the best example of coating, where one can observe it easily. Numerous examples of coating can be found in day-to-day life, starting from home utensils, decorative items, and industrial applications.

Generally, coatings have multipurpose uses and applications, like paints. Dual-usage coatings protect the substrate from rusting and decorate it using varying colors. Coatings applied for a particular function are termed functional coatings; they are known to change the substrate's surface properties, like corrosion resistance or wear resistance, wet-ability, adhesion, semiconductor device fabrication, etc. are some common functions of coatings. Most coating processes are applied by considering controlled coating thickness. To achieve the controlled thickness of the coating, various processes, like painting a wall, use a simple brush.

In the same way, special and expensive coating machines are used to coat various industrial instruments and electronic devices. In such coatings, several coating materials are used along with many coating techniques and parameters. Nozzles spray the coating material in industrial applications to get the required results. Coating materials may be wire powders with particle sizes up to nano-meters.

Some industrial applications require coating on a thin film substrate, like fabric, foil, film, paper, and many more. Some suitable techniques will be used in such applications. Coatings may be applied in any form, including solid, liquid, and gas.

1.2 Cold Spray Coating

It is alternatively recognized as supersonic particle deposition. Cold spray (CS) coating denotes a high-energy solid-state coating and powder consolidation procedure. In contrast to conventional thermal spraying methods like flame or plasma spraying, CS deposition does not require powder melting. In CS, solid powders, usually between 1 to 50 micrometers in diameter, are propelled by supersonic gas speeds up to 1200 m/s Dlouhy & Jan, [2018]. Upon impact on the substrate, the material particles undergo plastic deformation and adhere to the substrate surface. The kinetic energy (K.E.), sourced from gas expansion, transforms into plastic deformation energy during bonding.

The cold spraying inception dates back to the 1990s, originating from the research efforts of Russian scientists Dykhuizen & Smith, [1998]. Originally focused on particle erosion studies, scientists serendipitously discovered the rapid formation of coatings during their experiments. Subsequently, this technique underwent commercialization during the same period.

Cold Spraying offers versatility in depositing various materials, encompassing metals, polymers, ceramics, composite materials, nano-crystalline powders, and beyond. The primary bonding mechanism associated with the CS coating is attributed to “adiabatic shear instability.” Upon impact of spherical material particles traveling above the critical velocity with the substrate, a strong pressure field extends on both the material particle and substrate. This phenomenon triggers adiabatic shear instability, causing localized shear straining and material jetting. Consequently, material jetting induces viscous flow, with temperatures approaching the material’s melting point. The below Fig. 1.1 and Fig. 1.2 shows how the cold spraying process works and the conditions for it.

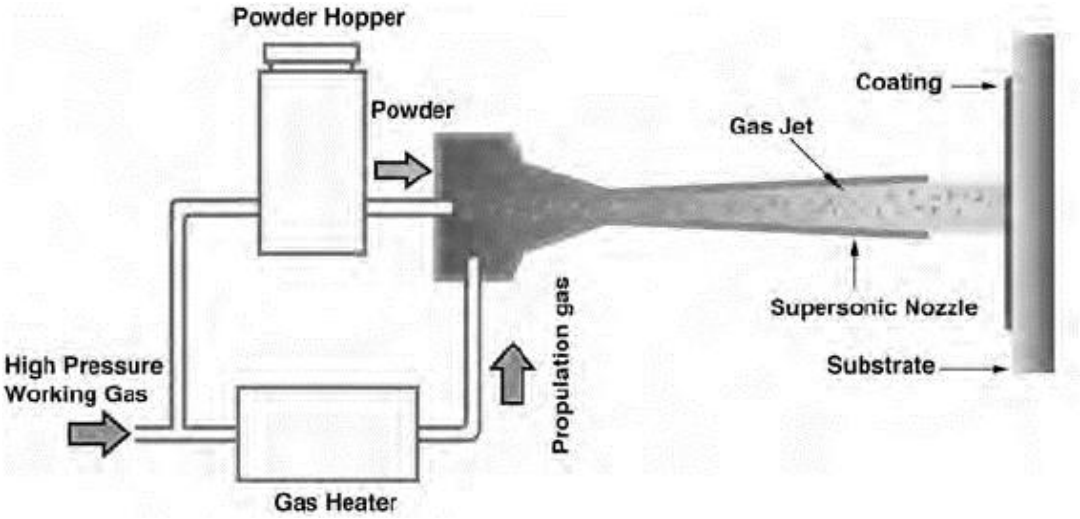

Figure 1.1 Cold Spraying with High-Pressure Working Gas

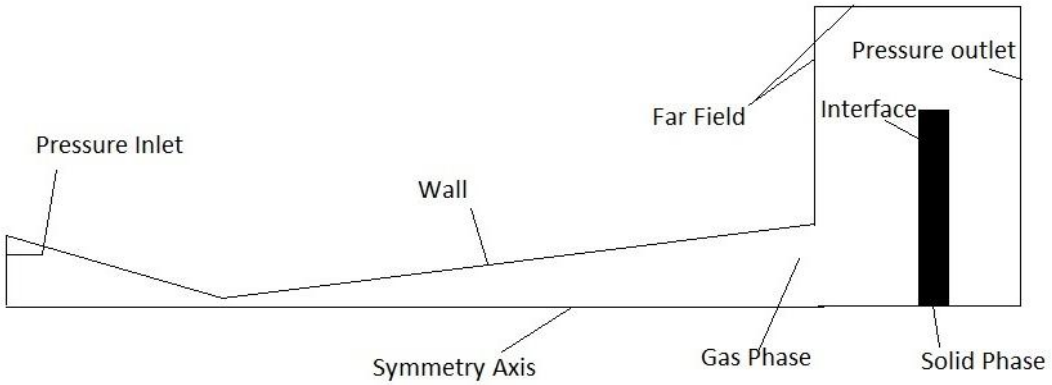

Figure 1.2 2D Spray Nozzle and Boundary Conditions for Cold Spray Coating.

CS coating boasts several advantages over other thermal spray techniques, including:

- High deposition efficiency
- High deposition rate
- Minimal or no masking is required
- Absence of grit blasting
- High coating density
- Versatility in substrate-coating selection
- Minimal thermal impact on the substrate
- High bond strength
- Generation of compressive residual stresses
- Ability to produce ultra-thick coatings
- Avoidance of phase changes
- Prevention of oxidation
- Inhibition of grain growth
- High thermal conductivity
- Enhanced corrosion resistance
- Elevated strength and hardness levels

However, despite its numerous advantages, cold Spraying does present some disadvantages, as elaborated below:

- Cold spraying coating has very little ductility in as-sprayed conditions, and mechanical properties compared to bulk values can only be acquired by post-spray heat treatment.

- Spraying composites using Cold Spraying is possible, but some work hardening alloys and pure ceramics can’t be processed.
- In the cold spraying method, a minimum ductility of the substrate is required to bond with powder particles. Due to this, limited bond strength has been shown on ceramic substrates.
- Till now, high-quality coatings can be achieved using helium gas only to achieve the required velocity for particle deposition.
- Coating on complex geometries or internal surfaces is difficult as this process is also a line-of-sight process like other thermal processes.

The superiority of cold spraying technology over the HVOF technique lies in its solid-state nature, which yields distinct results and coating properties. However, a disadvantage arises from plastic deformation, impacting the ductility of the coating.

Conversely, in thermal spray coating techniques, various forms of energy, such as mechanical, thermal, electrical, or chemical, are employed to generate high-temperature, high-velocity gas jets. The elevated temperatures melt the powder particles, forming splats upon the substrate. This process enhances the bonding mechanism between the substrate and the coating material, improving coating adhesion.

1.3 Classification

CS coating deposits a coating material on a substrate at moderately low temperatures, typically under the coating material's melting point. The classification of CS coating can be based on various factors, including process parameters, coating thickness, alloy-specific, and hybrid.

1.3.1 Process Parameters

1. Cold Spray (Low-Pressure): Involves using lower gas pressures for coating deposition.
2. Cold Spray (High-Pressure): Involves using higher gas pressures for coating deposition.
3. Cold Spray (Supersonic): Exploits supersonic speeds of the sprayed particles for coating deposition.

1.3.2 Coating Thickness

1. Thin-Film Cold Spray Coating: The deposition thickness is thin in this type of coating; therefore, it is called thin film coating.
2. Thick-Film Cold Spray Coating: The deposition thickness is thick in this coating; therefore, it is called thick film coating.

1.3.3 Alloy-Specific

1. Aluminium Cold Spray Coating: This coating focuses on aluminum particle involvement; therefore, such coating is known as Aluminium coating.
2. Titanium Cold Spray Coating: This type of coating focuses on titanium particle involvement; therefore, this type of coating is called titanium coating.

1.3.4 Hybrid

Metal-Ceramic Hybrid Cold Spray Coating: The combination of metal and ceramic particles is used to get enhanced properties.

The above classifications help to understand the variety of CS coatings and make it easy to select appropriate materials and process parameters based on particular requirements.

1.4 Applications

CS coating has many applications across several industries due to its capability to deposit materials at low temperatures without affecting the thermal impairment of the substrate material. Some distinguished applications of CS coating include:

1.4.1 Aerospace Industry

Corrosion Protection: CS coatings, usually made of aluminum or zinc, are used to coat aircraft components due to their corrosion resistance properties without negotiating the physical properties of the components.

Repair of Damaged Parts: CS coating technology is used to repair damaged or worn-out aerospace components, reducing the time consumption of making new components and maintenance costs.

1.4.2 Automotive Industry

Wear Resistance: CS coatings, typically made of metals like nickel or aluminum, are applied to critical automotive parts, such as engine cylinders and pistons, to improve wear resistance and extend the lifespan of such parts.

Corrosion Protection: CS coatings protect unprotected automotive parts from corrosion, especially in regions with strict weather conditions.

1.4.3 Electronics and Electrical Industry

Conductive Coatings: A thin layer can be deposited using CS Coating technology and conductive material powder. Conductive coatings can be made on

electronic components, and such coatings improve the electrical conductivity and performance of electrical and electronic components.

Thermal Management: CS coatings with higher thermal properties help proficiently dissipate heat and make the components more valuable for electrical and electronic devices where heat management is crucial.

1.4.4 Oil and Gas Industry

Corrosion Resistance: CS coatings are applied to oil and gas equipment, such as pipelines, joints, valves, etc., to provide corrosion resistance and enhance the service life of critical components, especially in the offshore atmosphere.

1.4.5 Medical Devices

Biocompatible Coatings: CS finds extensive application in the deposition of biocompatible coatings on medical implants; this confirms compatibility with the human body, mitigating the risk of rejection or contrary responses.

1.4.6 Military and Defense

Wear and Erosion Resistance: CS coatings are used on military equipment to enhance wear and erosion resistance, providing protection in harsh environments and extending the operational life of components.

1.4.7 Power Generation

Corrosion and Erosion Protection: Mainly in the area of power generation, the CS coating is applied to the components of power plants, like turbine blades, boiler tubes, etc., to protect them against corrosion and erosion, which also helps in improving efficiency and further leads to a reduction in maintenance needs and cost.

1.4.8 Tooling and Manufacturing

Wear-Resistant Coatings: CS deposits wear-resistant coatings on cutting tools, molds, and dies in manufacturing processes, improving tool life and reducing downtime for replacements.

1.4.9 Marine Industry

Corrosion Protection: In an industry like marine, CS coatings are used on components, like ship hulls, offshore structures, and many other components, to protect against corrosion in saltwater surroundings.

1.4.10 Infrastructure and Construction Industry

Corrosion Prevention: In construction and infrastructure, the CS coating is used for structural components, bridges, pipelines, etc., to prevent the components from corrosion, which extends the lifespan of the overall infrastructure.

1.4.11 Mining Industry

In the mining industry, the CS coatings are mainly utilized to provide wear protection for equipment exposed to abrasive conditions, such as drill bits, conveyor systems, etc.

1.4.12 Sports and Recreation Equipment

The CS coatings are applied to many sports equipment, including bicycle frames, golf clubs, etc., to improve the equipment's durability and enhance the wear resistance.

As we can see from the above industry-based applications, each component with a specific choice of coating material, process parameters, coating thickness, etc., is made to meet the industry’s norms, unique requirements, and the coated components’ planned function. The usefulness of CS technology makes it a valuable tool across diverse sectors for extending the life of different components with enhanced material properties.

CHAPTER 2

LITERATURE REVIEW

2.1 Introduction

This chapter explains the wide-ranging information about CS coating technology, encompassing various materials, different gases, and the mixtures used in the processes. It reviews numerous research papers on CS coating technology, providing insights and implications for further understanding and development.

Progressing CS coating process technology requires attractive coating quality, which can be achieved by increasing the impact velocity. Impact velocity can also be improved by using diverse propelling gases and changing the pressure conditions. Various models enhance bonding strength, deposition efficiency, and porosity control, which accurately evaluate particle velocity, deposition, and bonding, providing valuable insights for CS coating analysis.

The CS coating method represents a modern approach that minimally alters the coated material characteristics. The CS coating method has recently emerged as a significant area for research within coating technology. Generally, the properties of CS coatings are determined via experimental analysis. Still, numerical

analysis is an advanced technique because it can generate results that are meticulously aligned with experimental results. This study examines the optimal length for the particle injector, aiming to attain the most suitable substrate temperature throughout the coating process. The analysis of the injector length for particle impact velocity and temperature was carried out using numerical simulation under various states for cold sprays, like pressure, temperature, particle size, and particle speed for varying injector lengths.

2.2 Review

2.2.1 Experimental Work on Cold Spray

Cold spraying shows versatility across large temperature ranges, simplifying the observations for various phenomena such as re-crystallization, shear band formation, deformation, annealing, and the presence of sub-micron and nano-meter size grains through microstructural investigation Liu et al., [2020]. Chen et al., [2020] designed CS coatings in which various materials and high-pressure propelling gases are combined to simplify solid-state CS coating across a variety of powder size ranges and properties. Materials like SiC are used in the CS coating process because they are resistant to corrosion well and can withstand high temperatures in power generation, petrochemicals, mining, and other industries.

Barton et al., [2020] investigated the possibility of using larger grain sizes in the coating process without significantly increasing the substrate temperature or reducing the coating's hardness. This strategy improves the coating's performance and the coated material's overall performance.

Chen et al., [2020] designed CS coatings with high-pressure propelled gas and various materials to simplify solid-state cold spray coating across a spectrum of powder size ranges and properties. The CS coating process allows materials like SiC to be coated, which offers excellent corrosion resistance properties appropriate for high-temperature atmospheres in power generation, petrochemicals, mining, and more industries.

Barton et al., [2020] suggest raising the temperature of the substrate so that larger grain sizes can be used in the coating process without lowering the coating's hardness. This strategy not only improves the efficiency of the coating but also leads to notable improvements in the overall performance of the coated material.

Cetiner et al., [2020] found that integrating more than 5 wt.% of zinc into titanium feedstock powder in the CS deposition process results in asymmetrical coating and cavities on the coated surface. However, under dry sliding conditions, a zinc content of up to 5% lowers the coefficient of friction and increases wear resistance.

Using a Doehlert shell design, Lapushkina et al., [2020], determined that a temperature of 320°C and a pressure of 2.5 MPa, which represent high temperature and low pressure, were the ideal parameters for corrosion protection in Zn CS coatings. The coatings were categorized as heterogeneous or homogeneous, with varying densities based on temperature and pressure. The coating was found homogeneous and dense under conditions of 320°C and 2.5 MPa, providing the highest corrosion resistance properties.

2.2.2 Simulation Work on Cold Spray

Several methods can be used to simulate the CS process. It has been found that very little work has been done in the field of CS coating. As per the findings and challenges found in the previous research, the deformation of particles, strain rate, and temperature depend on the impact velocity of material particles. Most of the latest research has been reviewed, and the researchers' findings are discussed below.

S. Kumar et al., [2015] investigated the optimal nozzle injector length without a barrel and determined that 20 mm yielded the best results. Optimizing the injector length is crucial to achieving the desired particle velocity, particle temperature, and substrate temperature. Using Computational Fluid Dynamics

(CFD) simulations under several conditions for cold spraying, they assessed these parameters with the nozzle and substrate placed 35 mm apart in a horizontal setup.

Faizan-Ur-Rab et al. [2016] used a three-dimensional model to simulate the particle flight and stand-off distance for particle impact on the substrate from the spray nozzle. The model revealed that particle impacts against the nozzle wall led to an asymmetric coating zone influenced by particle size. As per the simulation results, the larger feedstock particles achieved higher temperatures than smaller ones and exhibited minor acceleration outside the nozzle. The results also highlight the improvement in deposition efficiency when the feedstock powder was pre-heated before impact.

Caruso et al., [2018] developed analytical solutions for evaluating Cold Spray (CS) process technology, employing both 2D and 3D modeling approaches. Their findings demonstrated that 3D models offer superior accuracy in simulating particle behavior and predicting coating outcomes compared to 2D models. The enhanced precision of 3D models allows for more detailed analysis of particle dynamics, impact patterns, and resultant coating characteristics, making them a valuable tool for optimizing CS processes in complex applications. This advancement supports better control over coating quality and process efficiency, offering insights critical for industries that rely on precise and durable coatings.

P. Zhao et al., [2020] examined, by employing molecular dynamics simulation, the crystal orientation of material particles on the substrate material

surface can be determined. It has been observed that particles at the bottom edge exhibit shapes such as square, rectangle, and hexagon.

Oyinbo et al., [2020] numerically examined the asymmetric deformation of particles using the molecular dynamic simulation at the coating interface, a phenomenon commonly observed during cold gas spray processes.

Jami & Jabbarzadeh, [2020] numerically analyzed the aerosol deposition (A.D.) technique, which represents a specific kind of cold spray (CS) coating process technique. Within this method, the formation and bonding of ceramic coatings are investigated through a combination of practical experimentation and Computational Fluid Dynamics (CFD) simulations.

Lupo et al., [2020] highlighted several factors influencing simulations for large samples, including density, transport variables, temperature non-uniformity, non-rigid rotation, deformation, and the non-instantaneous relaxation of fluids. They also noted that boundary condition challenges can lead to gas and vapor saturation, posing limitations in flow simulations.

Chakrabarty & Song, [2020]b conducted a numerical study on ceramic deposition in CS coating technology, analyzing deposition behavior across various substrate materials. Their findings indicate that crater depth is critical to effective ceramic retention. For soft substrates, significant deformation and depression formation occur, especially under high-velocity conditions, which impact ceramic

deposition. Uniform ceramic layers are achieved without jetting at crater edges, whereas jetting introduces highly localized plastic deformation, causing fragmentation and loss of ceramic material. Due to limited substrate thermal softening, ceramic retention is generally better for hard substrates, with minimal deformation and crater formation. Additionally, substrate roughness influences jetting; increased roughness moderates the jet effect, resulting in deeper depressions. However, crater formation on hard metal substrates is minimal, making them more suitable for ceramic retention without deformation.

Khan et al., [2020], [2021], and [2023]b proposed the CS coating process, which depends on three core parameters: (i) the pressure, (ii) the temperature mainly at the nozzle and particle inlet, and (iii) the stand-off distance from the substrate. The temperature can be controlled by pre-heating the substrate or heating the air at the nozzle inlet.

2.2.3 Critical Velocity of Cold Gas Spraying

In the cold spraying technique, bonding relies heavily on critical velocity, although various parameters can influence it. Nonetheless, the critical velocity is a representative parameter crucial for quality verification in cold spraying applications. Beyond the critical velocity, increased impact velocity leads to improved coating quality and enhanced critical velocity. Critical velocity, the impact velocity at which particles bond with the substrate, is challenging to determine through exploratory analysis but can be efficiently and accurately

calculated through numerical methods. Critical velocity depends on particle size, impact angle, pre-heat temperature, and material type.

Hemeda et al., [2020] calibrated the critical velocity; increased impact velocity leads to improved coating quality and enhanced critical velocity. However, the presence of oxide species has an adverse effect, diminishing particle jetting and flattening.

Ghelichi et al., [2011] examined the cold spraying technique; the critical velocity typically falls within the range of 400-585 m/s for particles sized at 20 μm. Bonding in this process relies heavily on the critical velocity, although various parameters can influence it. Nonetheless, the critical velocity is a representative parameter crucial for quality verification in cold spraying applications.

Takana et al., [2008] highlighted that achieving optimal CS coating requires carefully controlling particle velocity, size, and electrostatic forces. They emphasized that the coating process cannot exceed a critical velocity threshold unless specific parameters—such as particle size and applied electrostatic forces—are managed. These factors directly influence the coating thickness and uniformity, regulating the particle dynamics upon impact. By maintaining controlled conditions, including particle speed and size, the CS process can produce consistent and high-quality coatings, essential for applications demanding precise layer thickness and reliable material properties.

Goyal et al., [2012]; Lupoi et al., [2020] and Maledi et al., [2017] identified the primary parameters affecting the CS coating process: pressure, stand-off distance from the substrate, and temperature. The temperature may involve pre-heating the substrate or the air at the nozzle inlet. Critical velocity should not exceed particle velocity to achieve optimal coating, making pressure and temperature crucial factors. Various techniques can be employed to define optimal spraying parameters.

Fardan et al., [2021] used numerical methods to compute critical velocity, residual stresses, and deformation mechanisms, employing advanced techniques like molecular dynamics and Lagrangian-Eulerian models to provide precise predictions.

W. Y. Li et al., [2014] and [2016] highlighted the importance of impact velocity in achieving particle-substrate bonding, noting that higher impact velocities, such as 290 m/s for copper, are necessary for plastic deformation. This velocity is defined as the critical velocity for copper and has been validated through research. Jetting continues at velocities up to 400 m/s, marking the deposition range for copper between 290 m/s and 400 m/s, after which jetting ceases, as shown in simulations. Studies also reveal that increased impact velocity enhances jetting quality, crater size, and plastic deformation. Deposition efficiency improves with higher pre-heat temperatures for both substrate and particles, essential in CS

coating, which applies material layers at high speed without melting or oxidizing the particles.

Jiang et al., [2020] explored the CS process, also known as cold gas dynamic spraying (CGDS) or solid-state coating, which preserves particle properties and has expanded into additive manufacturing (AM). The choice of material is most important, and the biocompatible materials are very few. Therefore, opting for a bio-compatible material and carrier gas gives the best possible coating results. CS technology has proven effective for repairing damage in hydropower machinery from issues like cavitation.

Yeom et al., [2020] demonstrated that CS coating technology effectively maintains and protects nuclear fuel containers, particularly within Dry Cask Storage Systems (DCSS). This application is crucial for mitigating issues such as stress corrosion cracking and enhancing the integrity of fusion-welded regions, thereby extending the service life and ensuring the safety of these critical storage systems.

Yeom & Sridharan, [2021] highlighted that the CS coating method is especially advantageous due to its low heat input, which prevents phase transformation of the feedstock powder material and eliminates oxidation during the process. This characteristic ensures minimal phase changes occur, allowing for a high-quality, stable deposition that maintains the integrity of the original material properties throughout the application. Recent advancements in Cold Spray (CS)

technology have expanded its applications to light water reactors, nuclear fuel cladding tubes, nuclear energy systems, and many other sectors, particularly where corrosion resistance is critical, such as in nuclear fuel storage and reactor components.

This enhanced approach in CS technology is promising for corrosion resistance and improving the durability of components in high-stress environments like nuclear energy systems.

2.2.4 Process Parameters and Coating materials

Lin et al., [2019]; Oviedo & Valarezo, [2020]; Shayegan et al., [2014] and Yildirim et al., [2011] conducted studies demonstrating that impact velocity is a critical factor influencing residual stresses in Cold Spray (CS) technology. They also found that pre-heat temperature alters these residual stresses, impacting the overall coating quality.

Faizan-Ur-Rab et al., [2016] and Fallah et al., [2020] observed that the ideal impact velocity for deposition ranges between 500 m/s and 700 m/s, with optimal results seen when using particles approximately 20 Å in size and an impact angle of 90 degrees. They noted that particle size significantly affects how well the material adheres to the substrate surface, with adhesion largely driven by plastic

strain. This strain induces plastic flow due to thermal softening, allowing for effective bonding between the particles and the substrate.

Tortuero et al., [2020] investigated the relationship between impact velocity and material wear, finding that wear rate increases proportionally with impact velocity, regardless of the impingement angle. This finding underscores the importance of controlling impact parameters to manage coating longevity and minimize substrate wear.

X. Xie, Ma, et al., [2020] research on aluminum matrix composites revealed that the uniform dispersion of nano-sized TiB_2 particles within the matrix resulted in composites that were dense, crack-free, and highly durable. The study found that higher particle impact velocities increased particle deformation, grain refinement, tensile strength, and elongation, especially at elevated temperatures. These properties highlight the potential of Cold Spray in fabricating strong, resilient coatings and composites suitable for demanding applications.

Jia et al., [2020] studied the recent results, showing that splats' development mechanism occurs through the impact of the material droplet, followed by spreading and solidification. This process also occurs within textured grooves, where the wall temperature of the grooves plays a crucial role. It indicates that velocity or impact velocity significantly influences the CS coating process.

Khan et al., [2020] enhanced the working parameters of the Cold Spraying process technology through a CFD model, focusing on impact velocity by altering propelling gases and pre-heating particle temperatures. Titanium powder was selected due to its industrial demand and applications. Various input parameters were examined to study the powder particles' pre-heat temperature and impact velocity before substrate impact. Pre-heating the powder particles can improve deposition on the first layer. The maximum particle velocity was observed with pure nitrogen compared to oxygen. A particle size of 40 µm yielded a higher impact velocity than sizes of 20 µm, 60 µm, 80 µm, and 100 µm.

Khan et al., [2021], and [2023]b investigated the effect of pre-heat and impact velocity depending on the propelling gas type used in cold Spraying, as noted in the simulation results with helium gas. The pre-heat temperature improves at a low amount of helium, and with a high amount, the impact velocity. The particle size plays a vital role in enhancing velocity and temperature; with a large diameter of feedstock powder, the velocity and temperature are higher than smaller diameter particles.

Oyinbo & Jen, [2020] investigated the CS deposition process, concluding that the characteristics of the powder material particles, rather than the substrate material, predominantly influence deposition quality and deformation. Their research suggests that optimizing powder particle properties is key to

enhancing the efficiency of the CS process, with minimal impact from the substrate material itself.

X. Wang et al., [2020] explored the reinforcement potential of novel graphene (G) particles within the CS process. Their findings demonstrated that graphene-reinforced coatings exhibit enhanced plastic deformation and a more compact structure than those formed with pure metal particles. Moreover, the graphene-reinforced coatings showed superior corrosion resistance and a stronger re-passivation capacity, making them highly resilient in challenging environments. This study underscores the potential of graphene as a reinforcement in CS technology, offering benefits in structural integrity and durability that exceed those of traditional metal-based coatings.

Fallah et al., [2020] investigated using CS techniques to metalize polymeric materials, enhancing their electrical conductivity. This approach shows promise for developing conductive polymer surfaces, broadening the application potential of CS in electronics and other fields requiring conductive surfaces on non-metallic substrates.

Baidoo et al., [2020] applied machine learning methods to analyze particle behavior in CS technology, specifically identifying whether particles adhere to or bounce off the substrate during the spraying process. This innovative use of machine learning contributes valuable insights for optimizing CS parameters to improve deposition efficiency and coating quality.

Raoelison et al., [2020] noted that the temperature of coating material powders in Cold Spray additive manufacturing (AM) varies inconsistently during application. This temperature inconsistency may affect coating quality, suggesting the need for precise control of thermal conditions to ensure uniform coating properties.

Qin et al., [2020] examined the feasibility of using CS for ceramic coatings, noting that while CS can effectively deposit ceramics, it struggles on substrates with oxidized surfaces. The impact dynamics of metal particles in CS interfere with oxide adherence, limiting its success on oxidized materials.

Huang et al., [2014] observed that powder particles often collide with nozzle walls during the CS process, which reduces the nozzle's lifespan. This insight underscores the need for improved nozzle design or materials that can withstand the impact of high-velocity particles to enhance equipment durability.

Bhowmik et al., [2020] evaluated CS coating's effectiveness, finding that post-heat treatments can significantly improve the coating quality. The study indicated that increased post-treatment temperatures directly correlate with improved stress relief, enhancing coating durability and mechanical properties.

Sun et al., [2020] explored the formation of amorphous and nano-crystalline structures using CS. They found that pre-heating temperature inversely

affects the amorphous content, with lower temperatures favoring amorphous structure formation. This study offers insights into controlling the microstructure of CS coatings through temperature adjustments.

Bernard et al., [2020] discussed how coating formation in CS is influenced not only by gas pressure and temperature but also by nozzle design, including its length and inner shape. This effect is particularly notable with polymeric particles, which are sensitive to strain rate and temperature and impact coating quality and consistency.

Song et al., [2018] observed that particles with higher impact velocities in CS create high compressive stress parallel to the particle-substrate interface. This finding is important for applications where compressive stress contributes to coating adhesion strength and durability.

Yin et al., [2011] examined that, in Cold Spraying (CS) coatings, substrates can attain high surface temperatures and exhibit a significant temperature gradient, particularly in materials with lower thermal conductivity, which may contribute to generating residual stress. In CS coating technology, consistently pre-heating plays a crucial role in particle bonding and primary layer deposition, as shown by numerical and experimental studies on substrate pre-heating across various substrate materials. The Ti substrate exhibited the highest temperature gradient and surface temperature in the central region, likely generating residual stress. Starting from Steel, followed by Al and Cu, the order reversed in surface

gradient and heat flux. Cu had the highest surface heat transfer rate among the substrates, with the impact surface showing the most significant heat transfer compared to other materials. After Cu, Al, Steel, and Ti substrates were found in descending order of heat transfer rates.

Xu et al., [2020] demonstrated that post-heat treatment of Cold Spray (CS) coatings significantly enhances the microstructure by promoting re-crystallization and reducing dislocation density in particles near grain boundaries. Their research also found that internal oxidation of oxides within the coating increases proportionally with temperature, indicating that careful thermal management is essential to balance structural improvements and oxidation control in post-treated CS coatings.

A. S. Kumar et al., [2018] analyzed the surface roughness of sintered alumina, concluding that it is smoother compared to regular, unsintered alumina. This finding suggests that sintering can improve surface quality, potentially enhancing alumina's performance in applications requiring a fine, smooth finish, such as wear-resistant coatings and high-durability surfaces.

S. M. Hussain, [2022]b, and [2022]a studied the iron-based amorphous or nano-crystalline composite coatings exhibit significantly superior corrosion resistance properties compared to galvanized steel. Additionally, these coatings provide enhanced corrosion resistance and increased microhardness when applied to steel substrates, improving protective performance. Hassani-Gangaraj et al.

suggest that while adiabatic shear instability is prevalent, a hydrodynamic jetting mechanism might occur instead of an adiabatic process.

Singhal et al., [2018] found that the realizable k-ε model is a highly practical and robust two-equation turbulence model, making it an effective choice for simulating fluid dynamics in CS processes. This model's realism in capturing turbulent behavior contributes to more accurate predictions of particle flow and impact behavior in CS simulations.

Bagherifard et al., [2020] studied the deposition characteristics of Cold Spray coatings made from mixed powders, highlighting that this approach enables precise control over the phase volume fraction within the coating. They observed that powder deformability, particle shape irregularity, and oxide film presence significantly influence the final coating's residual stresses and porosity levels. Their work emphasizes the value of CS technology in fabricating bimodal materials with varied microstructures, broadening the scope for creating coatings with tailored properties for specific industrial applications.

Srikanth et al., [2019] observed that Cold Spraying (CS) coating technology is an advanced and highly effective deposition process due to its unique features. With a lower operating temperature than other coating techniques, this technology demonstrates high deposition efficiency and strong bonding between the substrate and particles. After deposition, the mechanical properties and

microstructure of the feedstock powder remain unchanged. CS also offers no oxidation, minimal porosity, and broad applicability across various materials, including ceramics, compounds, metals, and polymers.

Yeom & Sridharan, [2021] The study identified various constraints within the CS coating process that, when addressed, enhance the required functions. These constraints may disrupt the efficiency and the properties of the coating. However, improved coating efficiency, properties, and microstructure can be achieved with careful control of parameters such as gas temperature, pre-heating temperature, number of passes, particle morphology and size, substrate, powder material hardness, choice of propellant gas, and substrate roughness. Selecting coating materials is crucial for specific applications. An additional coating layer can protect nuclear power plant components exposed to extreme radiation, corrosion, and high temperatures. The nuclear industry has requirements, such as high throughput, transportability, and specific process temperatures, that are well-suited to the CS process. Additionally, the choice of feedstock powder material should be cost-effective for specific applications, and selecting the right propellant gas is also an essential consideration.

Da Silva et al., [2017] conducted an in-depth study on the effectiveness of Cold Spray (CS) technology across various applications, particularly for enhancing performance and facilitating repairs. Their research affirmed CS as a preferred technique due to its ability to extend the lifespan of both simple and complex components, reducing the need for part replacements. By providing

durable coatings and repairs without compromising the material integrity, CS contributes significantly to improving component longevity, thus lowering maintenance costs and downtime in applications that demand high durability. This study highlights the practicality and economic advantages of CS in industries where part longevity and minimal replacements are essential.

Nutt & Champagne, [2017] explored the versatility of Cold Spray (CS) coating technology, demonstrating its applicability to various materials, including metals such as aluminum and aluminum alloys. They emphasized that CS-coated materials, particularly in aeronautics, benefit from low oxidation rates, making them ideal for protective shielding in environments where corrosion resistance is crucial.

Koivuluoto et al., [2007] proposed using CS to coat fragments and components in nuclear power plants with cobalt and nickel alloys. This technique is particularly beneficial for maintaining and preserving nuclear systems, as the CS process supports the integrity and longevity of critical parts exposed to extreme conditions. These studies underscore CS technology's significance in enhancing durability and corrosion resistance across diverse, high-demand applications, from aeronautics to nuclear energy.

Khalkhali & Schmidt, [2017] found polyethylene and polyamides have been identified as excellent candidates for coating applications via the CS process.

These coatings have demonstrated remarkable effectiveness in shielding against corrosion.

Diab et al., [2017] investigated cold-sprayed aluminum coatings, which exhibit strong adhesion, low porosity, and improved corrosion resistance on substrates. However, pure aluminum coating material's low ultimate tensile strength leads to crack development, initiating localized corrosion and creating stress concentration sites. The fatigue life of both coated and non-coated materials decreases in corrosive environments compared to air. Cracks, pits, and ruptures in the oxide film at crack tips form due to the plasticity around the crack tips during the CS coating process.

Daroonparvar et al., [2020] observed that wear rates can be significantly reduced by applying a denser, double-layered coating of high-hardness materials. A notable improvement in corrosion resistance was found in coated Mg substrates. Applying a Ti layer on an Al-coated AZ31B Mg alloy substrate enhances hardness, protective efficiency, and electrolytic isolation while reducing pit formation and other localized corrosion issues. The electrochemical reaction rate at the electrode/electrolyte interface was measured to last about 48 hours, indicating a high protection rate.

Yao et al., [2020] developed a dual-layer CS coating that improves corrosion resistance and bioactivity on a degradable magnesium (Mg) alloy substrate. By incorporating layers of pure zinc (Zn) and hydroxyapatite (HA), the

coating offers protection and promotes bioactivity, making it ideal for biomedical applications.

X. Xie, Hosni, et al., [2020] studied the relationship between CS coating temperature and corrosion resistance, finding that higher temperatures reduce corrosion resistance. However, they also observed that elevated temperatures contribute to grain and precipitate growth within the coating, which may benefit certain structural characteristics.

Wu, Zhang, et al., [2020] investigated the addition of graphene to CS coatings, observing that graphene decreases the self-corrosion potential while enhancing the electrochemical potential difference between the coating and steel substrate. This adjustment improves the protective qualities of the coating, making it more effective in preventing corrosion in steel components.

Bai et al., [2017] found the utilization of CS to apply a Zn-Ni composite coating containing ten wt. % Ni has been found to offer superior corrosion protection for low-carbon steel substrates.

C. Xie et al., [2019] reported that coating pure zinc (Zn) improved the material corrosion potential and current density. The pure Zn coating did not introduce phase changes, oxidation, pore formation, or cracking. The cold-spray process used for applying the pure Zn resulted in a dense, uniform coating, with the density being influenced by the gas type, pressure, and temperature. Higher gas

pressures and temperatures produced even denser coatings, demonstrating the importance of optimizing these parameters to enhance coating quality.

Siddique et al., [2020] calibrated heat-treated and as-sprayed aluminum (Al) coatings on bulk Al substrates, finding that heat-treated Al coatings exhibited significantly improved anti-corrosion performance, enhancing substrate corrosion resistance by a factor of ten. Although as-sprayed Al coatings can also provide corrosion resistance, they result in lower wear resistance for the substrate. Applying heat treatment to as-sprayed Al coatings on magnesium (Mg) substrates for short durations at low temperatures densifies the microstructure and strengthens bonding by reducing interparticle boundaries, thereby improving wear resistance in Mg substrates.

K. Wang et al., [2020] conducted a comparative study of Zn-Al-Mg-TiO_2 and Zn-Al coatings. They found that the Zn-Al coating exhibited superior wear resistance and lower corrosion current density than the Zn-Al-Mg-TiO_2 coating, indicating better durability and corrosion protection. Additionally, the Zn-Al-Mg-TiO_2 coating showed an abrasive wear mechanism, while the Zn-Al coating demonstrated enhanced wear properties overall. In UV-rich solutions, the Zn-Al coating remained stable without degrading methyl blue, whereas the Zn-Al-Mg-TiO_2 coating quickly degraded the dye, highlighting its distinct reactivity under UV exposure.

Maledi et al., [2017] and Srikanth et al., [2019] observed the CS coating technique is a modern process that applies a material layer on a surface with low-temperature and high-velocity particles. The CS coating process has many benefits over other spray coating practices, such as avoiding thermal degradation and oxidation of the materials. Therefore, its importance has grown significantly over the decades.

Maledi et al., [2017] investigated coatings applied at high temperatures and pressures. They found that a specific particle velocity is required to enhance the mechanical bonding on substrate-coating. This velocity, achieved through plastic deformation and flattening of particles, results in increased coating hardness as temperature rises. However, higher temperatures also lead to material softening and a subsequent decrease in hardness. Pressure also affects coating microhardness, whereas increasing the stand-off distance reduces coating thickness and microhardness. Generally, high hardness is achieved at low pressures and high temperatures, with residual stress shown to be directly proportional to the stand-off distance. Additionally, increased temperature and pressure were found to lower residual stresses.

Schmidt et al., [2017] observed that particle bonding in CS technology is more effective with particles smaller than 10μm than larger particles. These findings suggest that finer particles promote stronger adhesion, likely due to greater surface area interaction, enhancing overall coating integrity.

Song et al., [2020] investigated the effect of substrate temperature on interface bonding and porosity control in coatings. They observed that porosity significantly decreases with increased particle velocity and substrate temperature. On the other hand, powder particles can be pre-heated to achieve higher porosity levels while keeping particle velocity constant, consenting for precise control over coating characteristics.

Suo et al., [2013] observed that the nozzle plays a significant role in powder particle dispersal during the CS process. Increasing the nozzle exit diameter results in particles broadening and flattening in the transverse direction. Conversely, reducing the nozzle exit diameter leads to sharper particles. Additionally, enlarging the throat size decreases the mean particle velocity, while increasing the injector size affects only the mean particle velocity.

Rizzo et al., [2013] designed a single-layered TiAlN coating, noting its cubic structure and inherent brittleness. In contrast, their development of a TiAlN/AlN-n multilayer coating demonstrated improved wear resistance, smoother surface finish, and increased hardness compared to the single-layer configuration, highlighting the advantages of a multilayered approach for durability and performance.

Liang et al., [2016] examined coating deposition using a cold-spray (CS) technique with a pre-heated substrate, achieving a 30% improvement in bonding strength. They also found that diffusion annealing did not enhance

bonding, indicating that substrate pre-heating is more beneficial than annealing for bonding quality in cold-spray coatings.

Z. po Zhao et al., [2018] explored hybrid nanostructures formed through chemical reactions and inter-diffusion between two materials (e.g., Cu and Zn) at the interface. The study reported forming an amorphous phase and intermetallic compounds (IMCs), effectively restricting boundary movement due to the high-velocity impact during deposition.

Khan et al., [2023]b; S. Kumar et al., [2015] examined the dynamics within convergent-divergent nozzles, finding that supersonic velocity can be reached in the divergent section if the Mach number remains below one at the throat. Beyond this, it can result in nozzle blockage. In cold-spray (CS) technology, particle temperature is influenced by particle characteristics and injector length. Lower particle temperatures are associated with longer injectors, whereas shorter injectors produce higher particle temperatures, which can be leveraged to optimize deposition conditions.

Liang et al., [2015] demonstrated that annealing CS coatings at 400°C for at least 120 minutes can significantly reduce stripping resistance, improving coating adhesion and durability. This post-treatment method is predominantly beneficial for coatings where high bonding strength is important.

Sabard et al., [2020] examined the properties of coated substrates after experiencing solution heat treatment and quenching. They observed that these treatments increase hardness and transform the precipitation state, which affects the deposition efficiency and the proportion of rebounding particles. These are key factors in achieving optimal coating performance.

Lupoi et al., [2020] identified Cold Spraying coating as a developing process due to its solid-state nature and high deposition rate, drawing significant interest for coating and additive manufacturing applications. Their analysis presented that collisional motion increases at the low-speed section of the nozzle, and the average particle velocity decreases notably with a rise in powder feed rate. A collisional model was developed to enhance particle distribution within and downstream of the nozzle, as simplified models could not accurately compute this feature. The location of the injector at the nozzle inlet was also critical for determining particle dwell time.

Pattison et al., [2008] introduced cold-spray coating technology, observing that deposition efficiency is directly related to the stand-off distance between the nozzle and the substrate. They also observed that the shape of particles impacts velocity behavior, with irregularly shaped particles exhibiting rapid fluctuations in velocity compared to more stable, spherical particles.

Liu et al., [2020]; Pattison et al., [2007]; Yeom & Sridharan, [2021]; Yin et al., [2018] proposed that in the CS coating process, feedstock powder was

sprayed through the nozzle to produce a high-velocity jet focused the substrate for coating deposition. This versatile coating technology combines various metals, composite materials, polymers, and ceramics tailored to specific applications and requirements. The technology is gaining traction within the manufacturing industry, leading to a dedicated cold spray additive manufacturing division. This solid-state powder-based deposition method is termed cold gas dynamic manufacturing.

M. Kumar et al., [2020] observed that surface roughness in CS coatings increases the particle size and decreases to the nanoscale. This association highlights the challenge of achieving smooth coatings with nanoparticles as feedstock powder because smaller particles can create rough surfaces upon deposition.

P. Das et al., [2019] investigated the effects of grinding on residual stresses in nanostructured coatings, finding that residual stress levels tend to increase with this post-processing method. This finding is important for applications where managing internal stresses is critical for coating stability and performance, as grinding can potentially influence the long-term durability of nanostructured coatings.

Klinkov et al., [2019] reported that the pre-heat-treated powder materials significantly enhanced Cold Spray deposition efficiency, doubling the deposition rate. Additionally, this pre-treatment reduced coating porosity by nearly four times, improving the coating’s density and overall structural integrity. This

approach provides a promising method for optimizing CS coatings, particularly when high-density and low-porosity coatings are required.

Winnicki et al., [2021] interpreted cladded powders, which can be produced by encapsulating alumina particles employing a nickel layer through hydrogen reduction. Due to high kinetic energy, plastic deformation and heat generation in the particles occur, directly affecting the microhardness and bond strength of CS coating. Microhardness impacts the microstructure, which results in porosity and cracks for lower microhardness. The microhardness of a layer with a high Nickel concentration is more complicated than having more alumina.

Vilardell et al., [2016] examined the formation of compact nano-crystalline grains found using CS coating technology in impact dynamics. Notably, a distinct moiré pattern emerges, attributed to the preserved tamping effect within the microstructure. Remarkably, no discernible size change occurs in the nano-sized grains despite these dynamic processes.

Cao et al., [2020] interpreted the Weibull distribution method has emerged as a viable and straightforward approach for characterizing the particle distribution in cold-sprayed coated composites.

Wu, Huang, et al., [2020] observed that surfaces coated through CS technology generally exhibit compressive residual stresses, primarily resulting from particle deformation and high-velocity impact. These compressive stresses

improve the mechanical robustness of the coating, contributing to improving wear resistance and structural integrity.

Chakrabarty & Song, [2020]a introduced an advanced model based on the Johnson-Cook (JC) material model, which effectively predicts both the stress distribution and the deformed shapes of particles during CS processes. This predictive model offers a valuable tool for optimizing CS coating parameters, easing better control over coating quality and particle behavior.

Singh et al., [2019] monitored the CS coating process, observing that it produces high thermal conductivity and strong adhesion strength coatings. These properties make CS coatings most suitable for applications requiring efficient heat transfer and durable bonding, such as the electronics and aerospace components industry.

Reddy & Kummitha, [2017] examined how coating applications significantly impact material properties, including porosity, hardness, and density. This influence extends to the coated material's middle and outer regions, mainly due to the reduction in grain size. The wear rate must also exhibit an upward movement as the applied loads increase.

B. Das et al., [2018] examine that the laser remelting of coating material significantly reduces the porosity of the thermal ceramic coatings and also exerts

notable consequences on mechanical properties such as microhardness, elastic modulus, and others when compared to the as-sprayed coating.

Seraj et al., [2020] deliberated the application of CS coatings using composite powders, which results in coatings characterized by low porosity, elevated hardness, and enhanced fracture toughness.

Tripathy et al., [2020] examined that CS coatings demonstrate exceptional corrosion resistance when applied at relatively low temperatures (approximately 500°C). Subsequent post-deposition heat treatment enhances interfacial bonding and mitigates porosity, further optimizing the overall coating properties.

Sabanayagam & Chockalingam, [2020] introduces When comparing uncoated materials with aluminum and chromium-coated ones, it is observed that aluminum-coated materials offer superior oxidation resistance in high-temperature working environments.

Mindivan & Mindivan, [2016] investigated pulse plasma nitriding but found that this technique alone does not substantially improve corrosion resistance. Their findings suggest that while nitriding may offer certain benefits, additional treatment methods may be necessary to achieve optimal corrosion protection.

Khan et al., [2021] investigated in CS coating technology a higher pre-heat temperature enhances the deposition of the first layer, thereby improving bonding strength. The material powder particles stuck at maximum temperature with a higher nitrogen gas concentration than the helium gas.

Rutkowska-Gorczyca, [2020] investigated the application of a low-pressure CS coating technique to copper, which results in a metallic structure, whereas copper-titanium dioxide coating yields an amorphous structure.

Dykhuizen & Smith, [1998]; W. Y. Li et al., [2007] and Lupoi et al., [2020] observed that Cold Spraying (CS) coating technology significantly influences manufacturing techniques and enables coating across various conditions and materials. The Russian Academy of Sciences developed this process in the 1980s. CS coating is a process that uses particles with low temperatures and high velocities to apply a layer of material on a surface. The particles do not melt or oxidize during the process. The Russian Academy of Science created and developed CS coating, a purely new finding and technique to coat, in the 1980s, and it has been used for different materials and conditions in manufacturing and coating applications.

W. Li, Yang, Zhang, Zhou, et al., [2016] and Y. Li et al., [2012] designed the Cold Spraying coating technique, the particle temperature is kept below its melting point, unlike in thermal spray coating techniques. In contrast to the thermal spray coating technique, the CS coating technique’s particle

temperature was kept lower than the melting point of the material particles. In this way, the CS coating technique did not affect the material properties.

Meyer et al., [2016] and Y. Xie et al., [2016] observed that the CS coating technique varies significantly from other spray coating methods, as it depends upon kinetic energy (K.E.) rather than thermal energy (T.E.). In CS coating, the temperature is kept below the melting point of the deposited material. This technique uses powder particles as the coating material, with the particle diameters ranging from nanometers to millimeters.

El Din et al., [2022]; S. M. Hussain, [2022]a, [2022]c, [2022]b, [2023]b, [2023]a and S. M. Hussain et al., [2022] extensively studied the CS coating technique, recognizing it as a modern and adaptable method that accommodates a wide range of coating materials with minimum impact on the substrate properties. Recently, the technique has been expanded to include nanomaterials and nanofluids, making it appropriate for various thermal systems where nanofluid-based coatings can improve thermal efficiency.

Shahzad et al., [2022] conducted a comprehensive analysis of CS coating properties, showing that experimental studies are often complemented by numerical analysis, which provides results closely aligned with practical outcomes. This dual experimental and numerical analysis approach has become popular due to its correctness in predicting real-world performance.

King et al., [2010] experimentally demonstrated that thermal softening in CS coating occurs with increased temperature and facilitating the particle deformation. This softening effect enables particles to deform more readily upon impact, enhancing coating adherence and quality.

W. Y. Li et al., [2014], [2016]; Yin et al., [2013], and Yu et al., [2013] investigated that the pre-heating of both the substrate and particles leads to more extensive particle deformation. They observed that the increase in temperature improves various impact characteristics, like crater depth, plastic strain, jet length, and flattening ratio, contributing to stronger and more cohesive coatings.

Yin et al., [2013] investigated the optimal substrate temperature, observing that the optimal substrate temperature varies based on the specific combination of coating material, substrate, and spray type. This insight suggests that tailoring temperatures is essential for achieving optimal coating performance.

W. Li, Yang, Zhang, & Zhou, [2016] found that the pre-heating influences the residual stress behavior in CS coatings, which converts from compressive to tensile with increased temperatures. This transition is attributed to quenching and thermal stresses overriding the peening stresses. Preheating effects differed across stress directions: radial and shear stresses were significantly influenced, whereas the axial stresses were less affected.

T. Hussain, [2012] analyzed the particle bonding mechanisms, highlighting Adiabatic Shear Instability (ASI), a widely accepted theory for explaining the strong bond between particles and substrates. This theoretical framework underscores the role of intense, localized deformation at the particle-substrate interface, facilitating robust bonding without post-heating.

Lin et al., [2019]; Oviedo & Valarezo, [2020]; Shah et al., [2017]; Shayegan et al., [2014] observed that the temperature of the substrate can affect the adhesion and other properties of the CS coatings. As per the studies, increasing the substrate temperature can improve the coatings' bond strength, electrical conductivity, and hardness and reduce the residual stress and porosity.

Lomas et al., [2011]; Maritime & 2020, n.d. and Willemen et al., [2020] investigated the impact of high substrate temperatures on Cold Spray (CS) coatings. According to their research, higher substrate temperatures promote better plastic deformation and material particle attachment upon impact. The temperature boost is because higher temperatures remove surface oxide layers from the particles and substrate, which leaves the surfaces cleaner and improves bonding. The stronger, more cohesive coatings that result from this temperature-induced oxide reduction and improved plasticity are especially useful in situations where material adherence and endurance are crucial.

With customized pre-heating improving coating qualities and promoting improved particle-substrate bonding across a range of materials and

stress orientations, our results highlight the significance of temperature control in Cold Spray.

The novelty of this research lies in finding the optimal injector length and stand-off distance at an unchanging inlet temperature and pressures and with particles of spherical shape. While previous studies have predominantly focused on critical velocity, coating thickness, and functionality of deposited material, our analysis specifically explores the optimal injector length and stand-off distance, which gives the best possible temperature and impact velocity. The shape of the material powder is also analyzed to get the best impact velocity and temperature on the substrate.

CHAPTER 3

OBJECTIVE OF THE STUDY

3.1 Introduction

This chapter focuses on identifying the research gaps in the present analysis. Research objectives have been framed based on these identified research gaps. This chapter centers on the identification of research gaps within the current analysis. Subsequently, research objectives are formulated based on these identified gaps.

3.2 Research Gaps

Based on the reviewed literature, the following research gaps have been identified:

1. As per the literature review, very little work has been proposed in cold spray coating.

2. Very few models are used in simulation-based research on cold spray coating works.

3. It has been found that the models analyzed for coating development are limited and thus need improvement.

4. It has been observed that no significant work has been done for the material selection, velocity and temperature selection, particle size selection, geometry, nozzle distance from the substrate, and much more for the cold spray coating.

5. Furthermore, from the available research, it is noted that no significant research has been found to give an impression of the particle shape and size effect.

6. In the literature, there is a lack of such work based on the concentration of propelling gas mixtures.

7. In the literature, there is a deficiency of work based on injector dimensions.

3.3 Research Objectives

As far as the literature gaps are concerned, the objectives formulated to carry this research work are as follows:

1. To develop a CFD model of spray coating for analysis and performance evaluation using different powder sizes of different materials and model validation.

2. To advance the proposed model using different geometrical parameters.

3. To develop a model of spray coating under pre-heat conditions and to analyze the effect for a wide range of operating parameters.

These objectives aim to enhance understanding of the CS dynamic spray coatings under different conditions, providing valuable insights for potential applications of developed models for further work.

These objectives are fulfilled in this research work as shown via the flow chart as shown in Fig. 3.1:

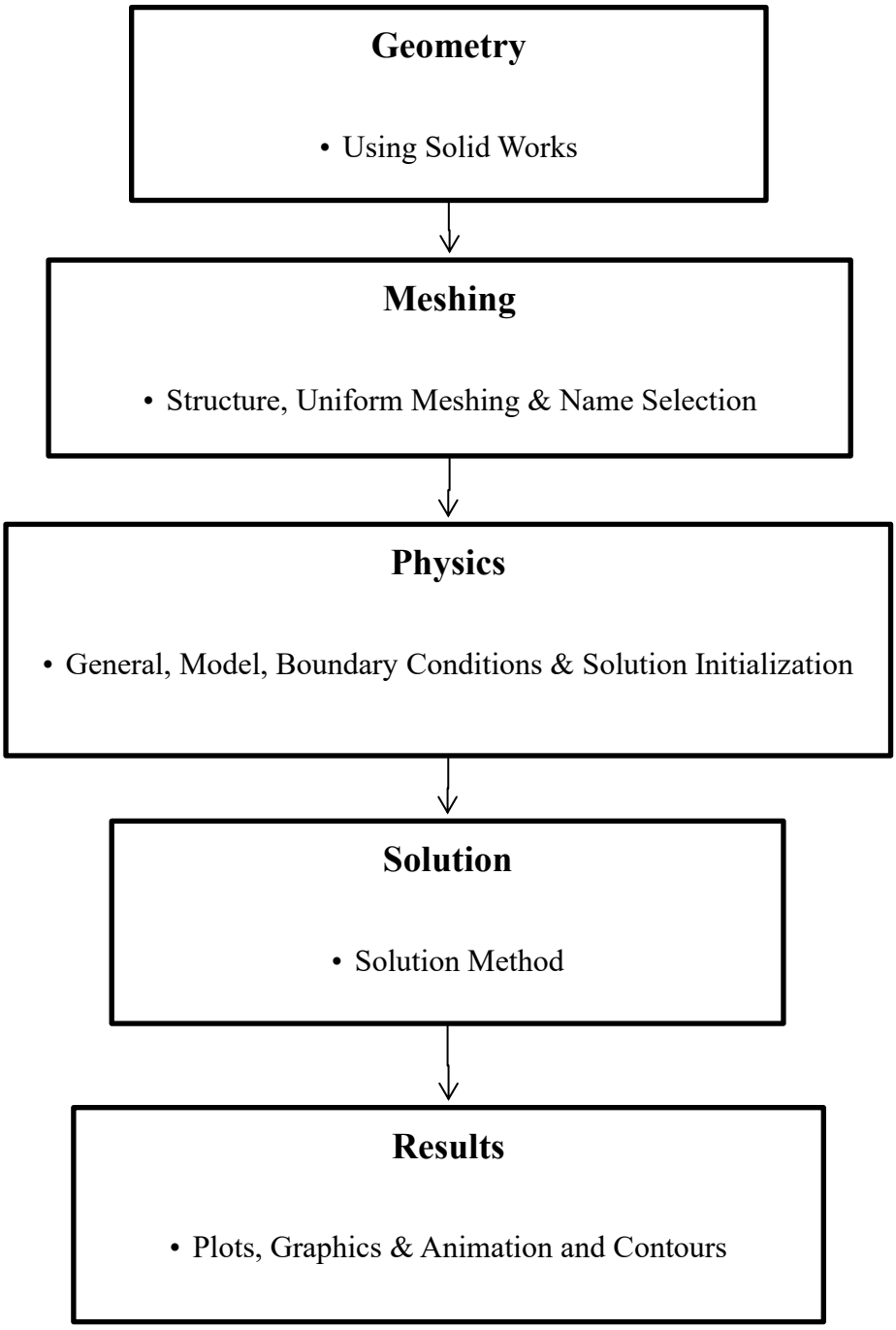

Figure 3.1 Flow chart to fulfill the objectives

3.4 Expected Research Outcome

1. A CFD model for the analysis of spray coating will be developed to obtain optimal results for industrial applications and performance parameters.

2. The model shall be validated with the existing results.

3. Powder particle size and material, substrate position and material, different geometrical nozzle parameters, temperature, and velocity distribution will be analyzed.

CHAPTER 4

METHODOLOGY AND MODELING

Chapter 4 explores the numerical methodology utilized to calibrate the CS coating process. This section encompasses the development of model geometry, the creation of the computational fluid domain, and mesh generation. It details the application of a CFD solver to resolve discretized governing equations using specified input parameters iteratively. CFD post-processing techniques extract data and visualize the effects of various process parameters. The chapter also covers the fundamental governing partial differential equations—continuity, momentum, and energy equations—essential for analyzing the influence of different nozzle process parameters. The study examines the behavior of different gases and gas mixtures and the effects of various powder particle materials, shapes, and sizes. Section 4.4 provides an in-depth discussion of the critical boundary conditions and numerical schemes utilized in the CFD solver. Section 4.6 elaborates on mesh generation and grid sensitivity analysis, including comparing results based on grid size within the flow domain. Finally, section 4.7 presents the endorsement of the computational methods employed in this thesis.

4.1 Research Methodology

1. A model for validation will be developed and solved with the help of Solid Works and FLUENT Workbench. The model will be updated and solved to improve the existing nozzle results with validation.

2. The above updated and improved model geometry is then analyzed and solved for different powder sizes of different materials under different conditions.

3. The advanced turbulent CFD model (using Fluent and Solid Works) is then developed by updating the geometrical parameters, considering the best results from the above objectives and improved data.

4. The above models are then analyzed under pre-heat conditions, and the pre-heat effect is observed.

5. The governing equations for the two-dimensional steady compressible flow are Huang et al., [2014]:

a. Continuity equation:

$$R = A \cdot v = \text{constant} \qquad (4.1.1)$$

Where:

R = The volume flow rate (m^3/s)

A = The flow area (m^2)

v = Fluid speed (m/s)

b. Momentum equation:

$$\rho \frac{D\boldsymbol{u}}{Dt} = \nabla \cdot \tau + \rho g \quad (4.1.2)$$

Where:

ρ = Fluid density (kg/m^3)

u = Velocity vector (m/s)

τ = Stress tensor (Pa or N/m^2)

g = Gravitational Acceleration (m/s^2)

c. Energy equation:

$$Q + (U + PE + KE + P.V)_{in} = W + (U + PE + KE + P.V)_{out} + (U + PE + KE + P.V)_{stored} \quad (4.1.3)$$

Where:

Q = Heat (Joules, J)

U = Internal energy (Joules, J)

PE = Potential energy (Joules, J)

KE = Kinetic energy (Joules, J)

P = Pressure (Pa or N/m^2)

V = Volume (m^3)

W = Work (Joules, J)

A. CFD process steps for simulation Fig. 4.1 of cold gas dynamic spray coating:

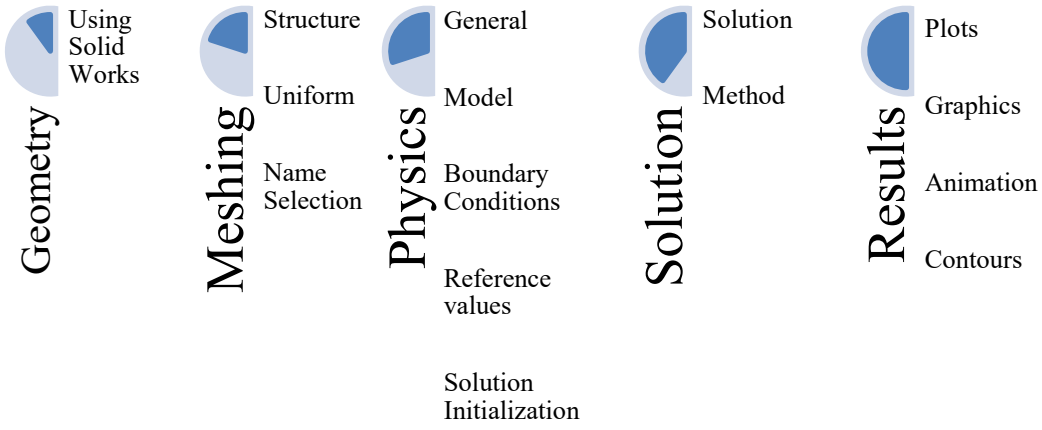

Figure 4.1 Steps Used in Simulation

4.2 Model and Domain Description

A 2-D model of the convergent-divergent nozzle with substrate is created for analysis on CAD software SOLIDWORKS. The governing equation is employed and solved using ANSYS Workbench, FLUENT. The General arrangement for the CS process technology primarily consists of a convergent-divergent nozzle and substrate, each with specific parameters as shown in Table 4.1. The developed geometry used in this work is designed and developed symmetrically for simplification, although it has been displayed as full geometry for better understanding, as shown in Fig. 4.2.

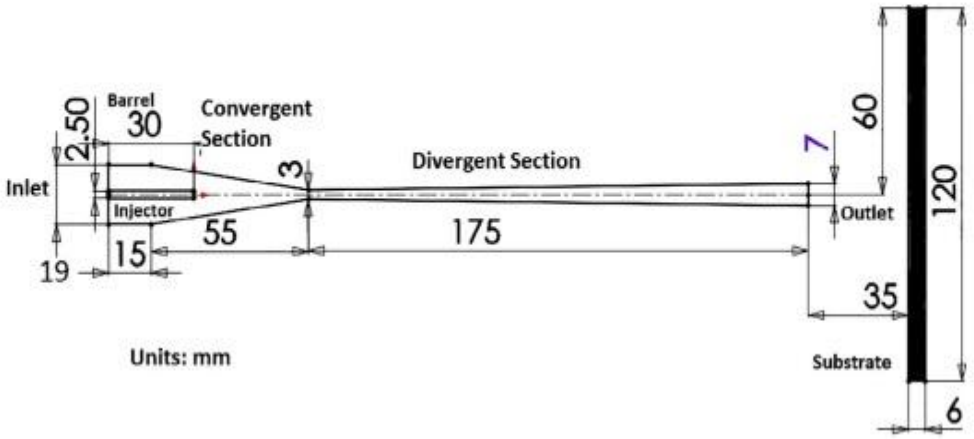

Figure 4.2 C-D Nozzle-Substrate arrangement with a stand-off distance of 35 mm.

Table 4.1 C-D Nozzle and Substrate Sections Dimensions Figure 4.2

S. No.	Particulars	Dimensions (mm)
1	Inlet Diameter	19
2	Injector Diameter	2.5
3	Injector Length	30
4	Barrel Length	15
5	Convergent Section Horizontal Length	55
6	Divergent Section Horizontal Length	175
7	Throat Diameter	3
8	Nozzle Outlet Diameter	7
9	Stand-off Distance	35
10	Substrate Diameter	120
11	Substrate Length	6

The general setup for CS process technology primarily involves a convergent-divergent nozzle and a substrate, each carefully designed with specific parameters. The nozzle begins with a circular inlet, 19 mm in diameter, leading to a convergent section of 55 mm in length. This section tapers down to a 3 mm throat, followed by a 175 mm divergent section, ending in a 7 mm diameter circular outlet. Attached to the beginning of the nozzle is a 15 mm barrel section to stabilize the flow.

For particle injection, a powder injector, measuring 30 mm in length and 2.5 mm in diameter, is situated 15 mm into the convergent section of the nozzle inlet. The substrate, onto which particles are deposited, is a rounded plate with a 60 mm radius and a 6 mm thickness, positioned 35 mm from the nozzle outlet. Additional parameter modifications are explored in subsequent sections to optimize performance and deposition efficiency in the CS process.

As previously discussed, the geometry used in this analysis has been designed symmetrically to streamline the modeling process. For clarity, the complete geometry is displayed in Fig. 4.3, providing a comprehensive view highlighting modifications to the setup shown in Fig. 4.2. This updated geometry includes adjustments in the substrate's position relative to the nozzle exit, with a substrate stand-off distance of 25 mm. The figure illustrates the arrangement of the nozzle and substrate, offering insight into how these modifications are intended to enhance the deposition process efficiency in the CS setup.

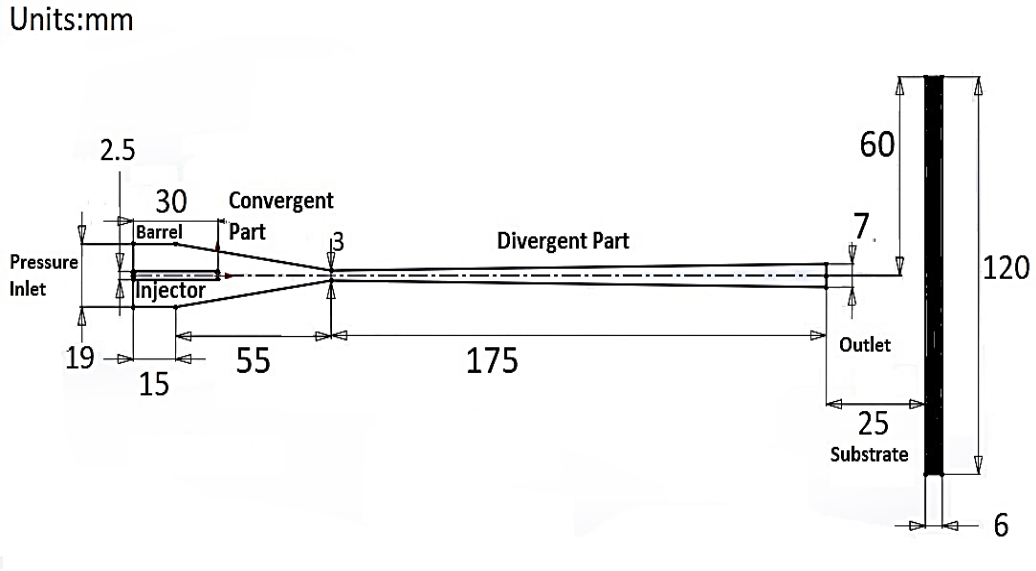

Figure 4.3 C-D Nozzle and substrate arrangement with the substrate stand-off distance of 25 mm.

The comparative general arrangement, as depicted in Fig. 4.2, illustrates the setup for CS process technology, which includes a modified barrel-convergent-divergent nozzle and substrate configuration. Table 4.2 details the specific parameters of this updated geometry. The primary modification in this model is the stand-off distance, which has been adjusted to 25 mm from the original 35 mm used in the initial model. This adjustment optimizes the deposition process by potentially enhancing particle impact and bonding efficiency.

Table 4.2 C-D Nozzle and Substrate Sections Dimensions

S. No.	Particulars	Dimensions (mm) Figure 4.2	Dimensions (mm) Figure 4.3
1	Inlet Diameter	19	19
2	Injector Diameter	2.5	2.5
3	Injector Length	30	30
4	Barrel Length	15	15
5	Convergent Section Horizontal Length	55	55
6	Divergent Section Horizontal Length	175	175
7	Throat Diameter	3	3
8	Nozzle Outlet Diameter	7	7
9	**Stand-off Distance**	**35**	**25**
10	Substrate Diameter	120	120
11	Substrate Length	6	6

In the series of modifications with the initially designed geometry Fig. 4.2, another modification was made, as displayed in Fig. 4.4, which is a full model of the modified geometry. Still, a symmetrical model was used to simplify simulation and calculations. The new modified geometry places the substrate at different positions from the nozzle exit.

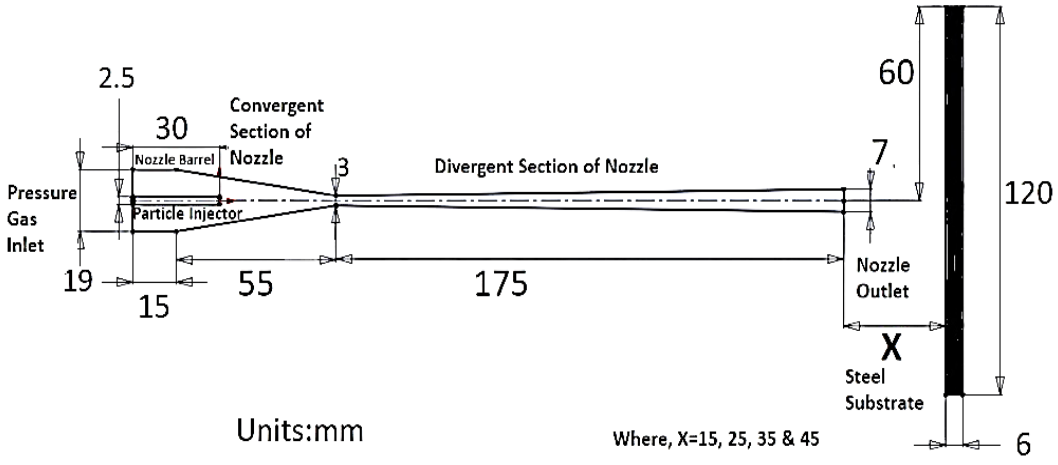

Figure 4.4 C-D Nozzle arrangement with the substrate having varying stand-off distance.

Fig. 4.4 exhibits the geometric modification of Fig. 4.2 with different substrate positions from the nozzle exit. The comparative general arrangement with Fig. 4.2 for the CS process technology, which primarily consists of a barrel-convergent-divergent nozzle and substrate having specific parameters of the modified geometry, is shown in Table 4.3. The modification mainly involves the stand-off distance. Upon updation, the stand-off distance starts from 15 mm to 45 mm with an interval of 10 mm.

Table 4.3 Comparison of Modified Geometry with Developed Geometry.

S. No.	Particulars	Dimensions (mm) Figure 4.2	Dimensions (mm) Figure 4.4
1	Inlet Diameter	19	19
2	Injector Diameter	2.5	2.5
3	Injector Length	30	30
4	Barrel Length	15	15
5	Convergent Section Horizontal Length	55	55
6	Divergent Section Horizontal Length	175	175
7	Throat Diameter	3	3
8	Nozzle Outlet Diameter	7	7
9	**Stand-off Distance**	**35**	**15, 25, 35, 45**
10	Substrate Diameter	120	120
11	Substrate Length	6	6

The developed geometry Fig. 4.2 was modified as shown in Fig. 4.5, which exhibits modification of injector lengths of material powder injector, starting from 15 mm to 30 mm with an interval of 5 mm. The modified geometry shown below is the actual geometry used for symmetry simulation.

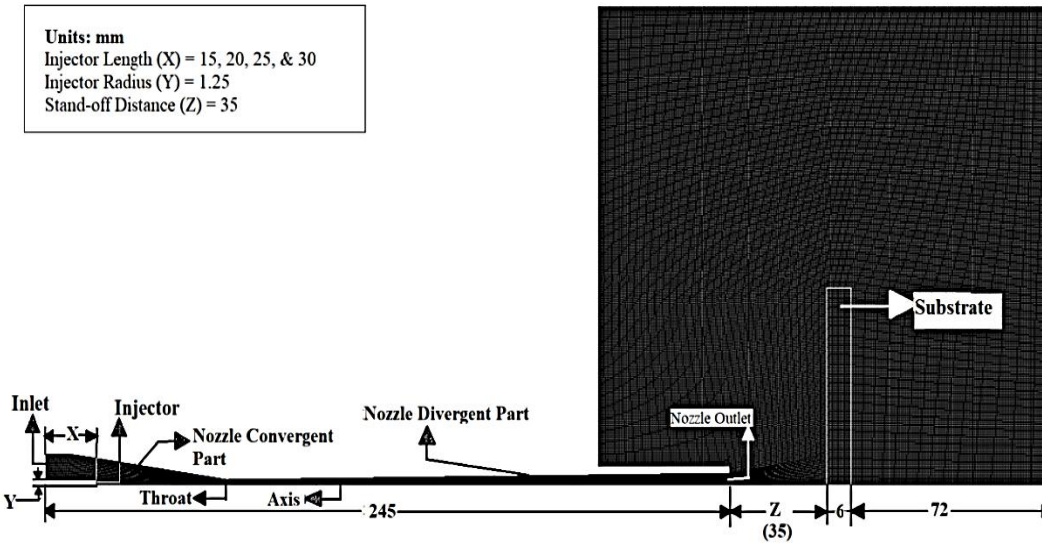

Figure 4.5 Computational Domain and C-D nozzle and substrate arrangement with varying injector length

Fig. 4.5 exhibits the geometric modification of Fig. 4.2 with different substrate positions from the nozzle exit. The comparative general arrangement with Fig. 4.2 for the CS process technology, which primarily consists of a barrel-convergent-divergent nozzle and substrate having specific parameters of the modified geometry, the modifications made are focused on the powder injector length, starting from 15 mm to 30 mm with an interval of 5 mm as shown in Table 4.4.

Table 4.4 Modified Geometry Comparision with Initially Developed Geometry.

S. No.	Particulars	Dimensions (mm) Figure 4.2	Dimensions (mm) Figure 4.5
1	Inlet Diameter	19	19
2	Injector Diameter	2.5	2.5
3	**Injector Length**	**30**	**15, 20, 25, & 30**
4	Barrel Length	15	15
5	Convergent Section Horizontal Length	55	55
6	Divergent Section Horizontal Length	175	175
7	Throat Diameter	3	3
8	Nozzle Outlet Diameter	7	7
9	Stand-off Distance	35	35
10	Substrate Diameter	120	120
11	Substrate Length	6	6

4.3 Governing Equations

4.3.1 The Continuity Equation

The continuity equation describes the movement of physical quantities, particularly conserved quantities such as mass, momentum, energy, and electric charge. It applies to understanding various physical phenomena, especially fluid dynamics, where fluids flow through tubes of varying diameters. Typically, fluids considered in such scenarios have constant density and are incompressible.

This idea can be compared to the human circulatory system, in which blood arteries divide into many capillaries, eventually forming veins. The continuity equation, a basic fluid dynamics principle, can determine the blood flow velocity through these veins. However, because blood vessels are elastic, other elements like vessel elasticity and diameter must be considered in addition to the continuity equation to obtain accurate predictions.

Let's first examine the flow rate (f) to comprehend the equation of continuity:

$$f = A \cdot v \tag{4.3.1}$$

Where,

f = rate of flow

A = the cross-sectional area of the pipe at a point

v = the average speed of the fluid in the pipe.

The volume of fluid flowing through a given point in a given amount of time is known as the flow rate, and it is commonly stated in milliliters per second (mL/s). It might, for instance, show how much water flows out of a pipe each minute.

The amount of blood pumped by the heart into the veins is determined by the continuity equation in medical applications, which is essential for evaluating cardiovascular health. It also helps identify possible problems like blocked arteries, which allows for prompt treatment to avoid heart-related problems.

Assumptions for the Equation of Continuity Derivation

The derivation of the continuity equation is grounded on several key assumptions:

- The tube or conduit under consideration has a single inlet and outlet.
- The fluid flowing through the tube is non-viscous (i.e., it experiences negligible internal friction).
- The fluid is incompressible, which means its density remains constant.
- The fluid flow is steady, with no fluctuations over time.

Continuity Equation Derivation

Consider a fluid flowing through a tube over a small interval of time, Δt. During this time, at the pipe's lower section, the fluid, moving with velocity v_1, will travel a distance of Δx_1.

The distance traveled in the time Δt, with speed v_1 by the fluid, is given by,

$$\Delta x_1 = v_1 \Delta t$$

Therefore, in the lower section, the volume of fluid flows in the pipe is,

$$V = A_1 \Delta x_1 = A_1 v_1 \Delta t \qquad (4.3.2)$$

As we know,

mass (m) = Density (ρ) × Volume (V)

Therefore, in the region Δx_1, the mass of fluid:

Δm_1= Density × Volume

$$\Rightarrow \quad \Delta m_1 = \rho_1 A_1 v_1 \Delta t \qquad (4.3.3)$$

To compute the mass flux at the lower section of the pipe, we define the mass flux as the entire mass of fluid passing through a specified cross-sectional area per unit of time.

Therefore, the mass flux for the lower section with cross-sectional area A_1 will be given by:

$$\Delta m_1/\Delta t = \rho_1 A_1 v_1 \quad (4.3.4)$$

Correspondingly, for the upper section of the pipe, the mass flux of the fluid will be:

$$\Delta m_2/\Delta t = \rho_2 A_2 v_2 \quad (4.3.5)$$

Where,

v_2 = velocity of the pipe's upper section of the flowing fluid.

Δx_2 = distance covered by the flowing fluid in the upper section of the pipe.

Δt = time.

A_2 = cross-section area of the upper section of the pipe.

The assumption is that the fluid density remains uniform throughout the pipe, from its lower to upper sections. This assumption allows us to consider the fluid flow as streamlined. Consequently, we can infer that the mass flux at the lower

section will be equivalent to the mass flux at the upper section of the pipe. Therefore, Eqn. 4.3.4 = Eqn. 4.3.5

Thus,

$$\rho_1 A_1 v_1 = \rho_2 A_2 v_2 \qquad (4.3.6)$$

Based upon the Eqn. 4.3.6 this can be stated as follows:

$$\rho.A.v = \text{constant}$$

The equation presented above serves as evidence supporting the law of conservation of mass in fluid dynamics. This assertion stems from the assumption that the fluid under consideration is incompressible, ensuring a constant density throughout the flow's steadiness.

So, $\rho_1 = \rho_2$

Applying this to Eqn. 4.3.6; it can be written as:

$$A_1 v_1 = A_2 v_2$$

The generalized form of this equation is:

$$A.\ v = \text{constant}$$

Let's denote R as the volume flow rate. Consequently, the above equation can be uttered as follows:

$$R = A.v = \text{constant} \quad (4.3.7)$$

Where:

R = The volume flow rate (m^3/s)

A = The flow area (m^2)

v = The average speed of the flowing fluid in the pipe (m/s)

This derivation outlines the continuity equation.

4.3.2 The Momentum Equation

The momentum equation embodies the principle of conservation of momentum in fluid motion. It states that the rate of change of total momentum within any infinitesimal unit in the flow field equals the sum of all external forces acting upon that unit. The fluid momentum equation (Eqn. 4.3.8) is expressed as follows:

$$\rho \frac{D\mathbf{u}}{Dt} = \nabla \cdot \tau + \rho \mathrm{g} \quad (4.3.8)$$

Where:

ρ = Fluid density (kg/m³)

u = Velocity vector (m/s)

τ = Stress tensor (Pa or N/m²)

g = Gravitational Acceleration (m/s²)

4.3.3 The General Energy Equation

The principle of energy conservation dictates that the energy can neither be created nor be destroyed, a concept synonymous with the First Law of Thermodynamics. This law was instrumental in formulating the energy equation discussed in the thermodynamics module. Eqn. 4.3.9 represents the general energy equation applicable to an open system.

$$Q + (U + PE + KE + P.V)_{in} = W + (U + PE + KE + P.V)_{out} + (U + PE + KE + P.V)_{stored} \quad (4.3.9)$$

Where:

Q = Heat (Joules, J)

U = Internal energy (Joules, J)

PE = Potential energy (Joules, J)

KE = Kinetic energy (Joules, J)

P = Pressure (Pa or N/m²)

V = Volume (m^3)

W = Work (Joules, J)

4.4 Fluid Mechanics of Particle Shapes

Several fluid mechanics principles govern the behavior of particles in a gas stream, especially **drag force** and **flow separation**.

Drag Force (FD): The resistance experienced by particles as they move through the gas medium. It is described by:

$$F_D = \frac{1}{2} C_D \, \rho v_p^2 A_D$$ D. Wang & Fan, [2013]

Where C_D is the drag coefficient, ρ is the fluid density, v_p is the particle velocity, & A_D is the cross-sectional area of the particle. Spherical particles have a lower C_D than irregular particles, resulting in a smaller drag force for the same velocity and fluid conditions.

Flow Separation: The degree of flow separation from the particle's surface increases with irregular shapes, leading to a larger turbulent wake behind the particle. This increased turbulence induces a larger drag force, reducing particle acceleration in the flow.

4.4.1 Shape Factor

The shape factor (SF) plays a significant role in determining the aerodynamic behavior of particles during the CS process. The SF is the deviation of a particle's geometry referencing from a perfect sphere, termed sphericity. The term sphericity can be explained as measuring an object and how spherical it is. Proposed by Waddell in 1935, the ratio of the surface area of an equal-volume sphere to the actual surface area of the particle gives the sphericity of a particle:

(Shape factor) $$\Psi = \frac{\pi^{1/3}(6V_p)^{2/3}}{A_p}$$ D. Wang & Fan, [2013]

Where,

Vp = Particle's volume, and

Ap = Particle's surface area.

The sphericity of a non-spherical particle is always less than 1. Particles with different shapes (e.g., spherical, elongated, irregular) exhibit varying drag forces, directly influencing their deposition efficiency and the velocity in the CS process.

4.5 Method of Solution

The geometry's flow domain is constructed utilizing SolidWorks, a widely accessible CAD modeling software. Subsequently, this modeled flow domain undergoes discretization into smaller elements and is solved numerically using the CFD solver within ANSYS Fluent workbench, which employs the finite volume method. This section deliberates fundamental aspects of Computational Fluid Dynamics (CFD), including coupling and discretization schemes, boundary conditions, and fluid properties essential for solving the discretized equations.

4.6 Some basic details regarding CFD

Computational Fluid Dynamics (CFD) is a branch of fluid mechanics that offers a cost-effective simulation of real flows through numerical solutions using governing equations. The Navier–Stokes formulations, fundamental to Newtonian fluid dynamics, have been extensively used for over a century. However, ongoing research focuses on advancing reduced forms of these equations, particularly for turbulent flow, such as Reynolds-averaged Navier-Stokes formulations. Yet, theoretical developments for non-Newtonian fluids, two-phase flows, and chemically reacting flows are comparatively less advanced.

In computational techniques, the governing differential equations are replaced by algebraic equations, facilitating straightforward computer computation. The exponential growth in computer power since the 1960s has been pivotal in the proliferation of CFD. This development makes it possible to examine cases outside of analytical solutions that are difficult or impossible to recreate experimentally.

Experimental techniques like wind tunnels and rig testing are essential to analyze and validate different approximations to governing equations and provide a more affordable option. For most real-world applications, the intricacy of flow-governing equations frequently excludes analytical solutions.

Based on input data, CFD uses various codes, including approved software like Ansys, to address particular issues. Although CFD offers problem-specific answers, its use is constrained by the scope of alternative testing techniques.

Depending on the particular issue, CFD simulates several flow methods in thermal design difficulties. Fluid flow conditions in microchannels are revealed by CFD, emphasizing the value of analytical solutions while describing fluid flow conditions.

4.7 Applications of CFD

4.7.1 Aerospace

CFD techniques, such as airflow analysis surrounding aircraft surfaces, are frequently used in aerospace applications to forecast and maximize component performance. These CFD approaches make possible comprehensive models of aerodynamic forces, turbulence, and pressure distribution throughout the wings, fuselage, and control surfaces. Engineers may evaluate lift, drag, and stability by simulating airflow patterns, which enables better flight control, structural safety, and fuel efficiency. Furthermore, CFD plays a key role in testing new design configurations, refining engine cooling systems, exhaust nozzles, and inlets, and assessing heat transfer and aerothermal effects at high speeds, particularly in the supersonic and hypersonic regions. This predictive ability lessens the need for intensive wind tunnel testing, enabling quicker and more economical development.

4.7.2 Automotive

Computational fluid dynamics, or CFD, is crucial in automotive applications for simulating vehicle aerodynamics, reducing drag, and enhancing efficiency in various operating scenarios. CFD assists engineers in improving designs for reduced drag coefficients, which improve handling, stability, and fuel efficiency by simulating airflow over the vehicle body. CFD also optimizes engine

parts, auxiliary systems like HVAC (heating, ventilation, and air conditioning), and cooling. It entails optimizing intake and exhaust systems, increasing airflow through radiators and intercoolers, and guaranteeing effective heat dissipation in the engine bay. These applications allow automotive manufacturers to meet environmental, energy, and performance regulations.

4.7.3 Chemical Engineering

In chemical engineering, computational fluid dynamics (CFD) has a wide and significant variety of applications in sectors like petrochemicals, waste treatment and recycling, fertilizer manufacture, pollution control, and food processing. CFD models and optimizes reactors, pipelines, and separation units in petrochemical operations to maximize yield and efficiency while consuming the least energy. CFD simulations aid in designing systems, such as scrubbers and filters, that effectively remove pollutants from the air and water. CFD models help optimize reaction conditions, mixing, and heat transfer in fertilizer manufacture, resulting in more efficient and sustainable procedures.

CFD helps design heating, cooling, and mixing systems in food processing, guaranteeing product quality and uniformity while adhering to food safety regulations. CFD applications help waste treatment and recycling by enhancing the performance and design of treatment facilities, like bioreactors and incinerators, which improves waste decomposition and resource recovery. CFD

allows engineers to evaluate and improve processes virtually in each domain, eliminating the need for expensive physical trials and enhancing environmental sustainability.

4.7.4 Biomedical

CFD helps design and simulate blood flow in inhalers, heart-assist devices, and cardiovascular systems. Researchers and engineers may precisely evaluate hemodynamic forces that impact vessel walls, flow patterns, and possible turbulence areas by employing computational fluid dynamics (CFD) to mimic blood flow's intricate, pulsatile nature through vessels. In inhalers and heart-assist systems, CFD helps optimize device design by analyzing airflow patterns, ensuring efficient drug delivery, and enhancing the performance of assistive cardiac devices. Overall, CFD enables the development of safer, more effective medical devices tailored to individual physiological conditions.

4.7.5 Power Generation

In the power sector, Computational Fluid Dynamics is applied extensively for analyzing economizers, superheaters, pulverized coal combustion, and designing low NOx burners, among other areas. These applications aim to enhance the performance and efficiency of power plants.

4.7.6 Electronic systems

The thermal challenges manufacturers encounter underscore the growing need for precise and cost-effective computational design tools to address intricate cooling-related thermal issues, which includes thermal analysis of electronic systems through Thermal Management Solutions (TMC).

4.8 Procedure of Computational Fluid Dynamics

- Partition the fluid volume or surface into manageable sections through gridding.
- Simplify the equations as necessary for the specific conditions.
- Define appropriate boundary conditions.
- Initialize the values on the grid.
- Proceed to solve the simplified equations step by step at the designated grid points.

4.9 Advantages

Several advantages of the CFD process are evident. While it involves multiple steps, it proves highly effective for 3-D volumes. The generation process is notably faster compared to manual operations.

- CFD significantly reduces time and costs.
- It enables the analysis of complex and hazardous problems.
- CFD techniques can handle problems beyond conventional limits.
- There's virtually unlimited capacity for detailed analysis.
- Various graphs are plotted to validate results for different purposes.
- Simplification of processes leads to good results.
- However, some challenges remain, including incomplete models for turbulence, multiphase flows, and other complex problems.

4.10 Disadvantages

- The initial setup costs may be higher compared to the provided data.
- Easy accessibility and low investment can lead to overtrading.

4.11 Computational Fluid Dynamics Code

Computational Fluid Dynamics codes are utilized across various categories in numerous applications. These codes enable the development of tools associated with CFD analysis, facilitating their application and generating valuable insights.

- **Computational Fluid Dynamics Commercial Codes**

  STAR-CD, FLUENT, FLUIDYN, CFX, CFDESIGN etc.

- **Computational Fluid Dynamics Research Codes**

  COOLFLUID, CFDSHIP IOWA, etc.

- **Computational Fluid Dynamics Public Codes**

  WINPIPED, HYDRO, etc.

- **Other Computational Fluid Dynamics codes**

Other codes like GAMBIT are employed in generation software, while grid visualization tools such as CFX-Post, ADINA-AUI, COMSOL, EnSight, Field View, and HyperView are utilized for visualization.

4.12 Computational Fluid Dynamics Process

- CFD is utilized across various applications, such as separating bubbly flows within a domain.

- Applications involve observing massive, uniform, and unsteady flows. The code assigns conjugate configuration rates in the process.

- The code enables various other applications, including multiphase fluids, marine, and biomedical applications.

- Flow tendencies are assessed by applying the code, which configures the steps in the process.

- The code application is tailored to the necessary steps in the generation process. If drawbacks occur, post-processing steps are applied.

4.12.1 Steps

- Geometry layout
- Application of physics
- Mesh generation
- Solution
- Reporting
- Feedback

4.13 Coupling and spatial discretization schemes

"Pressure-Based" solver and "steady" model has been used in the current analysis. The "Laminar" and "Species Transport" models have been used in ANSYS fluent. The "SIMPLE" algorithm has been used for pressure-velocity coupling and spatial discretization of pressure, momentum, and continuity, and "second-order upwind" has been selected. The convergence absolute criteria of residual for the continuity (X-velocity, Y-velocity) and the energy was picked as 10^{-8} and for the species were picked as 10^{-10}. Table 4.1 summarizes the numerical schemes employed in the computational simulations.

Table 4.1 Numerical schemes used for CFD solutions

S. No.	Particulars	Solution Methods
1	Pressure-velocity coupling Scheme	SIMPLE
2	Gradient	Least squares cell-based
3	Pressure	Second order
4	Energy	Second order upwind
5	Momentum	Second order upwind
6	Turbulent Kinetic Energy	Second order upwind
7	Turbulent Dissipation Rate	Second order upwind
8	Species	Second order upwind

4.14 Boundary Conditions

The CS coating process arrangement primarily involves a barrel-convergent-divergent nozzle with a circular cross-section. 2-D models with symmetry at the nozzle axis are used for simulation because this helps reduce computational time. The boundary conditions of the computational field consist of a gas phase and solid substrate, which includes pressure inlet, particle inlet, Axis of symmetry, Nozzle outlet, outer field, and Pressure outlet in the gas phase. In contrast, the Nozzle walls and the substrate to be coated are in solid phase. Fig. 4.6 indicates the axis-symmetric, 2-D model used in this analysis with boundary conditions and flow directions from the nozzle and injector's inlet to the computational domain's pressure outlet.

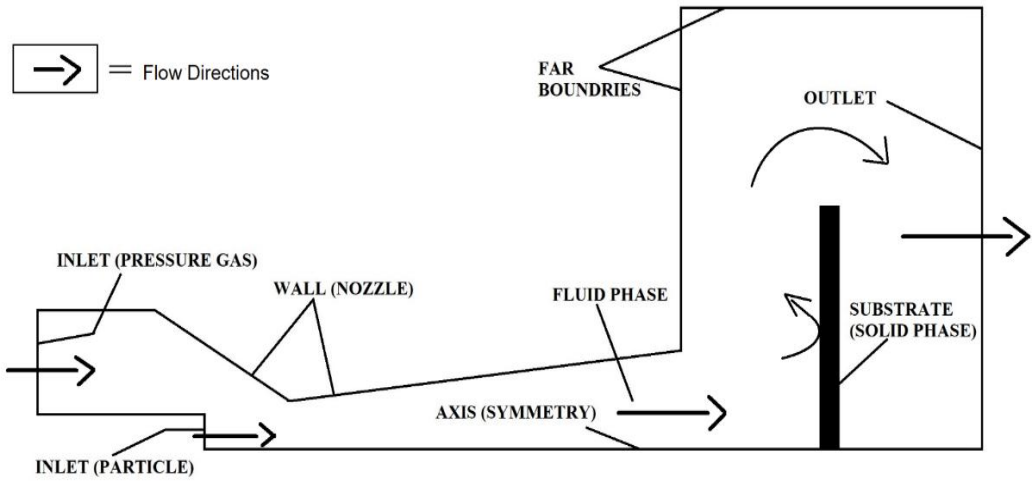

Figure 4.6 Boundary conditions and flow directions of the computational domain

This model neglects heat transfer between the gas and the nozzle walls. The nozzle inlet is characterized by a specific temperature and pressure, representing the pressure conditions applied at this point. Outside the nozzle exit, the surrounding atmospheric boundary serves as the outer far field, with the pressure outlet set to atmospheric pressure at the boundary of the computational domain. The substrate is positioned at the intersection of the gas mixture and the material particles, allowing for effective fluid-solid coupling. This setup enables accurate simulation of the interactions between the gas flow and solid particles as they impact the substrate.

4.15 Grid Generation and Sensitivity Analysis

The solution obtained from numerical calculations should ideally remain unaffected by the number of mesh elements, ensuring that it is independent of grid density. It must be determined to render the solution grid-independent to achieve an optimal mesh size with sufficient elements. It is achieved through a grid independence test, which verifies that further refinement does not significantly alter the results. According to the grid independence test illustrated in Fig. 4.7, the solution became stable with a mesh containing 70,000 elements or more, confirming that this density is adequate for reliable and accurate results.

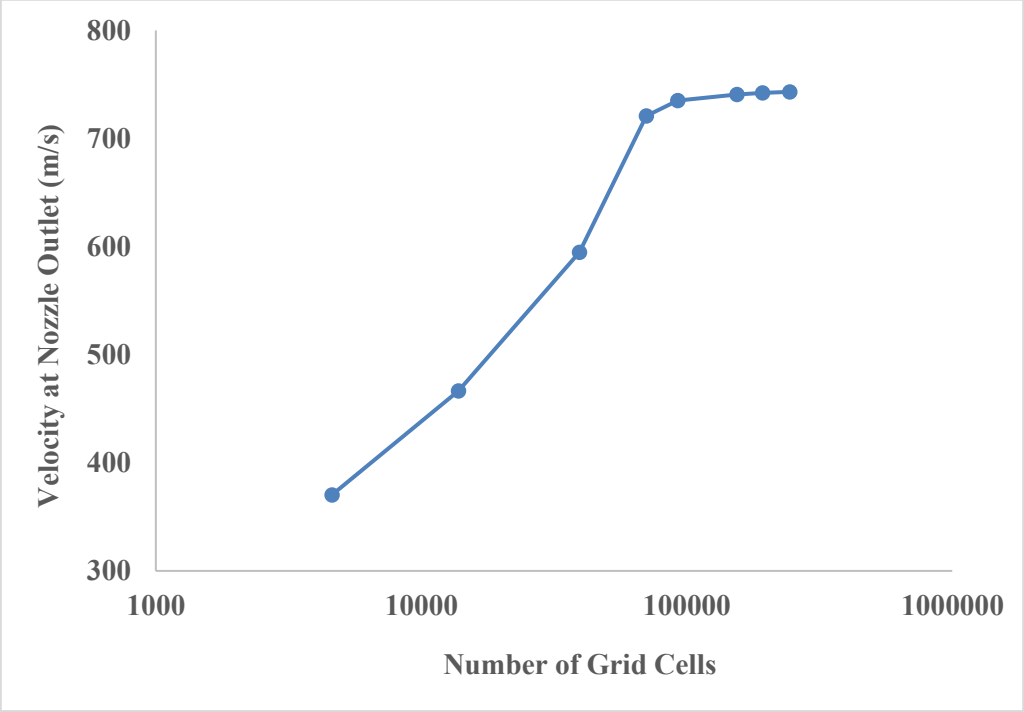

Figure 4.7 Velocity versus the number of grids.

The impression of enhancing the computational grid has been well analyzed regarding the precision of the C-D nozzle and substrate geometry outcomes. Fig. 4.8, Fig. 4.9, Fig. 4.10, and Fig. 4.11 show the quadrilateral meshing grid in the C-D nozzle and substrate, including computational geometry (far field) for the axisymmetric model. Fig. 4.8 shows the quadrilateral meshing grid of the whole geometry, Fig. 4.9 shows the mesh grid for the barrel, nozzle, and particle inlet, Fig. 4.10 shows the mesh grid for the nozzle throat area, where the pressure is maximum, and Fig. 4.11 shows the mesh grid for the nozzle outlet. The mesh grid shown in Fig. 4.8, Fig. 4.9, Fig. 4.10, and Fig. 4.11 are used for the axisymmetric model. Therefore, the results were shown for cut sections of the 2D geometry.

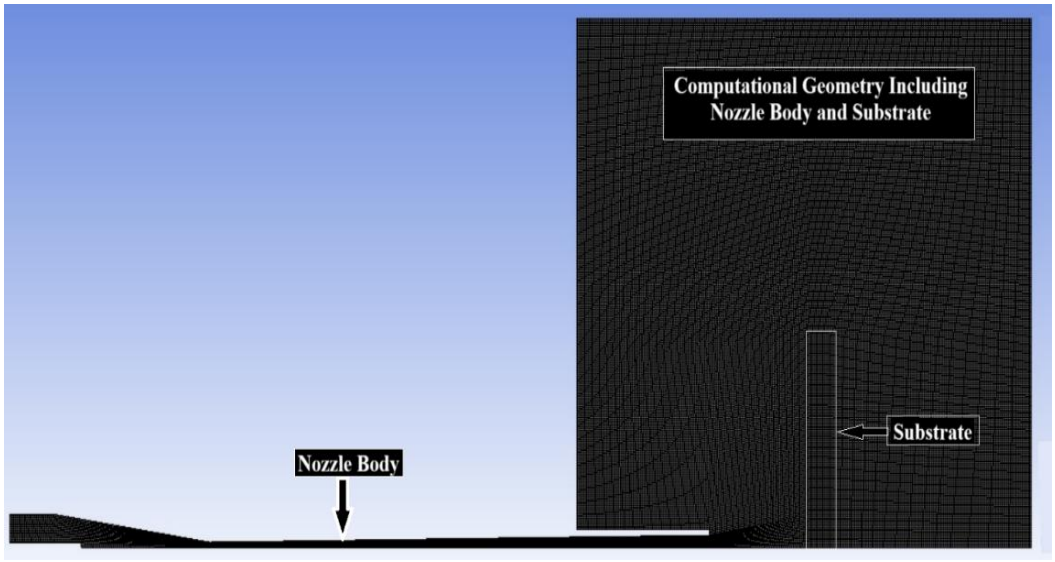

Figure 4.8 Quadrilateral Grid of the Symmetric Geometry's Meshing

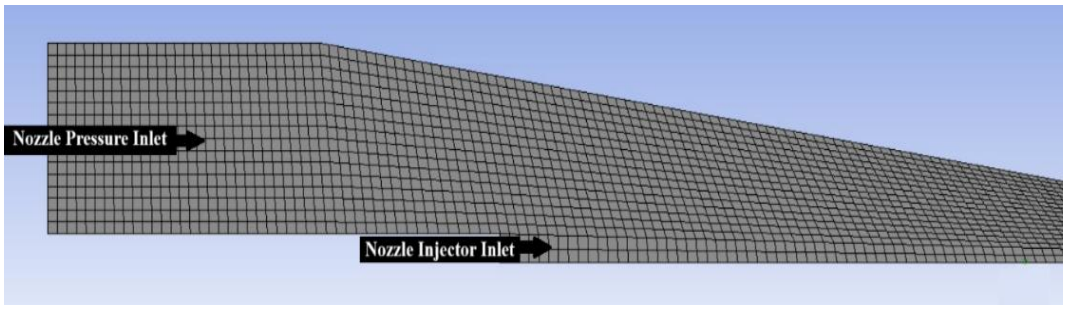

Figure 4.9 Quadrilateral Grid of the Mesh Grid for the Nozzle & Injector Inlet

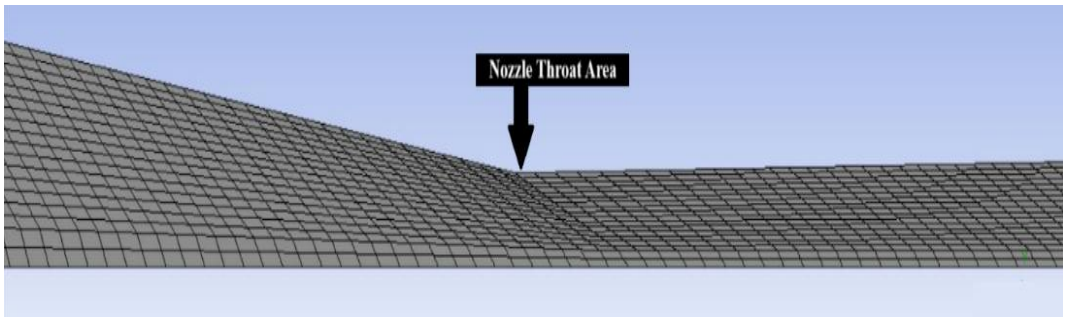

Figure 4.10 Quadrilateral Mesh Grid for the C-D Nozzle Throat Area

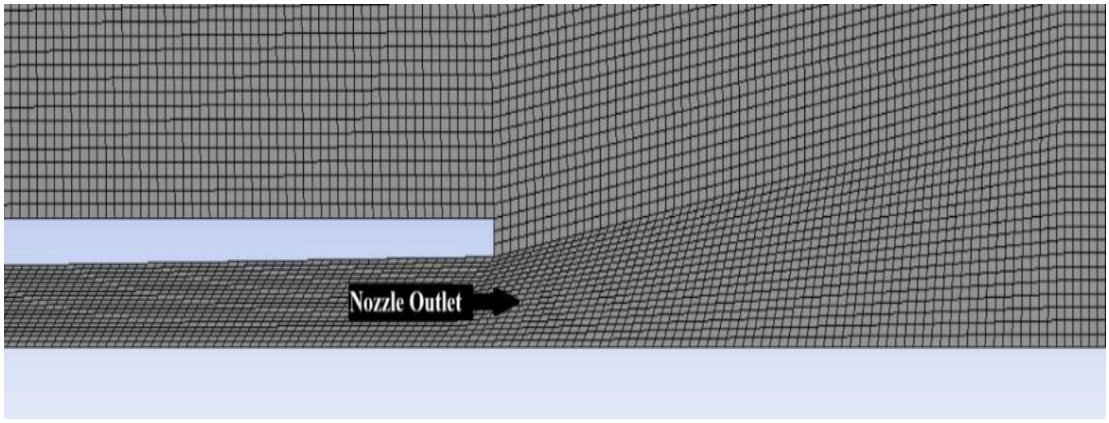

Figure 4.11 Quadrilateral Mesh Grid for the Nozzle Outlet.

In Fig. 4.12, Fig. 4.13, Fig. 4.14, and Fig. 4.15, the geometry shown is of the comprehensive meshing grid of the full geometry for illustration purposes. Still, geometries' symmetry was used in the Fluent workbench for computational work and analysis. The whole mesh grids of the nozzle inlet and the powder particle injector inlet are shown in Fig. 4.12, the nozzle throat area of the full geometry has been shown in Fig. 4.13, the whole mesh grid of the nozzle outlet of the geometry and the stand-off part has been displayed by Fig. 4.14, and the comprehensive mesh grid of the whole exit area of the nozzle including the nozzle outlet area, the substrate, the outer computational field are displayed by Fig. 4.15, where all the meshing grid of the barrel, nozzle, and injector inlet, the nozzle throat area, the meshing geometry of the nozzle outlet, and the meshing grid of the combined geometry including the substrate & outer computational field are used in symmetry for the simulation.

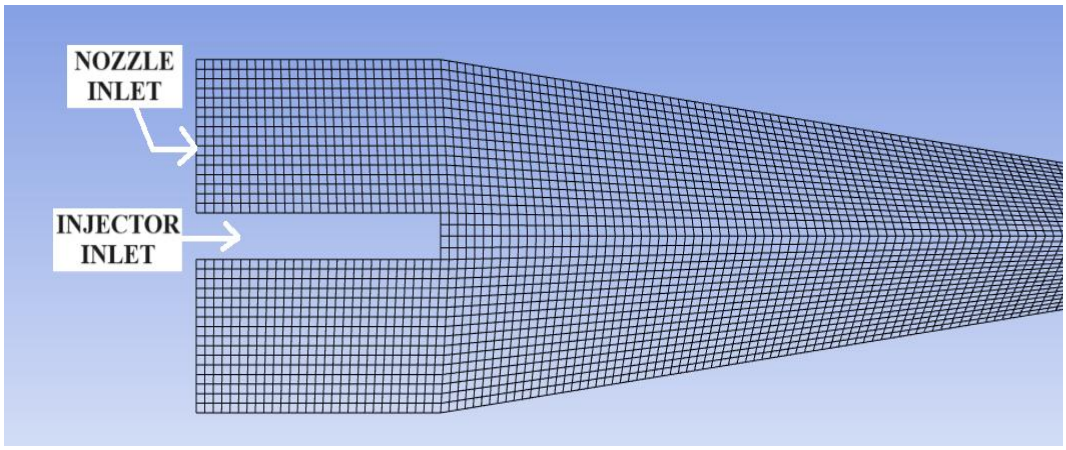

Figure 4.12 The Comprehensive Geometry Meshing Grid of the Nozzle and the Injector Inlet

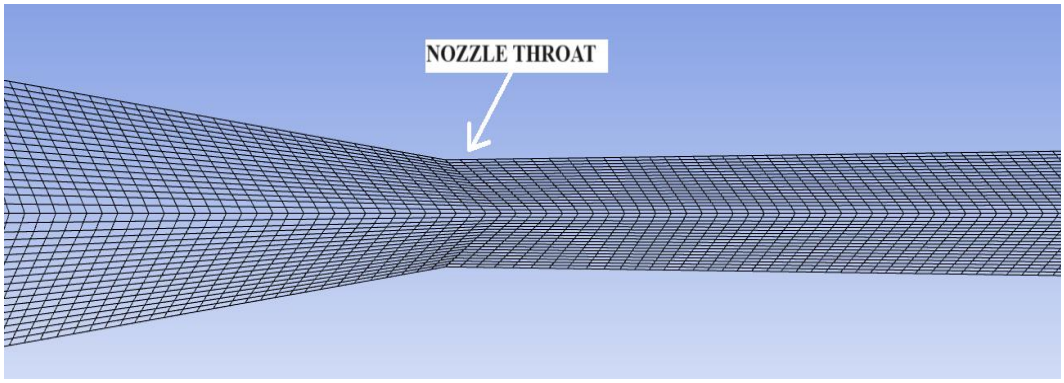

Figure 4.13 The Comprehensive Geometry Meshing Grid of the Nozzle Throat.

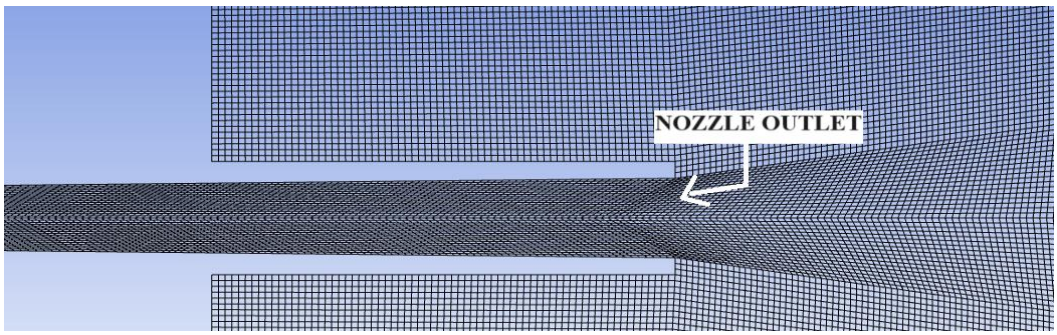

Figure 4.14 The Comprehensive Geometry Meshing Grid of the Nozzle Outlet.

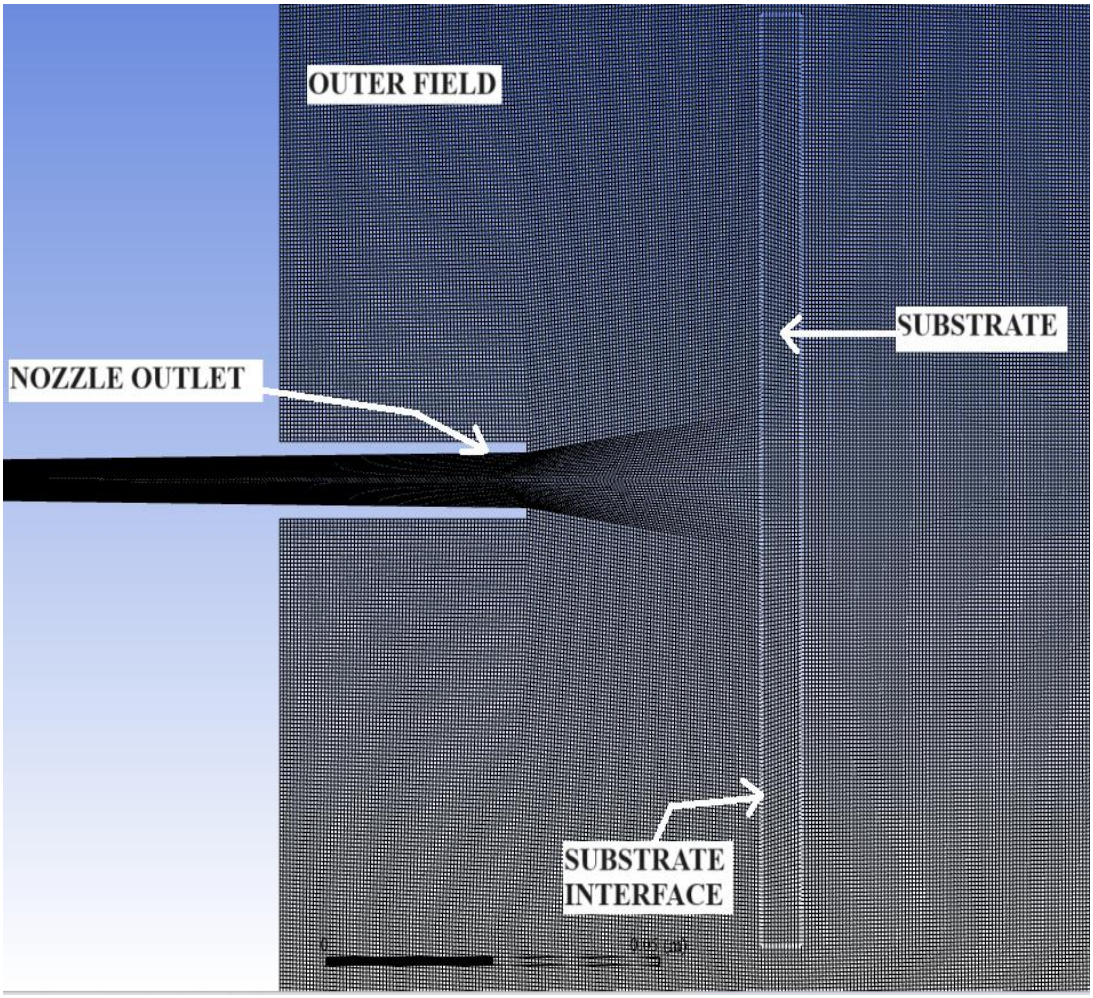

Figure 4.15 The Comprehensive Geometry Meshing Grid of the Substrate & Outer Field of the Whole Geometry.

4.16 Validation of the Computational Work

In our study, we used titanium as the material of choice to calibrate the numerical model. This process involved a detailed comparison of the results derived from our simulations with those obtained from actual experimental measurements.

The maximum percentage error during the whole process was below 5%. As depicted in Fig. 4.16, we could observe the substrate surface's temperature at various points. Upon analysis, it was found that the numerical results exhibited a high degree of agreement with the experimental data. This concurrence validates the precision of the numerical model employed in this simulation study, thereby reinforcing the reliability of our findings Yin et al., [2011].

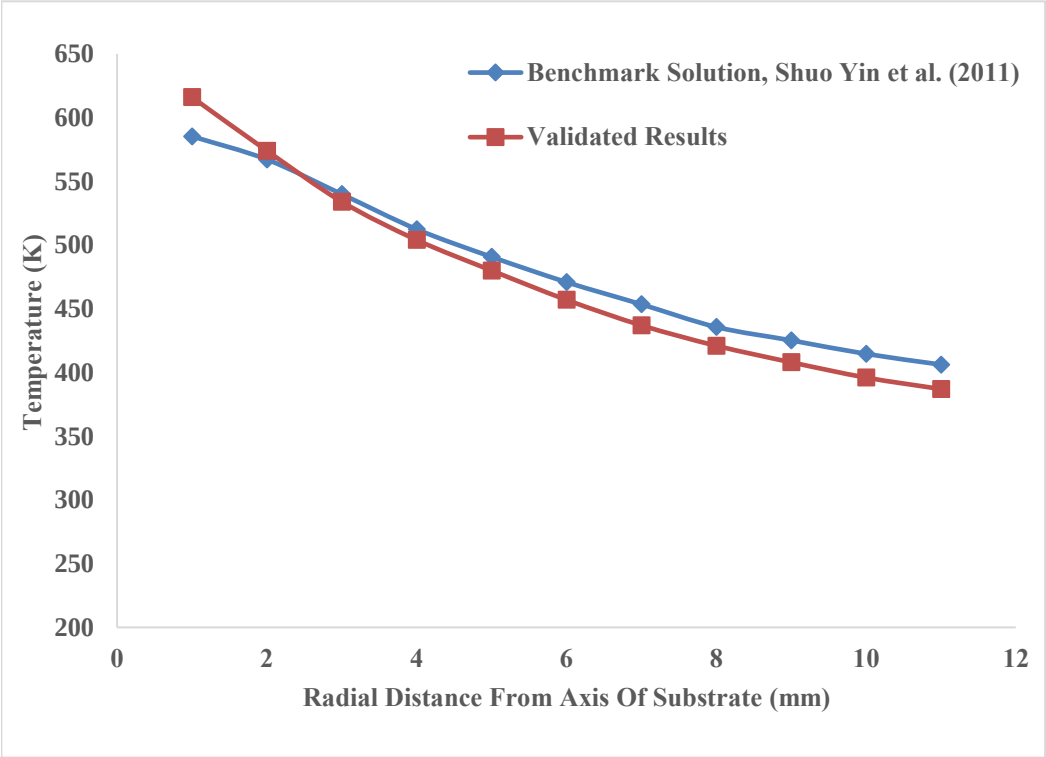

Figure 4.16 Experimental calibration with validated results (Shuo Yin et al. 2011).

CHAPTER 5

RESULTS AND DISCUSSION

The current chapter thoroughly discusses the numerical outcomes of powder material and gases. This chapter is divided into a few sections; the first one includes the velocity distribution near the substrate with a mixture of gasses with varying compositions passed through a convergent, divergent nozzle with coating material particles of varying sizes—The second includes the numerical results of pre-heating of feedstock powder and the impact velocity before impacting the substrate. The third one includes the particle shape and size effects on the velocity and the particle shape and size effects on temperature with significant considerations. Similarly, the impact of stand-off distance on impact velocity and temperature warrants careful examination. The fourth section includes the variation of injector length, computing the effect of the propelling gas type on impact velocity, substrate temperature, and particle temperature. The fifth and last ones include the effect of pressure change, temperature change, particle size, and powder particle speed on the substrate temperature.

5.1 Examination of Coating Material with Different Particle Sizes for Velocity

As discussed in Chapter 4, the cold-spray (CS) process technology setup primarily includes a barrel-convergent-divergent nozzle and a substrate, each with specific geometric parameters. The nozzle features a circular inlet with a diameter of 19 mm and a circular outlet with a diameter of 7 mm. It comprises a convergent section 55 mm long and a divergent section 175 mm long, connected by a throat section with a diameter of 3 mm. At the start of the nozzle, a 15 mm barrel section is attached to stabilize the flow.

For particle injection, a 30 mm-long injector with a diameter of 2.5 mm is positioned 15 mm into the convergent section of the nozzle inlet to introduce the powder particles. The substrate, designed as a rounded plate with a 60 mm radius and 6 mm thickness, is 35 mm from the nozzle outlet. The geometry has symmetrical features to simplify the analysis and facilitate parameter extraction. The subsequent sections discuss the behavior of temperature and velocity at the nozzle outlet and on the substrate, providing insights into the CS coating process parameters.

5.1.1 Computational Field and Boundary Conditions

In this simulation, 2D models with axis symmetry reduce computational time, making the analysis more efficient. Fig. 5.1 illustrates the detailed computational field boundary conditions. Heat transfer between the gas and nozzle walls is neglected, and a pressure inlet of 3 MPa with a temperature of 573 K is

applied at the nozzle inlet. Outside the nozzle outlet, the surrounding atmosphere is considered the outer far-field boundary.

The 2D model is discretized into quadrilateral parts, called cells or nodes, collectively forming the computational grid or field. The grid contains 70,402 cells or nodes for the present geometry, including a fine boundary layer near the substrate to capture interactions accurately. The grid density and cell count vary based on substrate location to ensure detailed results. Key boundary conditions within the grid include a pressure outlet at the computational domain's exit, and the substrate surface is modeled as the interface between gas and solid particles, facilitating accurate fluid-solid coupling. This approach allows for a reliable assessment of interactions between gas flow and the substrate.

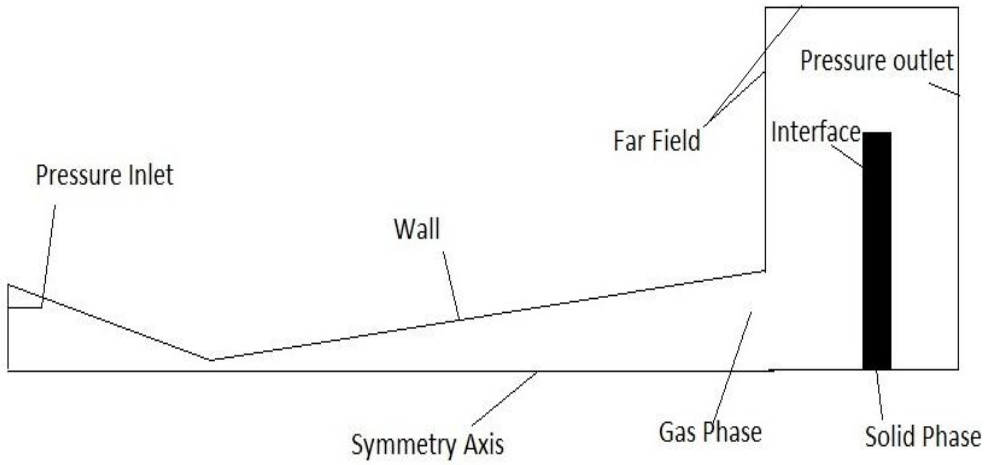

Figure 5.1 Boundary conditions of the geometry

5.1.2 Flow Pitch and Materials Properties

The compressibility effects of the gas phase are considered in this simulation, with air modeled as an ideal gas governed by the ideal gas law. Fundamental equations describe the gas flow, including continuity, momentum, and energy. An implicit, pressure-based solver with second-order precision ensures accuracy when solving the gas flow field. Steady-state conditions are assumed throughout the calculations, and turbulence is modeled using the standard k-ε turbulence model, effectively capturing the turbulent flow characteristics.

The energy equation is included to account for heat transfer in all modes present within the system. The substrate material in this setup is steel, with an initial temperature of 300 K. Key thermal properties for steel used in the simulation include a density of 8030 kg/m³, specific heat capacity of 502.48 J/kg·K, and thermal conductivity of 16.27 W/m·K. These parameters are essential for accurately simulating the fluid-solid interactions and heat transfer processes within the CS system.

C.P. Titanium serves as the coating material at a temperature of 401K. It is utilized with various particle sizes ranging from 20 μm to 100 μm. The material exhibits a 4850 kg/m³ density and a specific heat of 544.25 J/kg K.

5.1.3 Effect of particle size and proportions of the gas mixture

Fig. 5.2 illustrates the velocity distribution close to the substrate, positioned 35 mm from the nozzle outlet. As depicted in Fig. 5.3, the velocity near the substrate gradually decreases from the nozzle throat toward the substrate. This reduction reflects the energy dissipation and interaction of the flow as it approaches the substrate.

Additionally, the inlet gas ratio slightly affects the velocity profile, leading to minor variations in flow dynamics near the substrate. Notably, particles with a diameter of 40 μm exhibit the highest velocity at the nozzle exit, indicating a more efficient acceleration due to their smaller mass. In contrast, particles with larger diameters (60 μm, 80 μm, and 100 μm) show reduced velocities along the nozzle centerline, suggesting that larger particles encounter greater resistance and achieve lower speeds when they exit the nozzle. This variation underscores the impact of particle size on velocity, which is critical for optimizing particle deposition and coating quality in the CS process.

The velocity measurements at the nozzle exit and near the substrate show that using pure oxygen (0% nitrogen) as the propelling gas results in minimal velocity. In comparison, pure nitrogen (0% oxygen) achieves the highest velocity. Table 5.1 presents the velocities near the substrate for different particle sizes,

highlighting how gas composition influences particle acceleration and impact velocity.

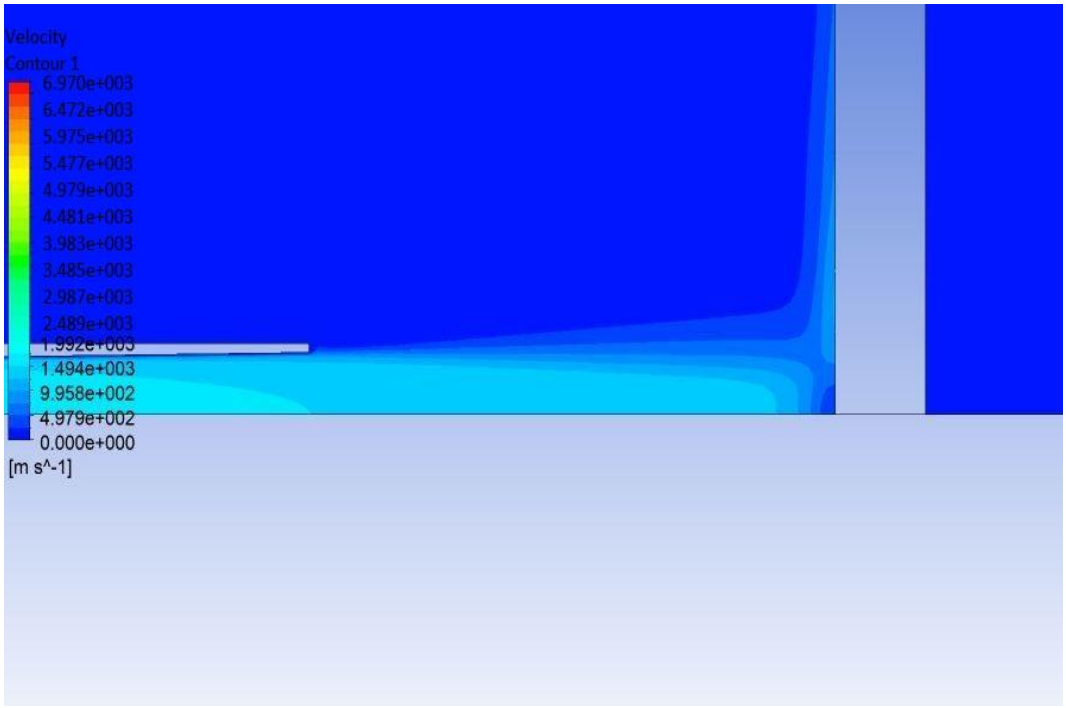

Figure 5.2 Velocity contour at the nozzle outlet at a stand-off distance of 35 mm.

The data further suggest that commercially pure titanium (C.P. Ti) particles within the 20 µm to 50 µm range attain optimal velocities for cold-spray (CS) coating. This size range appears ideal, as these particles achieve sufficient velocity to enhance deposition efficiency and coating quality. Thus, combining pure nitrogen as the propelling gas and particle sizes of 20–50 µm for C.P. Ti proves most effective for CS applications.

Table 5.1 Velocity of different particle sizes and proportions of the gas mixture

Gas Mixture Ratio (N_2: O_2)	**The velocity with particle size 20 µm**	**The velocity with particle size 40 µm**	**The velocity with particle size 60 µm**	**The velocity with particle size 80 µm**	**The velocity with particle size 100µm**
00:01	485	492	478	477	478
02:08	489	499	485	485	485
04:06	491	506	491	490	491
06:04	512	513	497	498	498
08:02	519	519	504	504	503
01:00	525	525	510	510	510

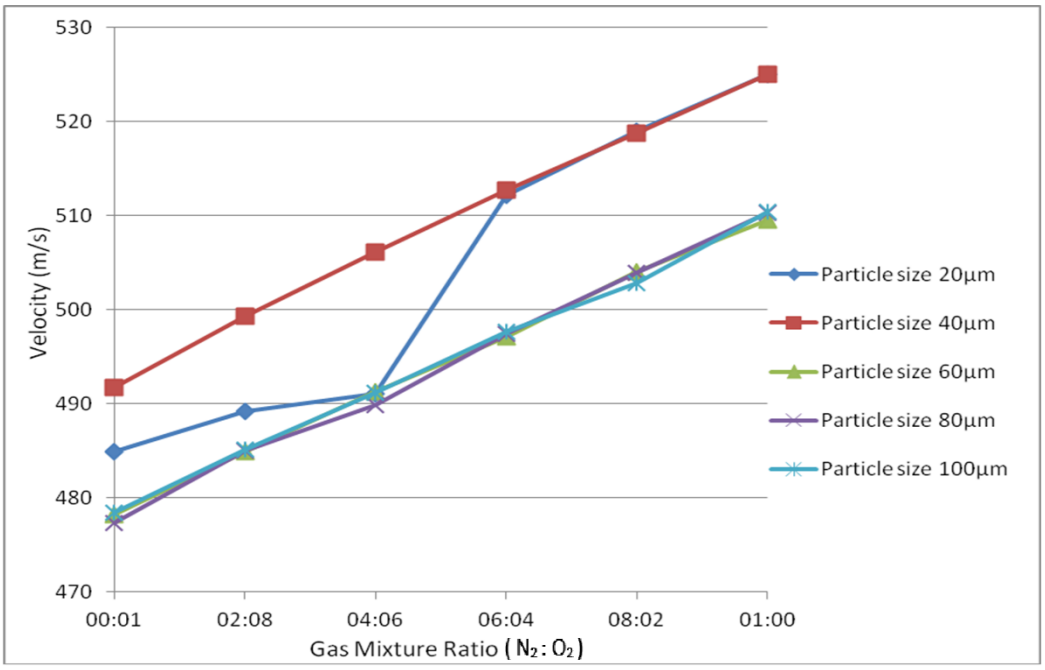

Figure 5.3 Velocity variations with different particle sizes and gas mixture proportions.

5.2 Simulation for Powder Pre-Heat and Impact Velocity

As detailed in Chapter 4, the setup for cold-spray (CS) process technology primarily involves a convergent-divergent nozzle and a substrate, each defined by specific geometric parameters. The nozzle features a circular inlet with a diameter of 19 mm and a circular outlet with a diameter of 7 mm. It includes a 55 mm convergent section and a 175 mm divergent section connected by a 3 mm diameter throat. A 15 mm barrel section is attached at the nozzle's entrance to stabilize the gas flow.

The particle injector, measuring 30 mm in length and 2.5 mm in diameter, is positioned 15 mm into the convergent section of the nozzle inlet. The substrate is modeled as a circular plate with a radius of 60 mm and a thickness of 6 mm, positioned 25 mm from the nozzle outlet to enable efficient deposition of coating material. The geometry is symmetrically built to simplify the simulation and capture crucial aspects of the CS coating process.

The impact velocity and pre-heat temperature fluctuations close to the substrate are examined in the following sections, considering various gas combinations and pressure levels. These parameters are critical in determining coating quality because they affect the CS process's particle acceleration, adhesion, and overall deposition efficiency.

5.2.1 CFD Analysis and Boundary Conditions

The impact velocity and pre-heat temperature were simulated using the conventional k-ε turbulence model with a non-equilibrium wall function. The feedstock material for the CS coating system in this model was titanium powder, and boundary conditions and a computational field controlled the particle flow.

The computational domain's pressure outlet was set at 0.1 MPa to simplify fluid-solid connection recognition. Variable pressure values between 3 and 7 MPa and various nitrogen and helium gas mixture ratios were applied at the nozzle inlet. Pure helium and nitrogen at different pressures were also included in the simulations, with a constant inlet temperature of 575 K.

Boundary constraints were consistently imposed throughout the simulation region to allow the gas to flow over boundaries in any direction. The interaction between the solid walls and the gas was assumed to be frictionless, resembling a free-slip wall boundary condition, which reduces the complexity of wall effects and enhances the model's focus on particle behavior and impact dynamics. This setup provides a robust framework for analyzing how gas composition, inlet pressure, and pre-heat temperature impact coating deposition in the CS process.

5.2.2 Governing Equations and Material properties

The effect of compressibility was incorporated into the model using air as the gas phase, governed by the ideal gas law. Equations of continuity, momentum, and energy were used to characterize the gas flow. The gas flow field was properly simulated using a second-order precision, implicit pressure-based

solver. The calculations assumed steady-state conditions, and the standard k-ε model was applied to account for turbulence in the flow.

The energy equation was used to determine heat transfer, and titanium particles were used as the feedstock material. The particles were delivered at a temperature of 475 K under changing pressure circumstances. The titanium particles were 10 µm in diameter, 4850 kg/m³ in density, and 544.25 J/kg·K in specific heat. Steel was designated as the substrate material with a surface temperature of 300 K, a density of 8030 kg/m³, a specific heat of 502.48 J/kg·K, and a thermal conductivity of 16.27 W/m·K. This configuration allows for a thorough examination of heat transport and particle behavior in the CS process, emphasizing how material characteristics, compressibility, and turbulence affect coating results.

5.2.3 Effect of Impact Velocity and Pre-Heat Temperature with Varying Pressure and Gas Mixtures

Fig. 5.4 and Fig. 5.5 illustrate how impact velocity and feedstock powder's pre-heating influence the substrate's deposition. The substrate was positioned at a stand-off distance of 25 mm from the nozzle outlet, with initial parameters set as previously defined. As shown in Fig. 5.6 and Table 5.2, the results highlight the role of pressure and gas mixture in determining impact velocity.

Figure 5.4 Impact Velocity contour at a stand-off distance of 25 mm.

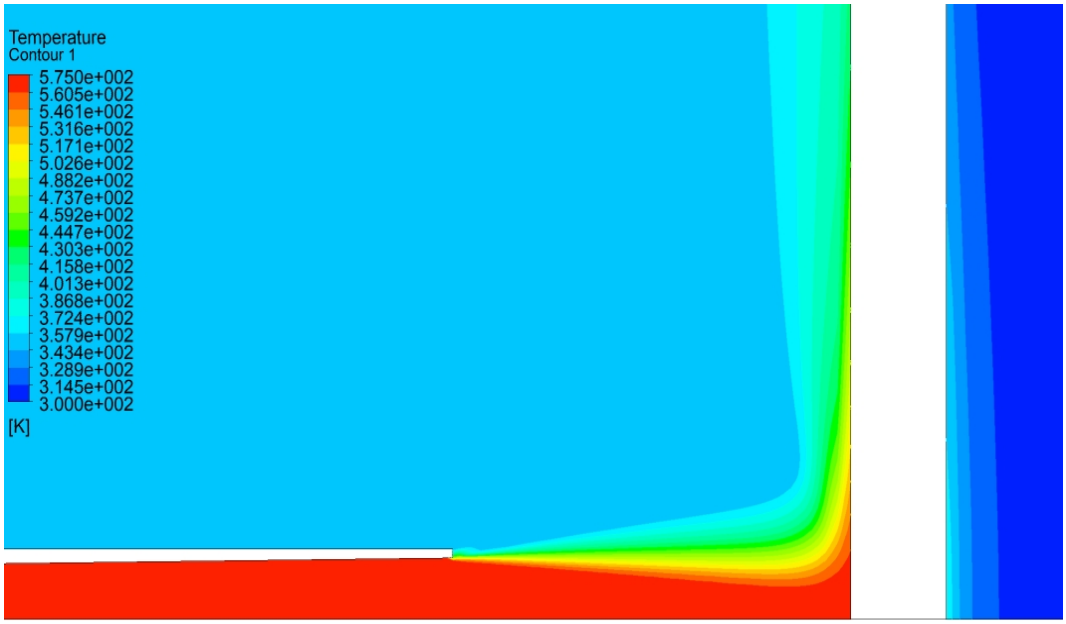

Figure 5.5 Pre-heat temperature contour at a stand-off distance of 25 mm.

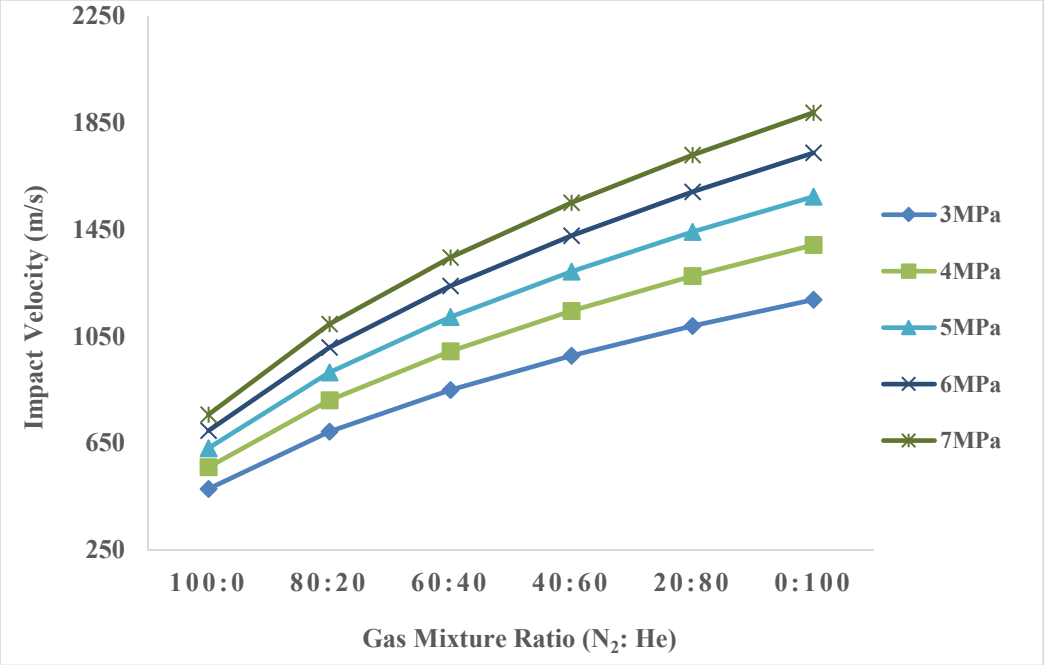

Figure 5.6 Impact velocity variations with varying pressure and gas mixture.

The impact velocity was relatively low across different pressure levels with pure nitrogen as the propellant gas. In contrast, the helium addition significantly enhanced the impact velocity; even a modest 20% helium concentration in the gas mixture led to a substantial increase in impact velocity. The impact velocity peaked across varying pressures with pure helium, underscoring its effectiveness in accelerating particle speed due to its lower molecular weight and greater compressibility. These observations emphasize the critical role of gas composition in optimizing impact velocity and, consequently, coating quality in the Cold Spray process.

Table 5.2 Impact Velocity (m/s) of feedstock particles with varying pressures and gas mixtures.

Gas Mixture Ratio (N_2: He)	Impact Velocity (3MPa)	Impact Velocity (4MPa)	Impact Velocity (5MPa)	Impact Velocity (6MPa)	Impact Velocity (7MPa)
100:0	478.84	559.71	631.35	696.46	756.69
80:20	693.12	810.67	914.52	1008.78	1095.79
60:40	849.54	994.28	1122.06	1237.89	1344.91
40:60	977.66	1145.11	1292.92	1426.80	1550.20
20:80	1088.16	1275.57	1440.65	1590.41	1728.25
0:100	1186.92	1391.77	1572.58	1736.40	1887.27

Fig. 5.7 and Table 5.3 demonstrate the impact of gas mixture concentration and pressure variation on powder particle behavior regarding pre-heat temperature. At lower pressures, introducing helium causes a consistent reduction in the pre-heat temperature of the particles, suggesting that helium's thermal conductivity influences heat transfer at these pressure levels.

As the pressure increases, the pre-heat temperature rises when helium is introduced at a concentration of 20% (with the remaining 80% nitrogen). However, the temperature decreases progressively beyond this concentration,

reaching its lowest values with pure helium. It indicates that while helium contributes to higher impact velocity, it affects thermal transfer differently at various pressures, influencing the pre-heat temperature dynamics. Additionally, an increase in inlet pressure reveals a decline in the effectiveness of pure nitrogen for achieving high pre-heat temperatures. The highest pre-heat temperature observed was at 7 MPa, with a gas mixture of 80% nitrogen and 20% helium. This combination thus appears optimal for maximizing particle pre-heat temperature, which can positively impact coating properties by enhancing particle deformation and bonding strength upon impact.

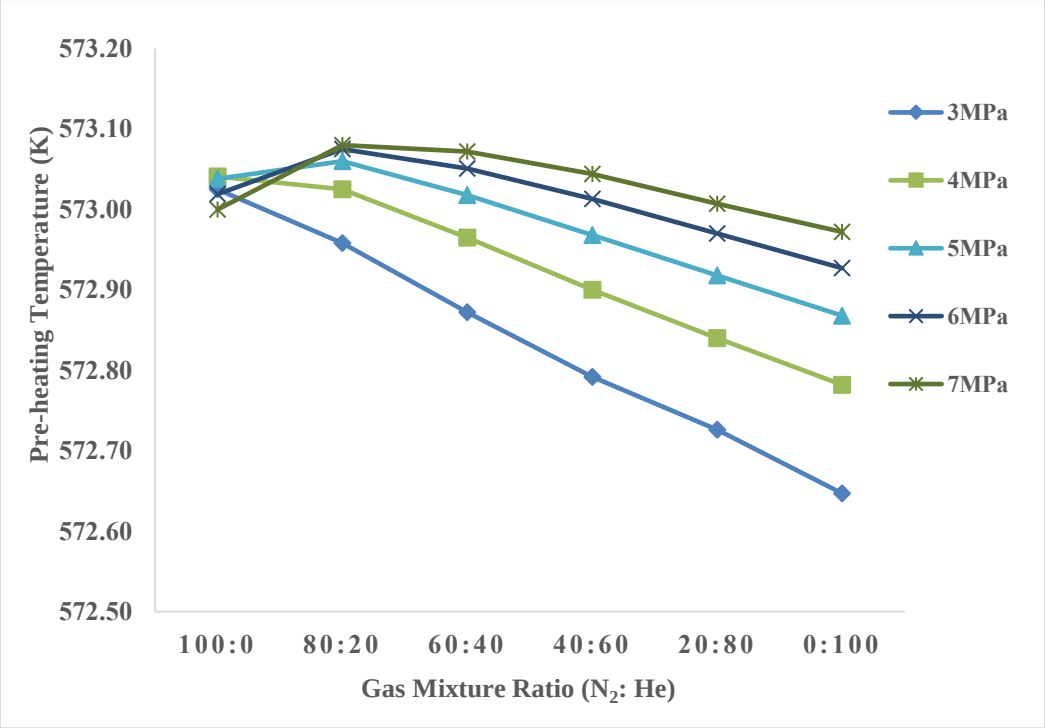

Figure 5.7 Pre-heating temperature variations with varying pressure and gas mixture concentrations.

The study's conclusion suggests that a pressure of 7 MPa is optimal for achieving high impact velocity and pre-heat temperature. Pure helium is the most effective gas or gas mixture for achieving maximum impact velocity. However, using pure helium results in a lower pre-heat temperature. On the other hand, a gas mixture comprising 80% (N_2) and 20% (He) yields the highest pre-heat temperature. Furthermore, simulation modeling reveals that larger feedstock powder particles attain higher temperatures than smaller particles and may experience slight acceleration outside the nozzle. The simulations also enumerated the advances in the deposition efficiency with pre-heat of feedstock powder before impact Faizan-Ur-Rab et al., [2016].

Table 5.3 Pre-heat temperature with varying pressures and gas mixtures.

Gas Mixture Ratio (N_2: He)	**Pre-Heat Temp. (3MPa)**	**Pre-Heat Temp. (4MPa)**	**Pre-Heat Temp. (5MPa)**	**Pre-Heat Temp. (6MPa)**	**Pre-Heat Temp. (7MPa)**
100:0	573.03	573.04	573.04	573.02	573.00
80:20	572.96	573.03	573.06	573.08	573.08
60:40	572.87	572.97	573.02	573.05	573.07
40:60	572.79	572.90	572.97	573.01	573.04
20:80	572.73	572.84	572.92	572.97	573.01
0:100	572.65	572.78	572.87	572.93	572.97

5.3 Analysis of Particle Shape and Size on Impact Velocity and Effect of Stand-off Distance

As discussed in Chapter 4, for analysis of particle shape and size on impact velocity, the geometry used is shown in Fig. 4.3. For the effect of stand-off distance, the distance varied from 15 mm to 45 mm with an interval of 10mm. The injector length & the diameter, nozzle inlet, and nozzle outlet were the same.

5.3.1 Governing Equations and Material properties

The gas phase behavior adheres to the ideal gas law, accounting for compressibility effects. Gas flow is governed by continuity, energy, and momentum equations, crucial for gas flow dynamics. The simulation employs a gas mixture of nitrogen and helium in a 40%:60% ratio (N_2: He). Copper metal particles of various shapes and sizes are used with a density of 8978 kg/m^3 and specific heat (Cp) of 381 J/kg-K. Particle shapes include spherical and non-spherical (SF=0.8), resembling crushed sandstone, ranging in size from 15 µm to 60 µm. The substrate material, steel, maintains a temperature of 300 K, with a density of 8030 kg/m^3, specific heat (Cp) of 502.48 J/kg-K, and thermal conductivity of 16.27 W/m-K.

CFD analysis, conducted using ANSYS software, explores the influence of particle shape, size, and stand-off distance on the CS process. The propelling gas enters at 675 K and 15 bar, while particle inlet conditions are set at 325 K and 1 bar.

The CS process simulation uses a pressure-based, axisymmetric numerical model. This simulation employed the two-equation Realizable k-ε turbulence model with standard wall functions, selected for its enhanced realism and accuracy in representing turbulent flow characteristics compared to other available models. The Realizable k-ε model effectively captures the complexities of particle-gas interactions and flow behavior within the CS process, making it a reliable choice for simulating the high-velocity impacts and turbulent flow dynamics characteristic of Cold Spray technology. This model enables detailed analysis of particle deposition behavior, coating quality, and the influence of varying parameters, supporting optimized process development.

Previous studies utilized 3-7 MPa pressures to optimize impact velocity for 10 µm particles. However, this study employs a pressure of 15 bar (1.5 MPa), varying particle shape and size. It aims to elucidate the impact of particle shape on velocity and temperature.

5.3.2 Effect of shape and size on impact velocity and temperature

The simulation analyses for impact velocity and temperature of particles, varying in shape and size, are showcased in Fig. 5.8 and Fig. 5.9. These figures offer a comprehensive view of the simulation results, which are further illustrated graphically in Fig. 5.10 and Fig. 5.11. Noteworthy is the discernible difference observed between spherical and non-spherical particle shapes, with spherical particles exhibiting notably higher velocities and temperatures. This discrepancy underscores the significant potential impact of particle shape on the quality of coatings, particularly in aspects such as porosity, hardness, and bond strength.

Figure 5.8 Velocity contour near the substrate

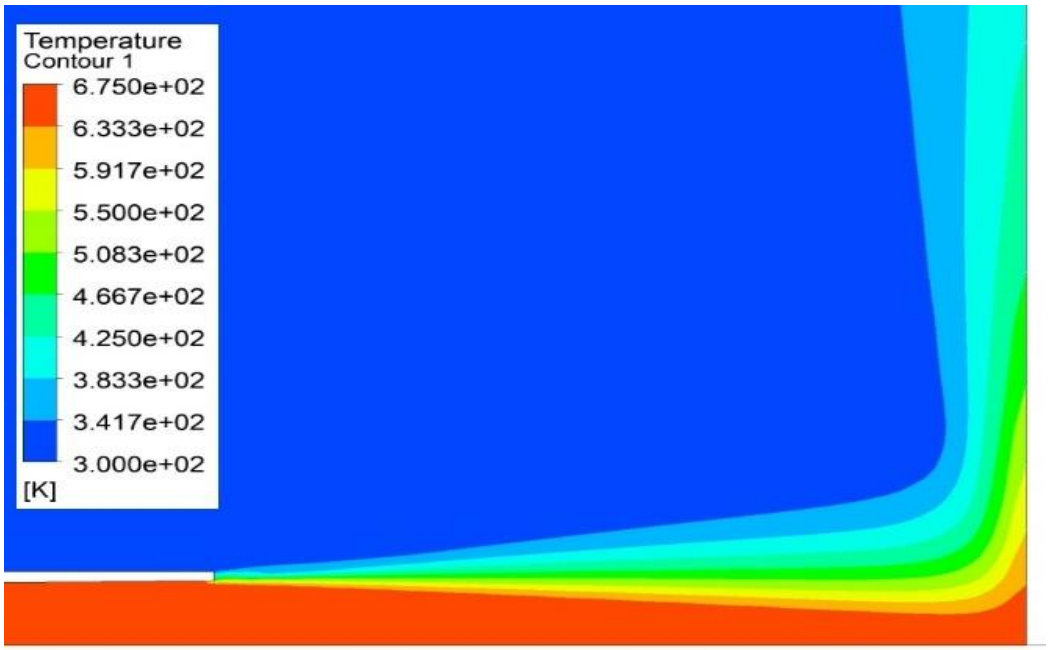

Figure 5.9 Temperature contour near the substrate

The specific impact velocities and temperatures of particles immediately before striking the substrate are delineated in Fig. 5.10 and Fig. 5.11. Here, spherical particles are recorded to have velocities of 1259.03 m/s and temperatures of 671.06 K at the substrate. In comparison, their non-spherical counterparts exhibit velocities of 1211.87 m/s and temperatures of 621.81 K. Consequently, spherical particles possess a higher impact velocity and temperature than non-spherical particles. It's worth noting that all simulations involving different particle shapes were conducted using a geometry with a 25 mm stand-off distance.

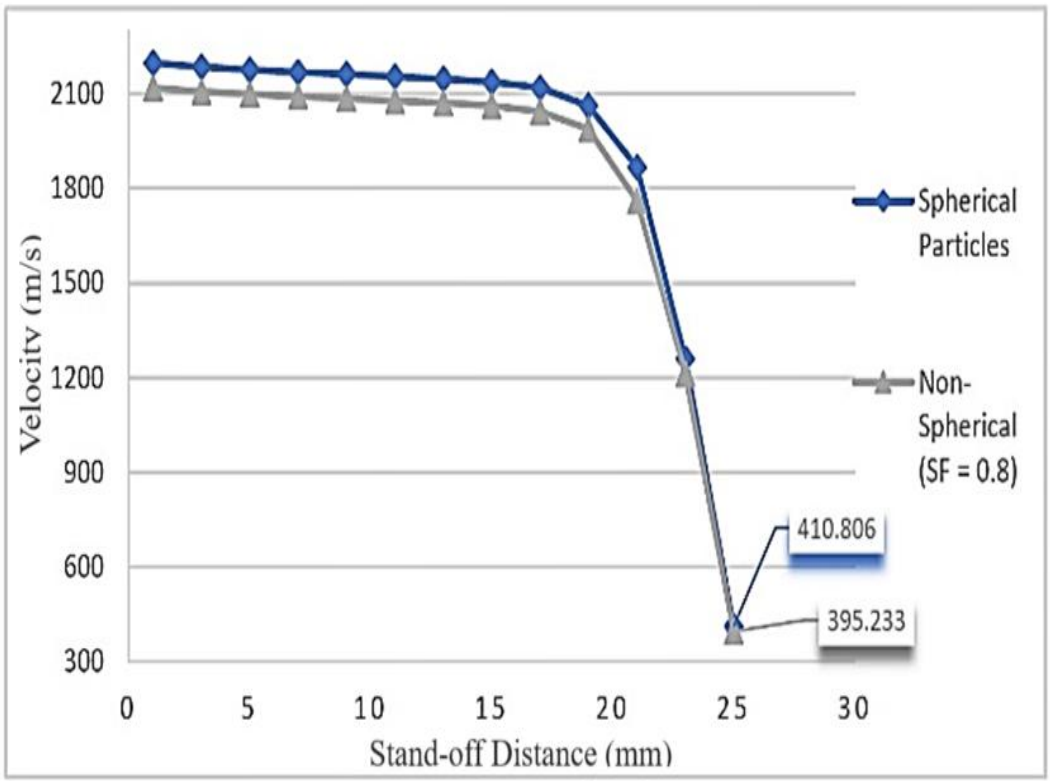

Figure 5.10 Effect of Particle Shape on Velocity

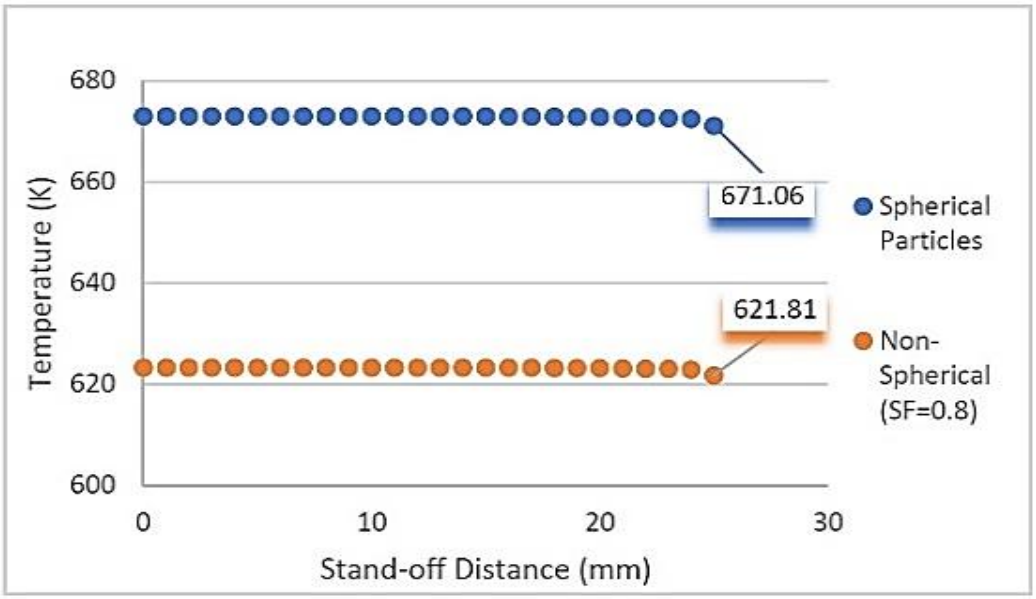

Figure 5.11 Effect of Particle Shape on Temperature

5.3.3 Effect of stand-off distance on impact velocity and temperature

The analysis of stand-off distance on the impact velocity and temperature of powder particles yielded distinct results, as shown in Fig. 5.12 and Fig. 5.13. The impact velocities recorded at stand-off distances of 15 mm, 25 mm, 35 mm, and 45 mm were 1234.84 m/s, 1259.03 m/s, 1325.06 m/s, and 1110.85 m/s, respectively. These values suggest that the highest impact velocity occurs at a 35 mm stand-off distance, while the lowest is at 45 mm.

For spherical and non-spherical particles, final impact velocities measured on the substrate surface were 403.806 m/s, 410.806 m/s, 443.216 m/s, and 381.448 m/s for 15 mm, 25 mm, 35 mm, and 45 mm stand-off distances, respectively. These results indicate that a 35 mm stand-off distance yields the highest particle velocity upon impact, supporting optimal coating conditions due to the increased deformation energy at the substrate.

The analysis also revealed that particle temperature increases with greater stand-off distances, likely due to extended exposure to the heated gas stream. The combination of velocity and temperature shows that a 35 mm stand-off distance is most efficient for Cold Spray coating, as it balances high impact velocity and favorable particle temperature, maximizing coating quality and adhesion.

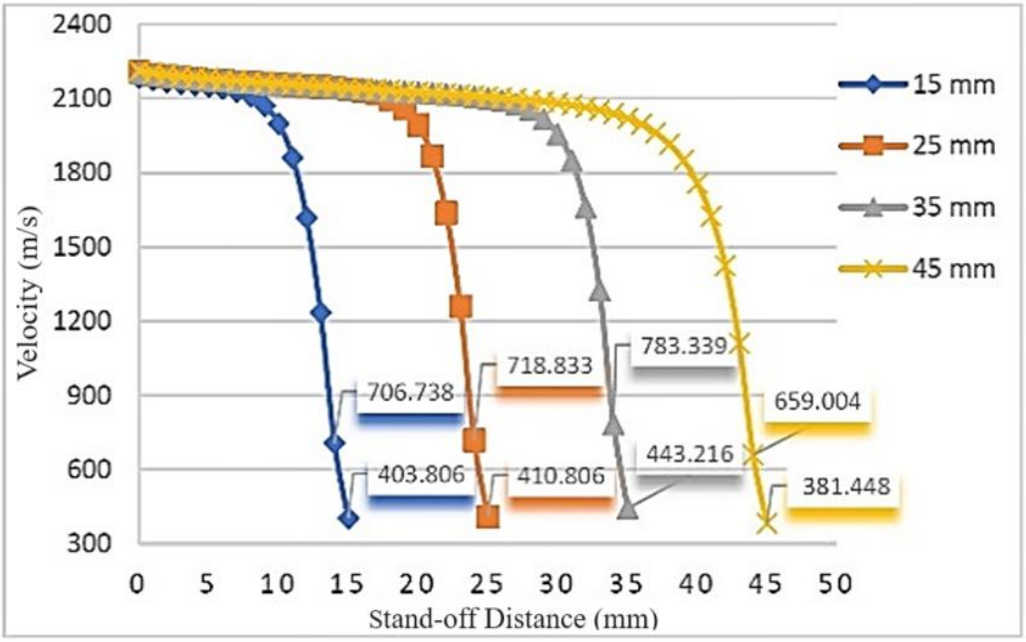

Figure 5.12 Effect of Stand-off Distance on Velocity

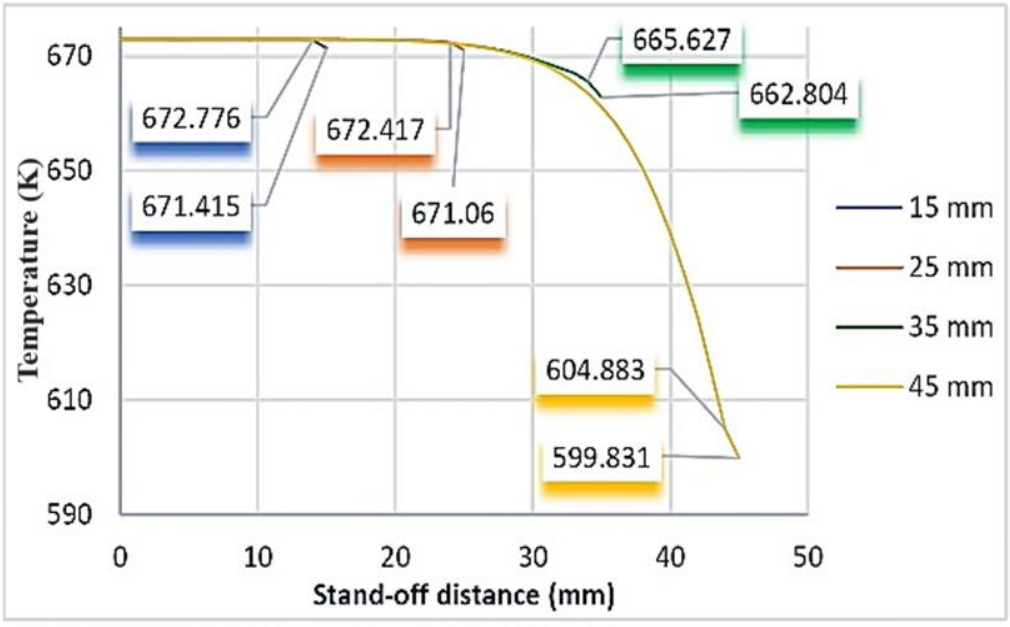

Figure 5.13 Effect of Stand-off Distance on Temperature

5.4 Simulation of Cold Spray Coating for Optimal Injector Length

As discussed in Chapter 4, for optimal injector length, the length of the injector varies from 15 mm to 30 mm with an interval of 5 mm without changing the injector diameter and nozzle dimensions, keeping other parameters same for impact velocity, substrate temperature and particle temperature with varying injector lengths and for different mixture of gasses.

5.4.1 Effect of gas type on optimization of particle injector length

The optimization of particle injector length in a gas-based Cold Spray (CS) system is influenced by factors such as the propelling gas. Fig. 5.14 shows particle impact velocity varies with injector length across different gas types—specifically, pure nitrogen, pure helium, and a 40% nitrogen to 60% helium mixture. The results indicate pure helium yields the highest particle impact velocity, while pure nitrogen produces the lowest. This variance is primarily due to the differing densities of the gases; helium’s lower density allows particles to reach higher velocities compared to nitrogen.

In addition, there is a nonlinear relationship between injector length and particle velocity. The particle impact velocity initially decreases as the injector length increases, reaching a minimum at a particular length. The particle velocity then rises in tandem with the injector length. Particle-gas interaction time and gas expansion dynamics may be to blame for this behavior, which suggests a minimum injector length. After reaching this ideal length, particles may re-accelerate as they pass through the injector, possibly due to additional energy transfer.

Understanding the relationship between injector length and gas type and the energy given to particles during the CS process is essential for maximizing particle impact velocity and obtaining desired coating characteristics.

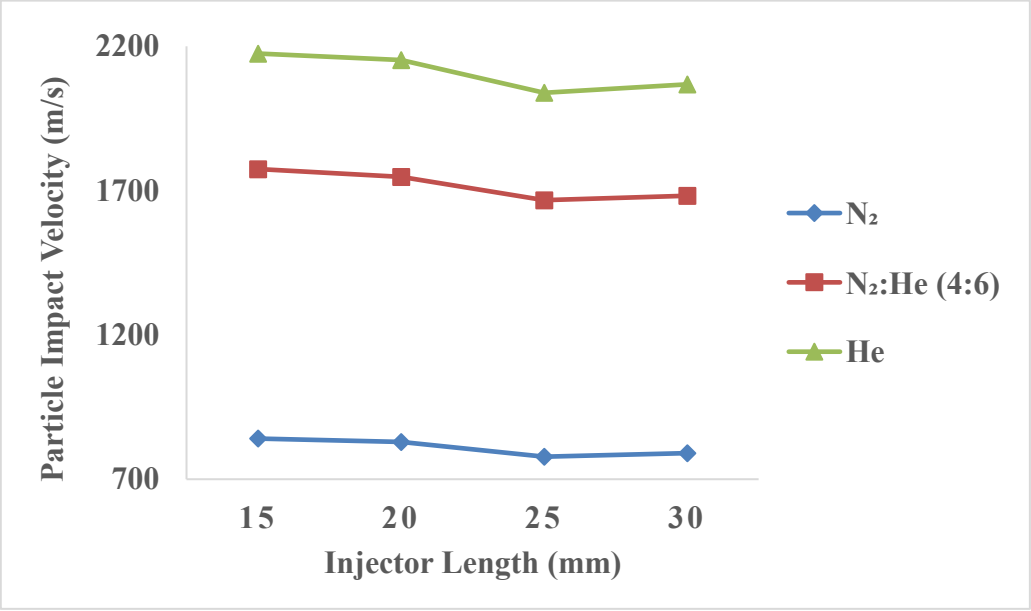

Figure 5.14. Effect of Propelling Gas Type on Impact Velocity with Varying Injector Length

According to the findings, injector length and gas type have a significant impact on substrate surface temperature and particle impact velocity in the Cold Spray (CS) method. When using various gases, including pure nitrogen, pure helium, and a mixture of nitrogen and helium, the particle impact velocity demonstrates a distinct pattern as the injector length shifts from 15 mm to 30 mm. The shortest injector length of 15 mm yields the maximum particle velocity, especially when pure helium is used. As injector length increases, particle velocity decreases, reaching a minimum of 30 mm before beginning to rise again, suggesting an optimal range where velocity modulation aligns with energy transfer dynamics in the gas stream.

In addition, Fig. 5.15 illustrates how substrate surface temperature responds to changes in injector length across different gases. The optimal injector length for achieving the desired surface temperature shifts from 15 mm to 30 mm, depending on the gas type. Notably, between 20 mm and 30 mm injector lengths, the substrate surface temperature approaches optimal under each gas condition. However, the highest temperature is recorded at 15 mm, aligning with the point of maximum impact velocity for helium.

Interestingly, the substrate temperature and particle temperature appear to increase as injector length grows, with this effect varying according to gas type. This correlation between injector length, gas type, and temperature suggests that adjusting injector parameters can fine-tune the CS process. Optimal injector length

balances high impact velocity and substrate temperature, enhancing particle bonding and coating quality for diverse applications.

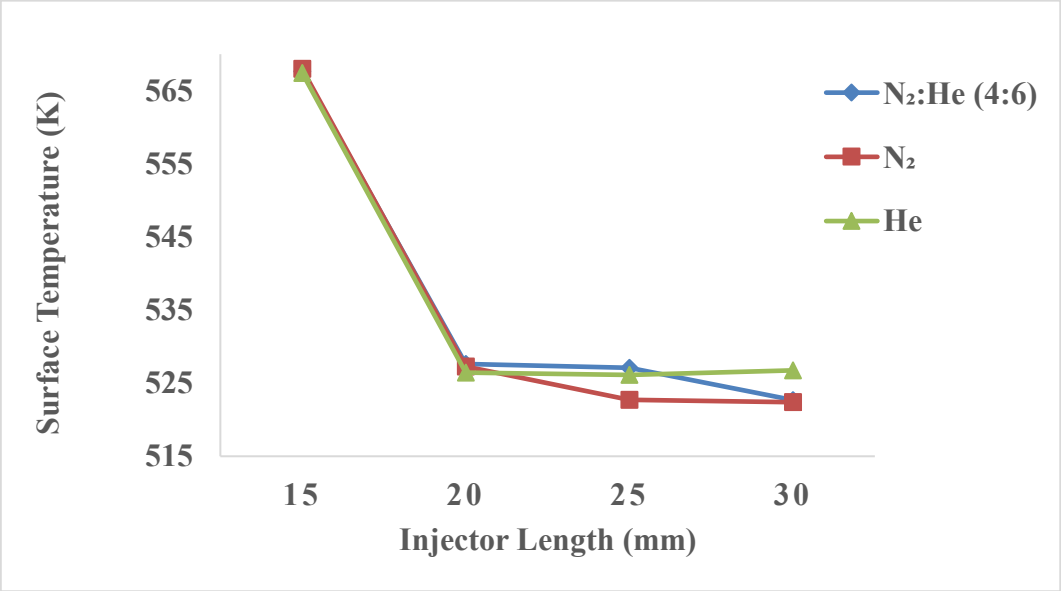

Figure 5.15. Effect of Propelling Gas Type on Substrate Temperature with Varying Injector Length

The analysis reveals that particle temperature in the CS process varies with injector length, reaching its peak at the shortest injector length of 15 mm, decreasing to a minimum at 25 mm, and rising slightly again at 30 mm, as depicted in Fig. 5.16. This pattern suggests an optimal injector length range where heat transfer to particles is minimized, possibly due to reduced residence time in the heated gas flow.

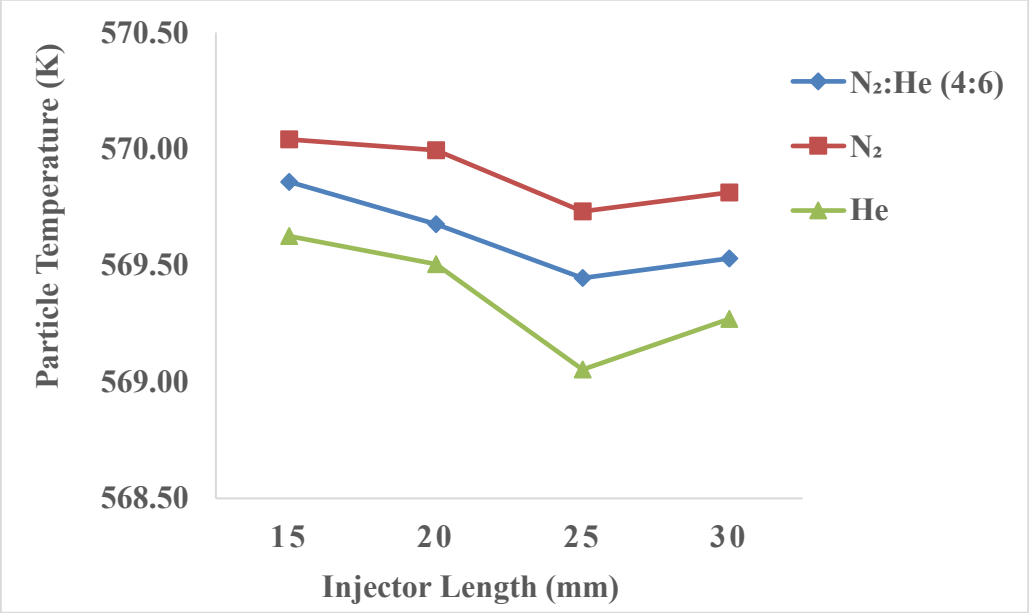

Figure 5.16. Effect of Propelling Gas Type on Particle Temperature with Varying Injector Length.

5.5 Effect of Process Parameters on the Substrate Surface

As discussed in Chapter 4, this exploration aims to identify the optimal length for the particle injector that would yield the highest possible particle velocity. It is a crucial aspect of our study as it directly influences the effectiveness of the process under investigation. To study the influence of various factors, we analyzed under different gas conditions, particle sizes, pressure and temperature conditions, etc. In some simulations, we fixed the nozzle dimensions and varied the injector length from 15mm to 30mm with 5mm increments. We also varied the pressure, temperature, propelling gas, particle size, and speed/velocity in each simulation.

The substrate reached the maximum temperature at its center. Therefore, we took all the observations at the center.

5.5.1 Simulation Parameters

ANSYS (Fluent) software was used to predict different parameters to optimize the best possible injector length. In the process of computational analysis, the domain under consideration was systematically divided into multiple quadrilateral cells to facilitate precise calculations and simulations. To attain a grid-independent solution, employing various cells, ranging from 75,000 to 125,000, within the computational domain was necessary. The most likely number of cells, which embraces nodes and elements, stayed at 96210 and 94926, respectively. The pressure and temperature of propelling gases were 3 MPa and 573 K, respectively, at the nozzle inlet. The pressure and temperature at the outlet of the computational domain were taken just above the atmospheric pressure 1 MPa and 300 K (likely a hot day), respectively, to stop the external influence, if any. Following the standard no-slip condition, it was assumed that both the wall of the nozzle and the substrate surface would exhibit zero velocity about the fluid, implying that there would be no relative motion between them and the fluid. The boundary of the nozzle was considered ideal, i.e., no heat flow through the wall was considered.

A study state solution was obtained using an implicit pressure-based solver in ANSYS Fluent workbench with second-order precision. We used the ideal gas law to compute the gas properties and assumed a constant density. In our study, we applied the standard k–ε turbulence model, a feature of computational fluid dynamics software FLUENT, to accurately simulate the turbulent flow conditions. The ability of this model to accurately depict the intricate behavior of turbulent flows is well known. We also used the standard wall function to deal with flow situations near the wall. Our decision was based on its dependability in managing near-wall flow dynamics, ensuring an accurate simulation of the flow field. To investigate the effects of applied pressure on the temperature and velocity of pushing gases through the nozzle intake and particle inlet, we performed simulations on titanium particles.

Additionally, we investigated the effects of temperature, particle size, and particle velocity on the nozzle injector's length. This thorough approach increased our comprehension of the dynamics in our setup. We examined the cold coating method using an axisymmetric model with different injector lengths. The substrate and the nozzle were positioned 35 mm apart and horizontally. We sprayed 40 µm-diameter spherical titanium powder particles. In our simulations, the particles were initially set to a velocity and temperature of 40 m/s and 300 K, respectively. The outcomes were assessed at a 35 mm stand-off distance from the exit of the nozzle.

This exploration aims to identify the optimal length for the particle injector that would yield the highest possible particle velocity. That is a crucial aspect of our study as it directly influences the effectiveness of the process under investigation. To study the influence of various factors, we analyzed under different gas conditions, particle sizes, pressure and temperature conditions, etc. In some simulations, we fixed the nozzle dimensions and varied the injector length from 15mm to 30mm with 5mm increments. We also varied the pressure, temperature, propelling gas, particle size, and speed/velocity in each simulation. The substrate reached the maximum temperature at its center. Therefore, we took all the observations at the center. Fig. 5.17 gives the temperature distribution of the substrate with injector lengths of 15 mm to 30 mm.

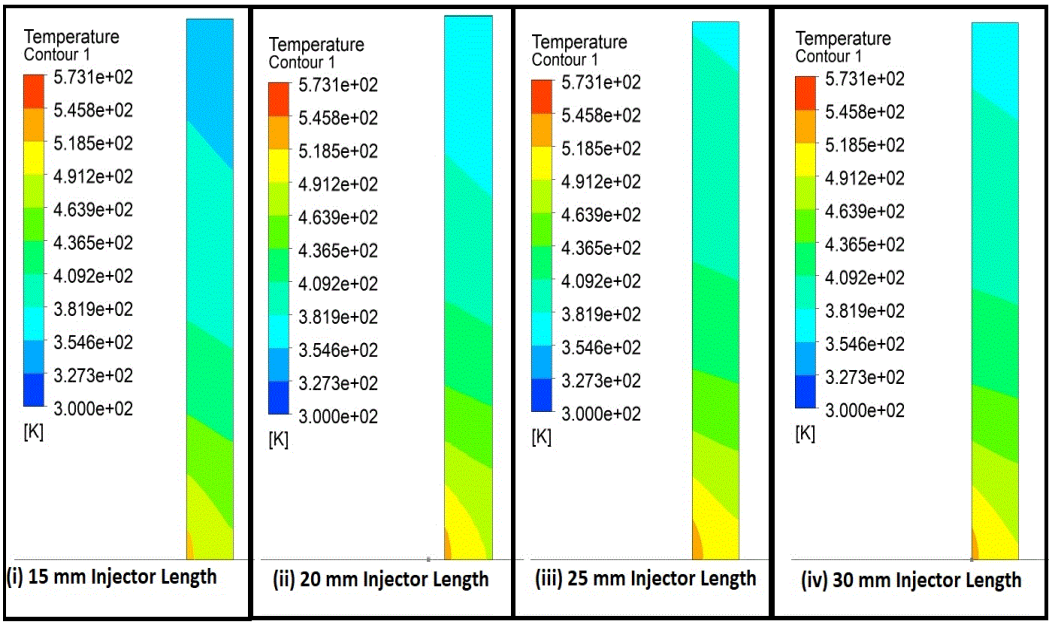

Figure 5.17: Temperature Contours of Substrate with Varying Injector Lengths.

5.5.2 Effect of Pressure on Substrate Surface Temperature

Inlet pressure increases from 2 MPa to 5 MPa with a 35 mm fixed stand-off distance for this case. The effect of substrate temperature and injector length are studied. The surface temperature distribution is shown in Fig. 5.18, Fig. 5.19, Fig. 5.20 & Fig. 5.21 under pressure, temperature, powder particle size, and powder particle velocity respectively. The substrate temperature decreases with an increase in particle injector length.

Our observations show that when the nozzle with the shortest particle injector length is used for fabrication, the resulting coating tends to be of superior quality, primarily because the substrate surface temperature reaches the maximum when the length of the particle injector is minimal. Therefore, a correlation between the particle injector length and the substrate surface temperature is crucial in determining the cold coating quality. Fig. 5.18 illustrates the influence of the particle injector length on the substrate temperature, with the latter being considered a function of particle velocity. This graphical representation provides a clear understanding of how these parameters interact in the context of our study.

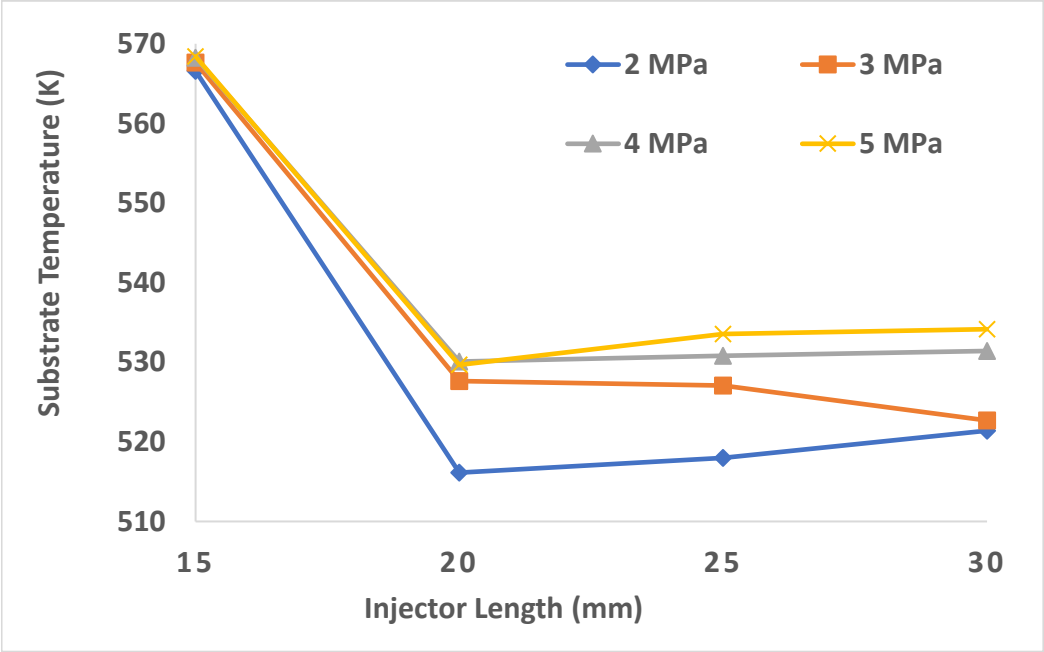

Figure 5.18: Effect of Pressure on Substrate Temperature

The substrate temperature decreases from injector length 15 mm to 20 mm, then slightly increases at 25 mm, and lastly, it decreases with low pressure and slightly increases at high pressure. Therefore, with no effect on the inlet pressure, the 15 mm length of the injector found the maximum temperature of the substrate surface, which means it had a low injector length. The powder particles and inlet air mixture were found to be best for keeping the temperature almost constant with changes in pressure. The turbulence present in the gas flow can indeed have an impact on the particle temperature. This outcome becomes particularly noticeable when the length of the particle injector is varied. In other words, changes in the length of the particle injector can lead to variations in the turbulence of the flow

gases, which in turn can influence the particle temperature. This interplay between the injector length, turbulence, and particle temperature is crucial in our study.

5.5.3 Effect of Temperature on Substrate Surface Temperature

In the simulation experiment, the gas temperature at the inlet was systematically increased from 473 K to 773 K, keeping the stand-off distance constant at 35 mm. A comprehensive study was conducted to comprehend the impact of the substrate's temperature and the injector's length.

The results of this study are presented in Fig. 5.19, which clearly illustrates the effect of an increase in the inlet gas temperature on the temperature of the substrate. As the inlet gas temperature rises, noticeable changes in the temperature of the substrate can be observed. It is very clear that the substrate's surface temperature increases with an increase in the inlet gas; the higher the inlet gas temperature, the higher the substrate surface temperature will be. Although injector length also affects the substrate surface temperature, with equal length of injector and barrel, the effect of temperature is maximum. As the injector length increases, the substrate surface temperature decreases comparatively.

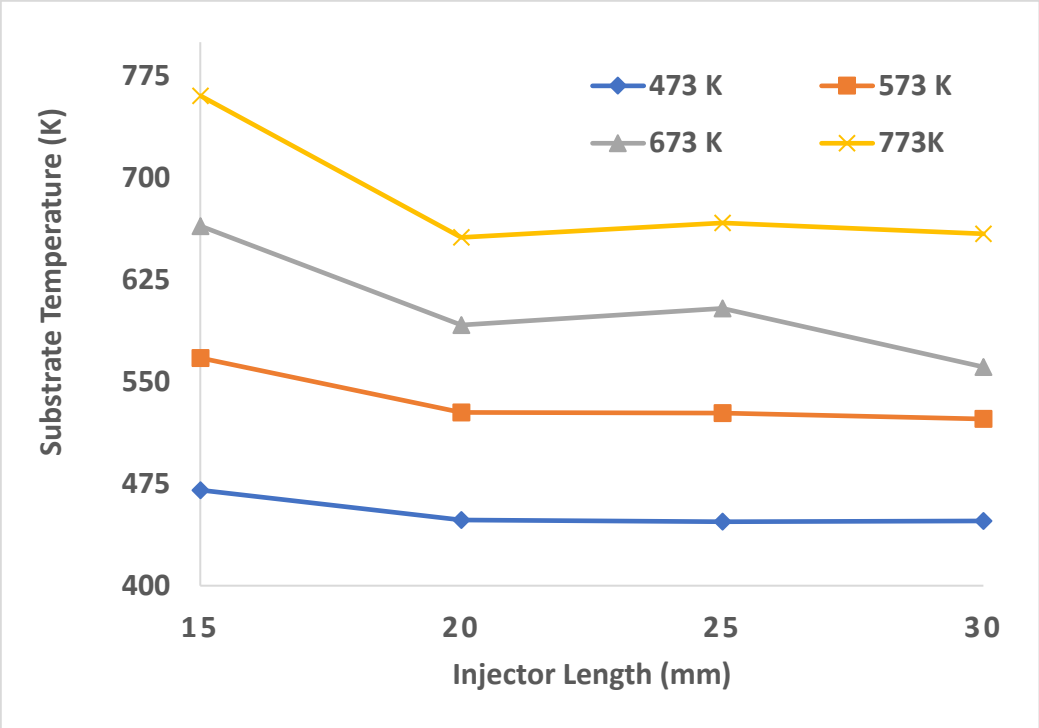

Figure 5.19: Effect of Temperature on the Substrate Temperature

Our observations indicate that the highest substrate temperature is achieved when the injector length is at a minimum of 15 mm, which coincides with the maximum temperature of the inlet gas. As the length of the particle injector increases, there is a corresponding decrease in temperature, reaching a minimum when the injector length is extended to 330 mm. It's worth noting that the quality of the coating fabricated using the nozzle is superior when the particle injector length is at its minimum. That is because the substrate surface temperature is at its maximum when the length of the particle injector is minimized. Therefore, the length of the particle injector plays a decisive part in determining both the temperature conditions and the quality of the coating.

5.5.4 Effect of Particle Size on Substrate Surface Temperature

The experiment systematically increased particle size from 20 µm to 80 µm while maintaining a 35 mm constant stand-off distance. The impact of particle size and the length of the particle injector on the substrate surface temperature is depicted in Fig. 5.20. It was observed that the particle injector's length predominantly determines the particles' behavior. Specifically, with the particle injector length of 15 mm, the substrate temperature was found to be high. However, as the length of the particle injector was increased from 20 mm to 30 mm, the substrate temperature declined. This declination in temperature can be attributed to the increased turbulence of the inlet gas caused by the longer injector length.

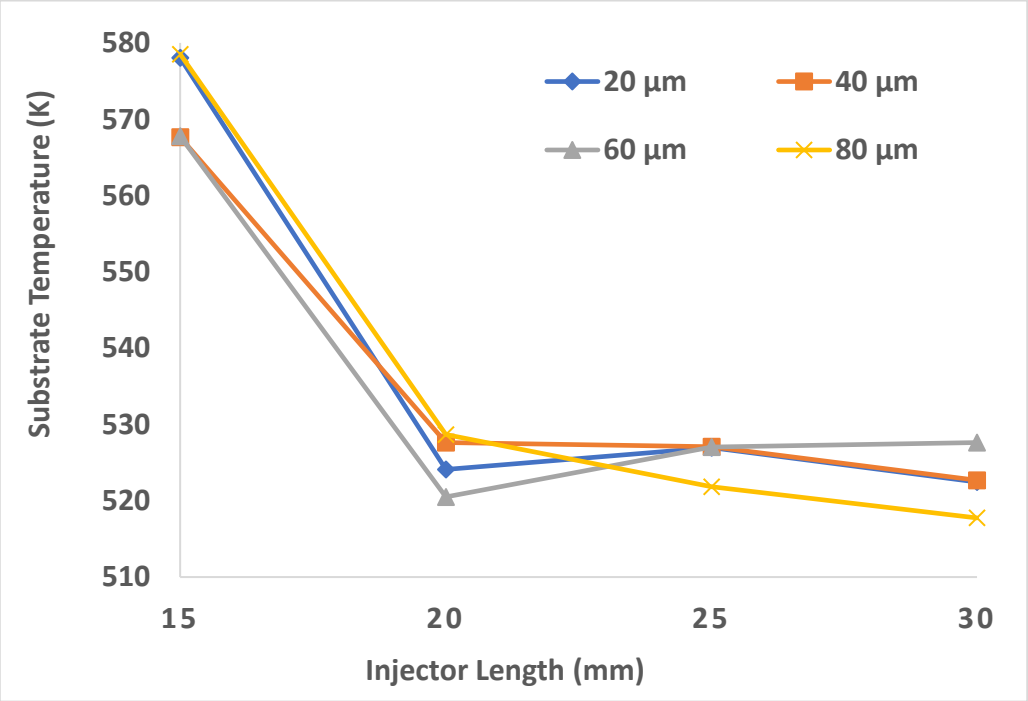

Figure 5.20: Effect of Particle Size on Substrate Temperature

5.5.5 Effect of Powder Particle Speed on Substrate Surface Temperature

The powder particle speed was increased from 20 m/s to 50 m/s, with a common stand-off distance of 35 mm. Fig. 5.21 shows the effect of powder particle speed and particle injector length on substrate surface temperature. The influence of turbulence can be observed from particle injector length 20 mm to 30 mm, without impact of powder particle speed. Our findings indicate that an injector length of 15 mm produces the highest substrate surface temperature. However, as the particle injector's length increases from 20 mm to 30 mm, there is a corresponding decrease in the substrate surface temperature.

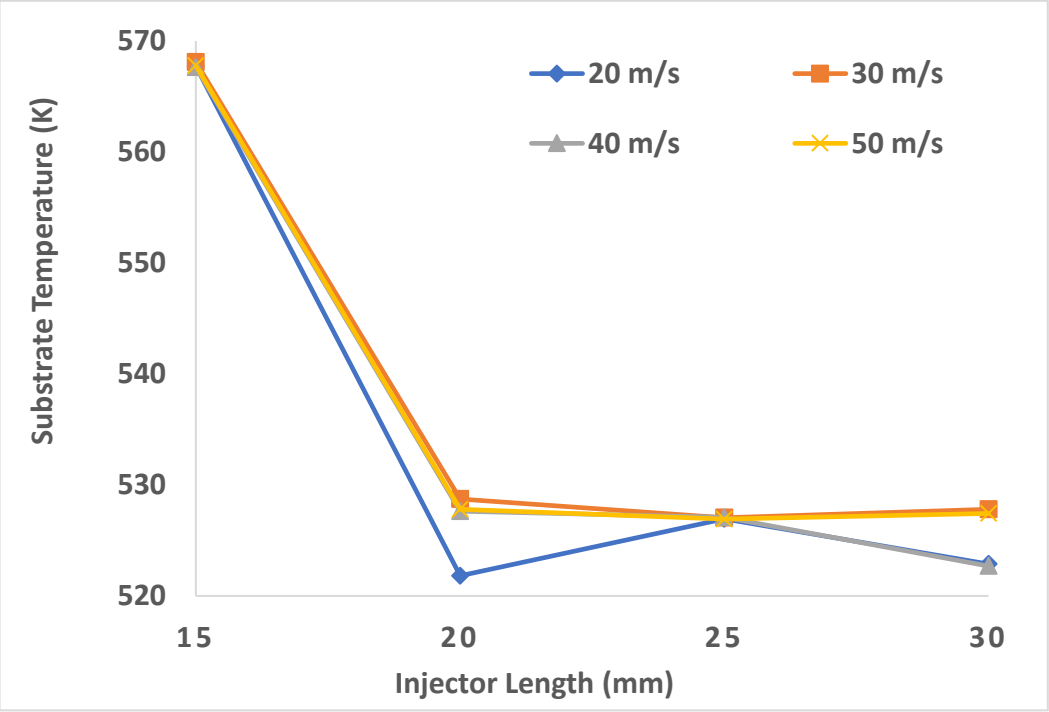

Figure 5.21: Effect of Powder Particle Speed on Substrate Temperature

This trend underscores the significant role that the length of the particle injector plays in influencing the temperature conditions within the system. Therefore, the influence of turbulence of inlet gas with the same barrel and particle injector length plays an important role in maintaining the higher temperature of particles and propelling gases. Therefore, considering the variations in substrate surface temperature with different parameters, an injector length of 15 mm emerges as the most optimal choice. This length provides the best balance between the various factors at play, ensuring the most effective performance for the process under investigation.

CHAPTER 6

CONCLUSION, FUTURE SCOPE AND SOCIAL IMPACT

In this research, the CS coating parameters are analyzed and optimized in five cases; firstly, the CS coating was examined for titanium powder for impact velocity using different particle sizes. Secondly, the CS coating simulation was carried out for powder pre-heat and impact velocity under varying pressure and gas mixtures. Then, the CS coating was analyzed for particle size and shape effect on impact velocity and stand-off distance. Fourthly, the CS coating was simulated for optimal injector length using a propelling gas type with varying injector lengths on impact velocity, substrate temperature, and particle temperature. Fifthly, the effect of process parameters- pressure, temperature, particle size, and particle speed- on the substrate surface in CS coating is being analyzed. A computational fluid dynamics simulation tool, ANSYS- FLUENT workbench, has been used to conduct simulations. The conclusions that can be made rely on simulated outcomes are mentioned below:

This study applies CS technology to investigate velocity distribution near the substrate using titanium powder particles of various sizes (20–100 μm) and different propelling gas compositions, specifically oxygen (O_2) and nitrogen (N_2). Particle sizes of 20 μm, 40 μm, 60 μm, 80 μm, and 100 μm were tested with pure

and mixed gas proportions. Results indicated that pure nitrogen produced the highest particle velocities, while pure oxygen yielded the lowest. Notably, particles of 40 µm achieved the maximum velocity near the substrate, enhancing bonding potential, whereas particles at 70 µm exhibited the lowest velocities across gas mixtures. For 20 µm particles, velocities ranged from 400 to 585 m/s, favorable for high-quality CS bonding.

When testing with different gas mixtures—including pure nitrogen, helium, and an N_2-He combination—results indicated that shorter injector lengths, particularly 15 mm, significantly enhanced parameters such as particle impact velocity, particle temperature, and substrate surface temperature. This finding suggests a 15 mm injector length is optimal for CS coating processes across varied gas conditions.

The findings also show that injector length significantly affects the gas flow dynamics inside the nozzle. Longer injector lengths were associated with greater pressure drops and shifts in the patterns of gas flow. These factors impacted particle velocity and trajectory, frequently lowering coating quality.

The ideal injector length for a Barrel-Convergent-Divergent type nozzle was 15 mm. With increasing nozzle barrel length, coating efficiency decreased. In addition, the temperature and velocity of the substrate are significantly affected by the gases nitrogen and helium: when similar conditions are present, nitrogen gas results in the highest substrate temperatures, while helium gas results in the highest

particle velocities. This relationship between injector design and gas composition emphasizes how crucial it is to choose parameters properly to maximize the efficiency of CS coating.

These results, taken as a whole, establish the significant roles that the type of gas, the length of the injector, and the particle size play in the optimization of the CS process. They also provide useful information for enhancing the quality of the coating and making it more useful in a variety of industrial applications.

In this work, a simulation analysis determined the ideal particle injector length for the CS coating process's best substrate surface temperature. The analysis shows the optimal particle injector length, i.e., 15 mm. Given that the relationship between the barrel length and the particle injector length must be determined, the minimum injector length used in this study is equal to the barrel length, even though the findings show that the ideal nozzle barrel length for compatibility is equivalent to the particle injector length.

The simulation results explain how feedstock powder particles behave under different pressure and gas mixture ratio variations. The study also takes into account how particle size, shape, and stand-off distance affect the results of the CS process:

i. When pure helium was used as the propelling gas, the maximum impact velocity was documented at a pressure of 7 MPa. This outcome is constant with helium's stronger compressibility and lower density, which enable particles to travel faster than other gases at the same pressure.

ii. Using a gas mixture of 80% nitrogen and 20% helium, the maximum pre-heat temperature for powder particles found was 7 MPa. This ratio improves particle adhesion and deformation in the Cold Spray (CS) process by achieving the ideal balance between heat transfer and thermal conductivity.

iii. Helium gas maximizes the impact velocity with higher concentrations and improves pre-heat temperature with lower concentrations. The high thermal conductivity and low density of Helium gas make it ideal for improving coating quality and efficiency.

iv. In Cold Spray (CS) applications, higher impact velocity and particle pre-heating enhance coating quality by improving adhesion, density, and bonding strength, especially for the initial layer—optimizing overall coating integrity and performance.

v. Spherical-shaped particles exhibit higher impact velocity and temperature than non-spherical particles (SF=0.8).

vi. Optimal CS coating is achieved with spherical powder particles at a stand-off distance of 35 mm.

vii. Deviating from this optimal stand-off distance (35 mm) affects coating properties, including porosity, bond strength, and efficiency.

viii. The surface temperature of the substrate is significantly influenced by the pressure of the gases entering the inlet—the substrate surface temperature peaks when the particle injector length is at its minimum, specifically 15 mm.

ix. The powder particle size and speed also influence the substrate surface temperature in the same manner as the pressure of the inlet gases.

FUTURE SCOPE

1. In future studies, the experimental implementation of the ideas presented in this thesis can be done to enhance cold coating performance.

2. Future research will check the compatibility of particle size and other parameters.

3. To design the next generation CS setup with improved outcomes, like impact velocity, the temperature of gases, type of gasses, and proportion of gases in the gas mixture.

4. Future research will check the compatibility of porous coating with the help of CS coating parameters.

5. The future scope will be centered on optimizing injector length and positions for particle injectors, either in the convergent part or with the divergent part.

SOCIAL IMPACT

This work helps the society in terms of making good quality of coating without disturbing the physical properties of the material.

The applications are most commonly used in medical industry.

1. Enhanced Industrial Efficiency – Optimized CS coating parameters lead to higher coating quality and durability, reducing equipment failure and maintenance costs across industries like aerospace, automotive, and biomedical sectors.

2. Environmental Sustainability – The CS process is a solid-state deposition method that eliminates the need for melting, reducing energy consumption and harmful emissions compared to traditional thermal spray or welding processes.

3. Resource Conservation – Optimizing gas mixtures and injector lengths minimizes material waste, making manufacturing more cost-effective and environmentally responsible.

4. Improved Product Longevity – Higher adhesion and better coating performance increase the lifespan of coated components, reducing frequent replacements and resource depletion.

5. Safer Working Conditions – Since CS operates at lower temperatures without combustion or toxic fumes, it enhances workplace safety by minimizing exposure to hazardous materials and thermal burns.

6. Cost-Effective Manufacturing – By reducing material loss, energy use, and defect rates, optimized CS coatings lower production costs, making high performance coatings more accessible to various industries.

7. Advancements in Medical Applications – High-quality titanium coatings can improve biomedical implants (e.g., prosthetics and orthopedic implants), enhancing patient outcomes and reducing the need for revision surgeries.

8. Sustainable Infrastructure Development – Durable and corrosion-resistant coatings enhance infrastructure components, such as bridges, pipelines, and marine structures, extending their service life and reducing maintenance costs.

9. Support for Aerospace and Defense – High-performance coatings improve the reliability and efficiency of critical aerospace and defense components, enhancing safety and reducing downtime for essential operations.

10. Technological Advancement and Job Creation – The optimization of CS technology fosters innovation, leading to new research opportunities, skill development, and job creation in advanced manufacturing sectors.

REFERENCES

[1] Bagherifard, S., Heydari Astaraee, A., Locati, M., Nawaz, A., Monti, S., Kondás, J., Singh, R., & Guagliano, M. (2020). Design and analysis of additive manufactured bimodal structures obtained by cold spray deposition. *Additive Manufacturing*, *33*(October 2019), 101131. https://doi.org/10.1016/j.addma.2020.101131

[2] Bai, Y., Wang, Z. H., Li, X. B., Huang, G. S., Li, C. X., & Li, Y. (2017). Corrosion behavior of low pressure cold sprayed Zn-Ni composite coatings. *Journal of Alloys and Compounds*, *719*, 194–202. https://doi.org/10.1016/j.jallcom.2017.05.134

[3] Baidoo, N., Wolter, M., & Leri, F. (2020). Window of Deposition Description and Prediction of Deposition Efficiency via Machine Learning Techniques in Cold Spraying. *Neuroscience and Biobehavioral Reviews*, 125871. https://doi.org/10.1016/j.neubiorev.2020.03.029

[4] Barton, D. J., Bhattiprolu, V. S., Thompson, G. B., & Brewer, L. N. (2020). Laser assisted cold spray of AISI 4340 steel. *Surface and Coatings Technology*, 126218. https://doi.org/10.1016/j.surfcoat.2020.126218

[5] Bernard, C. A., Takana, H., Diguet, G., Ravi, K., Lame, O., Ogawa, K., & Cavaillé, J. Y. (2020). Thermal gradient of in-flight polymer particles during cold spraying. *Journal of Materials Processing Technology*, *286*, 116805. https://doi.org/10.1016/j.jmatprotec.2020.116805

[6] Bhowmik, A., Wei-Yee Tan, A., Sun, W., Wei, Z., Marinescu, I., & Liu, E. (2020). On the heat-treatment induced evolution of residual stress and remarkable enhancement of adhesion strength of cold sprayed Ti–6Al–4V coatings. *Results in Materials*, *7*(July), 100119. https://doi.org/10.1016/j.rinma.2020.100119

[7] Cao, K., Yu, M., Liang, C. M., & Chen, H. (2020). Quantitative determination of SiC particles distribution of cold sprayed Al5056/SiC composite coatings. *Surface Engineering*, *36*(10), 1040–1048. https://doi.org/10.1080/02670844.2019.1609741

[8] Caruso, F., Meyer, M. C., & Lupoi, R. (2018). Three-dimensional numerical simulations of the particle loading effect on gas flow features for low pressure cold spray applications. *Surface and Coatings Technology*, *339*(October 2017), 181–190. https://doi.org/10.1016/j.surfcoat.2018.02.016

[9] Cetiner, D., Atar, E., Derin, B., & Cimenoglu, H. (2020). Thermal oxidation of cold sprayed Ti-5Al-XZn coatings for tribological applications. *Materials Letters*, *274*, 127959. https://doi.org/10.1016/j.matlet.2020.127959

[10] Chakrabarty, R., & Song, J. (2020a). A modified Johnson-Cook material model with strain gradient plasticity consideration for numerical simulation of cold spray process. *Surface and Coatings Technology*, *397*(April), 125981. https://doi.org/10.1016/j.surfcoat.2020.125981

[11] Chakrabarty, R., & Song, J. (2020b). Numerical simulations of ceramic deposition and retention in metal-ceramic composite cold spray. *Surface*

and Coatings Technology, *385*(July 2019), 125324. https://doi.org/10.1016/j.surfcoat.2019.125324

[12] Chen, C., Xie, Y., Yan, X., Ahmed, M., Lupoi, R., Wang, J., Ren, Z., Liao, H., & Yin, S. (2020). Tribological properties of Al/diamond composites produced by cold spray additive manufacturing. *Additive Manufacturing*, *36*, 101434. https://doi.org/10.1016/j.addma.2020.101434

[13] Da Silva, F. S., Cinca, N., Dosta, S., Cano, I. G., Guilemany, J. M., & Benedetti, A. V. (2017). Cold gas spray coatings: Basic principles, corrosion protection and applications. *Ecletica Quimica*, *42*(1), 9–32. https://doi.org/10.26850/1678-4618eqj.v42.1.2017.p09-32

[14] Daroonparvar, M., Khan, M. U. F., Saadeh, Y., Kay, C. M., Kasar, A. K., Kumar, P., Esteves, L., Misra, M., Menezes, P., Kalvala, P. R., Bakhsheshi-Rad, H. R., & Gupta, R. K. (2020). Modification of surface hardness, wear resistance and corrosion resistance of cold spray Al coated AZ31B Mg alloy using cold spray double layered Ta/Ti coating in 3.5 wt % NaCl solution. *Corrosion Science*, *176*(20), 109029. https://doi.org/10.1016/j.corsci.2020.109029

[15] Das, B., Bandyopadhyay, P. P., & Nath, A. K. (2018). An investigation on corrosion resistance and mechanical properties of laser remelted flame sprayed coating. *Advances in Materials and Processing Technologies*, *4*(4), 660–668. https://doi.org/10.1080/2374068X.2018.1489583

[16] Das, P., Bandyopadhyay, P. P., & Paul, S. (2019). Finish form grinding of thermally sprayed nano-structured coatings. *Advances in Materials and Processing Technologies*, *5*(1), 39–52.

https://doi.org/10.1080/2374068X.2018.1510680

[17] Diab, M., Pang, X., & Jahed, H. (2017). The effect of pure aluminum cold spray coating on corrosion and corrosion fatigue of magnesium (3% Al-1% Zn) extrusion. *Surface and Coatings Technology*, *309*, 423–435. https://doi.org/10.1016/j.surfcoat.2016.11.014

[18] Dlouhy, I., & Jan, V. (2018). Cold gas dynamic spray deposition as additive manufacturing of architectured materials. *Materials Engineering - Materiálové Inžinierstvo (MEMI)*, *24*(4), 115–123.

[19] Dykhuizen, R. C., & Smith, M. F. (1998). Gas Dynamic Principles of Cold Spray. *Journal of Thermal Spray Technology*, *7*(2), 205–212. https://doi.org/10.1361/105996398770350945

[20] El Din, S. M., Darvesh, A., Ayub, A., Sajid, T., Jamshed, W., Eid, M. R., Hussain, S. M., Sánchez-Chero, M., Ancca, S. M., Ramírez Cerna, J. M., & Dapozzo, C. L. A. (2022). Quadratic multiple regression model and spectral relaxation approach for carreau nanofluid inclined magnetized dipole along stagnation point geometry. *Scientific Reports 2022 12:1*, *12*(1), 1–18. https://doi.org/10.1038/s41598-022-22308-8

[21] Faizan-Ur-Rab, M., Zahiri, S. H., Masood, S. H., Phan, T. D., Jahedi, M., & Nagarajah, R. (2016). Application of a holistic 3D model to estimate state of cold spray titanium particles. *Materials and Design*, *89*, 1227–1241. https://doi.org/10.1016/j.matdes.2015.10.075

[22] Fallah, P., Rajagopalan, S., McDonald, A., & Yue, S. (2020). Development of hybrid metallic coatings on carbon fiber-reinforced polymers (CFRPs) by cold spray deposition of copper-assisted copper

electroplating process. *Surface and Coatings Technology*, 126231. https://doi.org/10.1016/j.surfcoat.2020.126231

[23] Fardan, A., Berndt, C. C., & Ahmed, R. (2021). Numerical modelling of particle impact and residual stresses in cold sprayed coatings: A review. *Surface and Coatings Technology*, *409*, 126835. https://doi.org/10.1016/j.surfcoat.2021.126835

[24] Ghelichi, R., Bagherifard, S., Guagliano, M., & Verani, M. (2011). Numerical simulation of cold spray coating. *Surface and Coatings Technology*, *205*(23–24), 5294–5301. https://doi.org/10.1016/j.surfcoat.2011.05.038

[25] Goyal, T., Walia, R. S., & Sidhu, T. S. (2012). Surface roughness optimization of cold-sprayed coatings using Taguchi method. *International Journal of Advanced Manufacturing Technology*, *60*(5–8), 611–623. https://doi.org/10.1007/s00170-011-3642-6

[26] Hemeda, A. A., Zhang, C., Hu, X. Y., Fukuda, D., Cote, D., Nault, I. M., Nardi, A., Champagne, V. K., Ma, Y., & Palko, J. W. (2020). Particle-based simulation of cold spray: Influence of oxide layer on impact process. *Additive Manufacturing*, *August*, 101517. https://doi.org/10.1016/j.addma.2020.101517

[27] Huang, G., Gu, D., Li, X., Xing, L., & Wang, H. (2014). Numerical simulation on syphonage effect of laval nozzle for low pressure cold spray system. *Journal of Materials Processing Technology*, *214*(11), 2497–2504. https://doi.org/10.1016/j.jmatprotec.2014.05.014

[28] Hussain, S. M. (2022a). Dynamics of radiative Williamson hybrid

nanofluid with entropy generation: significance in solar aircraft. *Scientific Reports*, *12*(1), 1–23. https://doi.org/10.1038/s41598-022-13086-4

[29] Hussain, S. M. (2022b). Irreversibility analysis of time-dependent magnetically driven flow of Sutterby hybrid nanofluid: a thermal mathematical model. *Https://Doi.Org/10.1080/17455030.2022.2089369*. https://doi.org/10.1080/17455030.2022.2089369

[30] Hussain, S. M. (2022c). Thermal-enhanced hybrid of copper–zirconium dioxide/ethylene glycol nanofluid flowing in the solar collector of water-pump application. *Https://Doi.Org/10.1080/17455030.2022.2066734*. https://doi.org/10.1080/17455030.2022.2066734

[31] Hussain, S. M. (2023a). Entropy generation and thermal performance of Williamson hybrid nanofluid flow used in solar aircraft application as the main coolant in parabolic trough solar collector. *Https://Doi.Org/10.1080/17455030.2022.2110624*. https://doi.org/10.1080/17455030.2022.2110624

[32] Hussain, S. M. (2023b). Numerical assessment of a sutterby hybrid nanofluid over a stretching sheet with a particle shape factor. *Https://Doi.Org/10.1080/17455030.2023.2166148*. https://doi.org/10.1080/17455030.2023.2166148

[33] Hussain, S. M., Mishra, M. R., Seth, G. S., & Chamkha, A. J. (2022). Dynamics of heat absorbing and radiative hydromagnetic nanofluids through a stretching surface with chemical reaction and viscous dissipation. *Https://Doi.Org/10.1177/09544089221096103*. https://doi.org/10.1177/09544089221096103

[34] Hussain, T. (2012). Cold Spraying of Titanium: A Review of Bonding Mechanisms, Microstructure and Properties. *Key Engineering Materials*, *533*, 53–90. https://doi.org/10.4028/www.scientific.net/kem.533.53

[35] Jami, H., & Jabbarzadeh, A. (2020). Molecular simulation of high-velocity deposition of Titanium dioxide nanoparticles on titanium. *Applied Surface Science*, *542*(November 2020), 148567. https://doi.org/10.1016/j.apsusc.2020.148567

[36] Jia, D., Liu, Y., Yi, P., Zhan, X., Ma, J., & Mostaghimi, J. (2020). Splat formation mechanism of droplet-filled cold-textured groove during plasma spraying. *Applied Thermal Engineering*, *173*(October 2019), 115239. https://doi.org/10.1016/j.applthermaleng.2020.115239

[37] Jiang, X., Overman, N., Smith, C., & Ross, K. (2020). Microstructure, hardness and cavitation erosion resistance of different cold spray coatings on stainless steel 316 for hydropower applications. *Materials Today Communications*, *25*(February), 101305. https://doi.org/10.1016/j.mtcomm.2020.101305

[38] Khalkhali, Z., & Schmidt, D. (2017). Optimization of Cold Spray Deposition of High-Density Polyethylene Powders. *Journal of Thermal Spray Technology*, *November*. https://doi.org/10.1007/s11666-017-0627-5

[39] Khan, M., Zunaid, M., & Murtaza, Q. (2020). Examination of titanium powder with different particle sizes for velocity. *Materials Today: Proceedings*, *43*, 383–387. https://doi.org/10.1016/j.matpr.2020.11.682

[40] Khan, M., Zunaid, M., & Murtaza, Q. (2021). Simulation of cold spray

coating for powder pre-heat and impact velocity. *Materials Today: Proceedings*, *46*(46), 10837–10844. https://doi.org/10.1016/j.matpr.2021.01.780

[41] Khan, M., Zunaid, M., & Murtaza, Q. (2023a). CFD Analysis of Particle Shape and Size on Impact Velocity and Effect of Stand-off Distance in the Cold Spray Process. In A. Maurya, A. K. Srivastava, P. K. Jha, & S. M. Pandey (Eds.), *Lecture Notes in Mechanical Engineering* (pp. 109–119). Springer Nature Singapore. https://doi.org/10.1007/978-981-19-7709-1_11

[42] Khan, M., Zunaid, M., & Murtaza, Q. (2023b). *CFD Analysis of Particle Shape and Size on Impact Velocity and Effect of Stand-off Distance in the Cold Spray Process* (A. Maurya, A. K. Srivastava, P. K. Jha, & S. M. Pandey (eds.); pp. 109–119). Springer Nature Singapore. https://doi.org/10.1007/978-981-19-7709-1_11

[43] Khan, M., Zunaid, M., & Murtaza, Q. (2023c). Computational simulation of cold spray coating for optimal injector length. *Case Studies in Thermal Engineering*, *51*(March), 103655. https://doi.org/10.1016/j.csite.2023.103655

[44] King, P. C., Bae, G., Zahiri, S. H., Jahedi, M., & Lee, C. (2010). An experimental and finite element study of cold spray copper impact onto two aluminum substrates. *Journal of Thermal Spray Technology*, *19*(3), 620–634. https://doi.org/10.1007/s11666-009-9454-7

[45] Klinkov, S. V., Kosarev, V. F., Shikalov, V. S., Vidyuk, T. M., Chesnokov, A. E., & Smirnov, A. V. (2019). Influence of preliminary heat treatment

and ball milling of copper powder on cold spray process. *Materials Today: Proceedings*, *25*(xxxx), 360–362. https://doi.org/10.1016/j.matpr.2019.12.090

[46] Koivuluoto, H., Lagerbom, J., & Vuoristo, P. (2007). Microstructural studies of cold sprayed copper, nickel, and nickel-30% copper coatings. *Journal of Thermal Spray Technology*, *16*(4), 488–497. https://doi.org/10.1007/s11666-007-9060-5

[47] Kumar, A. S., Kar, S., Bandyopadhyay, P. P., & Paul, S. (2018). Grinding of ceramics–sintered ceramics versus ceramic coatings. *Advances in Materials and Processing Technologies*, *4*(4), 538–547. https://doi.org/10.1080/2374068X.2018.1479820

[48] Kumar, M., Singh, H., & Singh, N. (2020). Effect of increase in nano-particle addition on mechanical and microstructural behaviour of HVOF and cold-spray Ni-20Cr coatings on boiler steels. *Materials Today: Proceedings*, *21*, 2035–2042. https://doi.org/10.1016/j.matpr.2020.01.321

[49] Kumar, S., Zunaid, M., Murtaza, Q., Ansari, N., & Arora, A. (2015). Simulation of Injector in Cold Spray Process by Fluent-6. *International Conference of Advance Research and Innovation (ICARI-2015)*, 464–472.

[50] Lapushkina, E., Yuan, S., Mary, N., Adrien, J., Ogawa, K., & Normand, B. (2020). Contribution in optimization of Zn Cold-sprayed coating dedicated to corrosion applications. *Surface and Coatings Technology*, *400*(July), 126193. https://doi.org/10.1016/j.surfcoat.2020.126193

[51] Li, W. Y., Liao, H., Douchy, G., & Coddet, C. (2007). Optimal design of a cold spray nozzle by numerical analysis of particle velocity and

experimental validation with 316L stainless steel powder. *Materials and Design*, *28*(7), 2129–2137. https://doi.org/10.1016/j.matdes.2006.05.016

[52] Li, W. Y., Yang, K., Yin, S., & Guo, X. P. (2016). Numerical Analysis of Cold Spray Particles Impacting Behavior by the Eulerian Method: A Review. *Journal of Thermal Spray Technology*, *25*(8), 1441–1460. https://doi.org/10.1007/s11666-016-0443-3

[53] Li, W. Y., Zhang, D. D., Huang, C. J., Yin, S., Yu, M., Wang, F. F., & Liao, H. L. (2014). Modelling of impact behaviour of cold spray particles: Review. *Surface Engineering*, *30*(5), 299–308. https://doi.org/10.1179/1743294414Y.0000000268

[54] Li, W., Yang, K., Zhang, D., & Zhou, X. (2016). Residual Stress Analysis of Cold-Sprayed Copper Coatings by Numerical Simulation. *Journal of Thermal Spray Technology*, *25*(1–2), 131–142. https://doi.org/10.1007/s11666-015-0308-1

[55] Li, W., Yang, K., Zhang, D., Zhou, X., & Guo, X. (2016). Interface behavior of particles upon impacting during cold spraying of Cu/Ni/Al mixture. *Materials and Design*, *95*, 237–246. https://doi.org/10.1016/j.matdes.2016.01.122

[56] Li, Y., Wang, X., Yin, S., & Xu, S. (2012). Influence of Particle Initial Temperature on High Velocity Impact Process in Cold Spraying. *Procedia Environmental Sciences*, *12*, 298–304. https://doi.org/10.1016/j.proenv.2012.01.281

[57] Liang, Y. L., Wang, Z. B., Zhang, J. B., & Lu, K. (2015). Formation of interfacial compounds and the effects on stripping behaviors of a cold-

sprayed Zn-Al coating on interstitial-free steel. *Applied Surface Science*, *340*, 89–95. https://doi.org/10.1016/j.apsusc.2015.02.118

[58] Liang, Y. L., Wang, Z. B., Zhang, J., Zhang, J. B., & Lu, K. (2016). Enhanced bonding property of cold-sprayed Zn-Al coating on interstitial-free steel substrate with a nanostructured surface layer. *Applied Surface Science*, *385*, 341–348. https://doi.org/10.1016/j.apsusc.2016.05.142

[59] Lin, E., Chen, Q., Ozdemir, O. C., Champagne, V. K., & Müftü, S. (2019). Effects of Interface Bonding on the Residual Stresses in Cold-Sprayed Al-6061: A Numerical Investigation. *Journal of Thermal Spray Technology*, *28*(3), 472–483. https://doi.org/10.1007/s11666-019-00827-7

[60] Liu, Z., Wang, H., Haché, M. J. R., Chu, X., Irissou, E., & Zou, Y. (2020). Prediction of heterogeneous microstructural evolution in cold sprayed copper coatings using local Zener-Hollomon parameter and strain. *Acta Materialia*, *193*, 191–201. https://doi.org/10.1016/j.actamat.2020.04.041

[61] Lomas, J. P., Contraros, P. D., & Papadakis, G. (2011). COATINGS AND PERMANENT MEANS OF ACCESS – THE ANTI-CORROSION CHALLENGES. *Transactions of the Royal Institution of Naval Architects Part A: International Journal of Maritime Engineering*, *153*(A4), A243–A246. https://doi.org/10.5750/ijme.v153iA4.868

[62] Lupo, G., Gruber, A., Brandt, L., & Duwig, C. (2020). Direct numerical simulation of spray droplet evaporation in hot turbulent channel flow. *International Journal of Heat and Mass Transfer*, *160*, 120184. https://doi.org/10.1016/j.ijheatmasstransfer.2020.120184

[63] Lupoi, R., Meyer, M., Wits, W. W., & Yin, S. (2020). The role of particles

flow characteristics in the performance of cold spray nozzles. *CIRP Annals*, *69*(1), 189–192. https://doi.org/10.1016/j.cirp.2020.04.061

[64] Maledi, N. B., Oladijo, O. P., Botef, I., Ntsoane, T. P., Madiseng, A., & Moloisane, L. (2017). Influence of cold spray parameters on the microstructures and residual stress of Zn coatings sprayed on mild steel. *Surface and Coatings Technology*, *318*, 106–113. https://doi.org/10.1016/j.surfcoat.2017.03.062

[65] Maritime, A. W.-I. J. of, & 2020, undefined. (n.d.). THE CHALLENGES OF MAJOR TANK COATING REFURBISHMENT PROJECTS FOR ON-STATION FLOATING ASSETS. *Intmaritimeengineering.OrgA WestwellInternational Journal of Maritime Engineering, 2020•intmaritimeengineering.Org*. Retrieved February 10, 2024, from http://www.intmaritimeengineering.org/index.php/ijme/article/view/1126

[66] Meyer, M. C., Yin, S., McDonnell, K. A., Stier, O., & Lupoi, R. (2016). Feed rate effect on particulate acceleration in Cold Spray under low stagnation pressure conditions. *Surface and Coatings Technology*, *304*, 237–245. https://doi.org/10.1016/j.surfcoat.2016.07.017

[67] Mindivan, F., & Mindivan, H. (2016). Surface properties and tribocorrosion behaviour of a thermal sprayed martensitic stainless steel coating after pulsed plasma nitriding process. *Advances in Materials and Processing Technologies*, *2*(4), 514–526. https://doi.org/10.1080/2374068X.2016.1247232

[68] Nutt, M. R. R. S. R., & Champagne, C. A. W. V. K. (2017). Review of Relationship Between Particle Deformation , Coating Microstructure , and

Properties in High-Pressure Cold Spray. *Journal of Thermal Spray Technology*, *26*(6), 1308–1355. https://doi.org/10.1007/s11666-017-0575-0

[69] Oviedo, F., & Valarezo, A. (2020). Residual Stress in High-Velocity Impact Coatings: Parametric Finite Element Analysis Approach. *Journal of Thermal Spray Technology*, *29*(6), 1268–1288. https://doi.org/10.1007/s11666-020-01026-5

[70] Oyinbo, S. T., & Jen, T. C. (2020). Investigation of the process parameters and restitution coefficient of ductile materials during cold gas dynamic spray (CGDS) using finite element analysis. *Additive Manufacturing*, *31*, 100986. https://doi.org/10.1016/j.addma.2019.100986

[71] Oyinbo, S. T., Jen, T. C., Zhu, Y., Ajiboye, J. S., & Ismail, S. O. (2020). Atomistic simulations of interfacial deformation and bonding mechanism of Pd-Cu composite metal membrane using cold gas dynamic spray process. *Vacuum*, *182*(August), 109779. https://doi.org/10.1016/j.vacuum.2020.109779

[72] Pattison, J., Celotto, S., Khan, A., & O'Neill, W. (2008). Standoff distance and bow shock phenomena in the Cold Spray process. *Surface and Coatings Technology*, *202*(8), 1443–1454. https://doi.org/10.1016/j.surfcoat.2007.06.065

[73] Pattison, J., Celotto, S., Morgan, R., Bray, M., & O'Neill., W. (2007). Cold gas dynamic manufacturing: A non-thermal approach to freeform fabrication. *International Journal of Machine Tools and Manufacture*, *47*(3–4), 627–634. https://doi.org/10.1016/j.ijmachtools.2006.05.001

[74] Qin, J., Huang, Q., Wang, X., Suo, X., Wang, J., & Li, H. (2020). Interfacial metal/ceramic bonding mechanism for metallization of ceramics via cold spraying. *Journal of Materials Processing Technology*, *288*(July 2020), 116845. https://doi.org/10.1016/j.jmatprotec.2020.116845

[75] Raoelison, R. N., Guéchi, M. R., & Padayodi, E. (2020). In-flight temperature of solid micrometric powders during cold spray additive manufacturing. *International Journal of Thermal Sciences*, *157*(April). https://doi.org/10.1016/j.ijthermalsci.2020.106422

[76] Reddy, B. V. R., & Kummitha, O. R. (2017). Characterization of spray formed and cold rolled Al-Pb alloy. *Materials Today: Proceedings*, *4*(2), 267–276. https://doi.org/10.1016/j.matpr.2017.01.021

[77] Rizzo, A., Mirenghi, L., Massaro, M., Galietti, U., Capodieci, L., Terzi, R., Tapfer, L., & Valerini, D. (2013). Improved properties of TiAlN coatings through the multilayer structure. *Surface and Coatings Technology*, *235*, 475–483. https://doi.org/10.1016/j.surfcoat.2013.08.006

[78] Rutkowska-Gorczyca, M. (2020). X-ray diffraction and microstructural analysis of Cu–TiO2 layers deposited by cold spray. *Materials Science and Technology (United Kingdom)*, *0836*. https://doi.org/10.1080/02670836.2020.1738069

[79] Sabanayagam, S., & Chockalingam, S. (2020). Analysis of high temperature oxidation behaviour of SS316 by Al2O3 and Cr2O3 coating. *Materials Today: Proceedings*, *xxxx*, 3–7. https://doi.org/10.1016/j.matpr.2020.01.218

[80] Sabard, A., McNutt, P., Begg, H., & Hussain, T. (2020). Cold spray deposition of solution heat treated, artificially aged and naturally aged Al 7075 powder. *Surface and Coatings Technology*, *385*(October 2019), 125367. https://doi.org/10.1016/j.surfcoat.2020.125367

[81] Schmidt, K., Buhl, S., Davoudi, N., Godard, C., Merz, R., Raid, I., Kerscher, E., Kopnarski, M., Müller-Renno, C., Ripperger, S., Seewig, J., Ziegler, C., & Antonyuk, S. (2017). Ti surface modification by cold spraying with TiO2 microparticles. *Surface and Coatings Technology*, *309*, 749–758. https://doi.org/10.1016/j.surfcoat.2016.10.091

[82] Seraj, R. A., Abdollah-Zadeh, A., Assadi, H., Hajipour, H., & Kadkhodaee, M. (2020). Effect of substrate on the properties of cold sprayed coating of WC-10Ni. *Advances in Materials and Processing Technologies*, *00*(00), 1–14. https://doi.org/10.1080/2374068X.2020.1794228

[83] Shah, S., Lee, J., & Rothstein, J. P. (2017). Numerical Simulations of the High-Velocity Impact of a Single Polymer Particle During Cold-Spray Deposition. *Journal of Thermal Spray Technology*, *26*(5), 970–984. https://doi.org/10.1007/s11666-017-0557-2

[84] Shahzad, F., Jamshed, W., Safdar, R., Hussain, S. M., Nasir, N. A. A. M., Dhange, M., Nisar, K. S., Eid, M. R., Sohail, M., Alsehli, M., & Elfasakhany, A. (2022). Thermal analysis characterisation of solar-powered ship using Oldroyd hybrid nanofluids in parabolic trough solar collector: An optimal thermal application. *Nanotechnology Reviews*, *11*(1), 2015–2037. https://doi.org/10.1515/ntrev-2022-0108

[85] Shayegan, G., Mahmoudi, H., Ghelichi, R., Villafuerte, J., Wang, J., Guagliano, M., & Jahed, H. (2014). Residual stress induced by cold spray coating of magnesium AZ31B extrusion. *Materials and Design*, *60*, 72–84. https://doi.org/10.1016/j.matdes.2014.03.054

[86] Siddique, S., Bernussi, A. A., Husain, S. W., & Yasir, M. (2020). Enhancing structural integrity, corrosion resistance and wear properties of Mg alloy by heat treated cold sprayed Al coating. *Surface and Coatings Technology*, *394*(April), 125882. https://doi.org/10.1016/j.surfcoat.2020.125882

[87] Singh, S., Singh, P., Singh, H., & Buddu, R. K. (2019). Characterization and comparison of copper coatings developed by low pressure cold spraying and laser cladding techniques. *Materials Today: Proceedings*, *18*, 830–840. https://doi.org/10.1016/j.matpr.2019.06.509

[88] Singhal, C., Murtaza, Q., & Parvej, P. (2018). Simulation of Critical Velocity of Cold Spray Process with Different Turbulence Models. *Materials Today: Proceedings*, *5*(9), 17371–17379. https://doi.org/10.1016/j.matpr.2018.04.150

[89] Song, X., Everaerts, J., Zhai, W., Zheng, H., Tan, A. W. Y., Sun, W., Li, F., Marinescu, I., Liu, E., & Korsunsky, A. M. (2018). Residual stresses in single particle splat of metal cold spray process – Numerical simulation and direct measurement. *Materials Letters*, *230*, 152–156. https://doi.org/10.1016/j.matlet.2018.07.117

[90] Song, X., Ng, K. L., Chea, J. M. K., Sun, W., Tan, A. W. Y., Zhai, W., Li, F., Marinescu, I., & Liu, E. (2020). Coupled Eulerian-Lagrangian (CEL)

simulation of multiple particle impact during Metal Cold Spray process for coating porosity prediction. *Surface and Coatings Technology*, *385*(January), 125433. https://doi.org/10.1016/j.surfcoat.2020.125433

[91] Srikanth, A., Mohammed Thalib Basha, G., & Venkateshwarlu, B. (2019). A Brief Review on Cold Spray Coating Process. *Materials Today: Proceedings*, *22*, 1390–1397. https://doi.org/10.1016/j.matpr.2020.01.482

[92] Sun, C., Zhou, X., Xie, C., Xu, L., Li, R., & Liu, B. (2020). Formation of Al-based amorphous/nanocrystalline coatings by cold spraying. *Surface and Coatings Technology*, *389*(November 2019), 125644. https://doi.org/10.1016/j.surfcoat.2020.125644

[93] Suo, X. K., Liu, T. K., Li, W. Y., Suo, Q. L., Planche, M. P., & Liao, H. L. (2013). Numerical study on the effect of nozzle dimension on particle distribution in cold spraying. *Surface and Coatings Technology*, *220*, 107–111. https://doi.org/10.1016/j.surfcoat.2012.09.029

[94] Takana, H., Ogawa, K., Shoji, T., & Nishiyama, H. (2008). Computational simulation of cold spray process assisted by electrostatic force. *Powder Technology*, *185*(2), 116–123. https://doi.org/10.1016/j.powtec.2007.10.005

[95] Tortuero, S., Garrido, M. A., Poza, P., & Rodríguez, J. (2020). Evaluating the erosion resistance of Ti6Al4V coatings deposited by cold spray. *Wear*, *454–455*(March), 203337. https://doi.org/10.1016/j.wear.2020.203337

[96] Tripathy, S., Behera, A., Pati, S., & Roy, S. (2020). Corrosion resistant nickel coating on mild steel by cold gas dynamic spraying. *Materials Today: Proceedings*, *xxxx*. https://doi.org/10.1016/j.matpr.2020.09.668

[97] Vilardell, A. M., Cinca, N., Cano, I. G., Concustell, A., Dosta, S., Guilemany, J. M., Estradé, S., & Peiró, F. (2016). Dense nanostructured calcium phosphate coating on titanium by cold spray. *Journal of the European Ceramic Society*. https://doi.org/10.1016/j.jeurceramsoc.2016.11.040

[98] Wang, D., & Fan, L. S. (2013). Particle characterization and behavior relevant to fluidized bed combustion and gasification systems. In *Fluidized Bed Technologies for Near-Zero Emission Combustion and Gasification* (pp. 42–76). https://doi.org/10.1533/9780857098801.1.42

[99] Wang, K., Wang, S., Xiong, T., Wen, D., Wang, G., Liu, W., & Du, H. (2020). Properties of Zn-Al-Mg-TiO2 coating prepared by cold spraying. *Surface and Coatings Technology*, *387*(February), 125549. https://doi.org/10.1016/j.surfcoat.2020.125549

[100] Wang, X., Zhang, L., Zhou, X., Wu, W., & Jie, X. (2020). Corrosion behavior of Al2O3-reinforced graphene encapsulated Al composite coating fabricated by low pressure cold spraying. *Surface and Coatings Technology*, *386*(January), 125486. https://doi.org/10.1016/j.surfcoat.2020.125486

[101] Willemen, R., Luyckx, D., Meskens, R., Lenaerts, S., & De Baere, K. (2020). A STUDY INTO THE COATING THICKNESS OF SHIP BALLAST TANKS. *Transactions of the Royal Institution of Naval Architects Part A: International Journal of Maritime Engineering*, *162*(A3), A277–A288. https://doi.org/10.5750/ijme.v162iA3.1137

[102] Winnicki, M., Kozerski, S., Małachowska, A., Pawłowski, L., &

Rutkowska-Gorczyca, M. (2021). Optimization of ceramic content in nickel–alumina composite coatings obtained by low pressure cold spraying. *Surface and Coatings Technology*, *405*(October 2020). https://doi.org/10.1016/j.surfcoat.2020.126732

[103] Wu, H., Huang, C., Xie, X., Liu, S., Wu, T., Niendorf, T., Xie, Y., Deng, C., Liu, M., Liao, H., & Deng, S. (2020). Influence of spray trajectories on characteristics of cold-sprayed copper deposits. *Surface and Coatings Technology*, *405*(July 2020), 126703. https://doi.org/10.1016/j.surfcoat.2020.126703

[104] Wu, H., Zhang, L., Liu, C., Mai, Y., Zhang, Y., & Jie, X. (2020). Deposition of Zn-G/Al composite coating with excellent cathodic protection on low-carbon steel by low-pressure cold spraying. *Journal of Alloys and Compounds*, *821*, 153483. https://doi.org/10.1016/j.jallcom.2019.153483

[105] Xie, C., Li, H., Zhou, X., & Sun, C. (2019). Corrosion behavior of cold sprayed pure zinc coating on magnesium. *Surface and Coatings Technology*, *374*(May), 797–806. https://doi.org/10.1016/j.surfcoat.2019.06.068

[106] Xie, X., Hosni, B., Chen, C., Wu, H., Li, Y., Chen, Z., Verdy, C., Kedim, O. E. I., Zhong, Q., Addad, A., Coddet, C., Ji, G., & Liao, H. (2020). Corrosion behavior of cold sprayed 7075Al composite coating reinforced with TiB2 nanoparticles. *Surface and Coatings Technology*, *404*(October), 126460. https://doi.org/10.1016/j.surfcoat.2020.126460

[107] Xie, X., Ma, Y., Chen, C., Ji, G., Verdy, C., Wu, H., Chen, Z., Yuan, S.,

Normand, B., Yin, S., & Liao, H. (2020). Cold spray additive manufacturing of metal matrix composites (MMCs) using a novel nano-TiB2-reinforced 7075Al powder. *Journal of Alloys and Compounds*, *819*. https://doi.org/10.1016/j.jallcom.2019.152962

[108] Xie, Y., Yin, S., Chen, C., Planche, M. P., Liao, H., & Lupoi, R. (2016). New insights into the coating/substrate interfacial bonding mechanism in cold spray. *Scripta Materialia*, *125*, 1–4. https://doi.org/10.1016/j.scriptamat.2016.07.024

[109] Xu, Y., Li, W., Qu, L., Yang, X., Song, B., Lupoi, R., & Yin, S. (2020). Solid-state cold spraying of FeCoCrNiMn high-entropy alloy: an insight into microstructure evolution and oxidation behavior at 700-900 °C. *Journal of Materials Science & Technology*. https://doi.org/10.1016/j.jmst.2020.06.041

[110] Yao, H. L., Yi, Z. H., Yao, C., Zhang, M. X., Wang, H. T., Li, S. Bin, Bai, X. B., Chen, Q. Y., & Ji, G. C. (2020). Improved corrosion resistance of AZ91D magnesium alloy coated by novel cold-sprayed Zn-HA/Zn double-layer coatings. *Ceramics International*, *46*(6), 7687–7693. https://doi.org/10.1016/j.ceramint.2019.11.271

[111] Yeom, H., Dabney, T., Pocquette, N., Ross, K., Pfefferkorn, F. E., & Sridharan, K. (2020). Cold spray deposition of 304L stainless steel to mitigate chloride-induced stress corrosion cracking in canisters for used nuclear fuel storage. *Journal of Nuclear Materials*, *538*, 152254. https://doi.org/10.1016/j.jnucmat.2020.152254

[112] Yeom, H., & Sridharan, K. (2021). Cold spray technology in nuclear

energy applications: A review of recent advances. *Annals of Nuclear Energy*, *150*, 107835. https://doi.org/10.1016/j.anucene.2020.107835

[113] Yildirim, B., Muftu, S., & Gouldstone, A. (2011). Modeling of high velocity impact of spherical particles. *Wear*, *270*(9–10), 703–713. https://doi.org/10.1016/j.wear.2011.02.003

[114] Yin, S., Cavaliere, P., Aldwell, B., Jenkins, R., Liao, H., Li, W., & Lupoi, R. (2018). Cold spray additive manufacturing and repair: Fundamentals and applications. *Additive Manufacturing*, *21*(April), 628–650. https://doi.org/10.1016/j.addma.2018.04.017

[115] Yin, S., Wang, X. F., Li, W. Y., & Guo, X. P. (2011). Examination on substrate preheating process in cold gas dynamic spraying. *Journal of Thermal Spray Technology*, *20*(4), 852–859. https://doi.org/10.1007/s11666-011-9623-3

[116] Yin, S., Wang, X., Suo, X., Liao, H., Guo, Z., Li, W., & Coddet, C. (2013). Deposition behavior of thermally softened copper particles in cold spraying. *Acta Materialia*, *61*(14), 5105–5118. https://doi.org/10.1016/j.actamat.2013.04.041

[117] Yu, M., Li, W. Y., Wang, F. F., Suo, X. K., & Liao, H. L. (2013). Effect of particle and substrate preheating on particle deformation behavior in cold spraying. *Surface and Coatings Technology*, *220*, 174–178. https://doi.org/10.1016/j.surfcoat.2012.04.081

[118] Zhao, P., Zhang, Q., Guo, Y., Liu, H., & Deng, Z. (2020). Atomic simulation of crystal orientation effect on coating surface generation mechanisms in cold spray. *Computational Materials Science*, *184*(March),

109859. https://doi.org/10.1016/j.commatsci.2020.109859

[119] Zhao, Z. po, Tang, J. rong, Du, H., Gyansah, L., Wang, J. qiang, & Xiong, T. ying. (2018). In-situ chemical interaction in cold-sprayed Zn/Cu composite coating. *Materials Letters*, *228*, 246–249. https://doi.org/10.1016/j.matlet.2018.06.024

BIOGRAPHICAL PROFILE OF RESEARCHER

Mohsin Khan works at Mewat Engineering College (Waqf), Nuh, Haryana, as an Assistant Professor in the Department of Mechanical Engineering. He completed his Bachelor of Technology in Mechanical Engineering at the same college, i.e., Mewat Engineering College (Waqf), Nuh, Haryana. He received his Master's degree (M. Tech.) in Thermal Engineering from M.V.N. University, Palwal, Haryana as the class topper. He has published and presented 15 research papers in SCI, SCOPUS, UGC Care Journals, and National and International Conferences. He got various certificates, Medals, & Prices in Art, Technical Presentation, Academic & other Co-Curricular Activities. He has worked as an assistant professor in the mechanical engineering department at the World Institute of Technology, Sohna, Gurugram, Haryana, and RAWAL INSTITUTIONS at the College of Engineering & Technology, Faridabad, Haryana. He has more than eight years of core teaching experience.